CANADIAN JOURNAL OF RESEARCH

VOLUME 28 JULY, 1950 NUMBER 4

— SECTION A —

PHYSICAL SCIENCES

Contents

NATIONAL RESEARCH COUNCIL
OTTAWA, CANADA

CANADIAN JOURNAL OF RESEARCH

The *Canadian Journal of Research* is issued in six sections, as follows:

A. Physical Sciences	D. Zoological Sciences
B. Chemical Sciences	E. Medical Sciences
C. Botanical Sciences	F. Technology

For the present, Sections A, C, D, and E are to be issued six times annually, and Sections B and F, twelve times annually, each under separate cover, with separate pagination.

The *Canadian Journal of Research* is published by the National Research Council of Canada under authority of the Chairman of the Committee of the Privy Council on Scientific and Industrial Research. The *Canadian Journal of Research* is edited by a joint Editorial Board consisting of members of the National Research Council of Canada, the Royal Society of Canada, and the Chemical Institute of Canada.

Sections B and F of the *Canadian Journal of Research* have been chosen by the Chemical Institute of Canada as its medium of publication for scientific papers.

Manuscripts should be addressed:

Editor-in-Chief,
Canadian Journal of Research,
National Research Council, Ottawa, Canada.

Canadian Journal of Research

Issued by THE NATIONAL RESEARCH COUNCIL OF CANADA

VOL. 28, SEC. A. JULY, 1950 NUMBER 4

PRECISION DETERMINATION OF NUCLEAR GYROMAGNETIC RATIOS[1]

BY E. W. GUPTILL, W. J. ARCHIBALD, AND E. S. WARREN

Abstract

The ratio of the Larmour frequency of precession for hydrogen and fluorine, and for sodium and aluminum have been measured with an accuracy of one part in 10^5:

$$\nu_H/\nu_F = 1.062917 \pm 0.00001$$
$$\nu_{Na}/\nu_{Al} = 1.015081 \pm 0.00001$$

These ratios are corrected for the atomic diamagnetism giving for, γ, the *nuclear* gyromagnetic ratios:

$$\gamma_H/\gamma_F = 1.06245 \pm 0.00002$$
$$\gamma_{Na}/\gamma_{Al} = 1.01494 \pm 0.00002$$

A brief description is given of the relevant equipment used in obtaining these measurements.

Several methods for measuring nuclear gyromagnetic ratios have been developed in the past few years (1, 7, 8). The present article describes a slightly different method which lends itself to an accurate determination of the ratios of nuclear moments. The technique involves the use of a single sample in which both nuclei are to be found. The measurement of a ratio has been reduced to the measurement of the Larmour frequencies of the two nuclei, both resonances being detected by the same electronic device, the change from one resonance to another being effected with no physical adjustments other than the resetting of an oscillator.

Apparatus

Fig. 1 contains a block diagram of the apparatus. Element *A* of the diagram is a combination oscillator and detector, a detailed circuit diagram of which is to be found in Fig. 2. The coils which in Bloch's experiment are called the driver coil and pickup coil are in this apparatus respectively the plate coil and grid coil of the oscillator. The amplitude of oscillation of *A* is determined (among other things) by the mutual inductance of these two coils, which is altered by the nuclear precession when it occurs.

The magnetic field is modulated about 0.0025% by the 30 cycle oscillator *D*. This slight modulation, as in Purcell's method (2), is a small fraction of the

[1] *Manuscript received January 31, 1950.*
Contribution from the Department of Physics, Dalhousie University, Halifax, N.S.

natural line width. When in the region of the resonance, there is a 30 cycle amplitude modulation of the oscillator A. The oscillations of A are detected, giving a 30 cycle signal which is amplified by B, which is in turn detected by the phase-sensitive detector (3) C. The 30 cycle oscillator D is coupled to C in order that only those signals having the same frequency as D may give rise to a unidirectional current through the meter E.

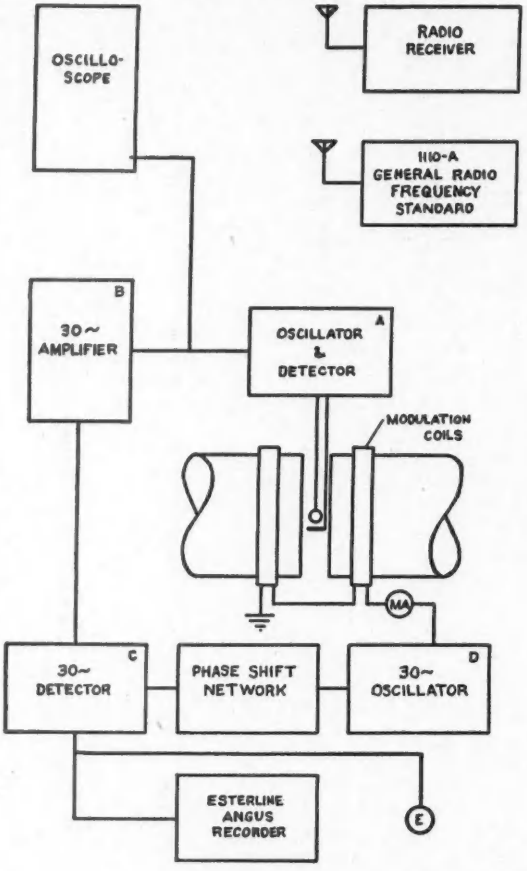

FIG. 1. *Block diagram of apparatus.*

It is essential that the perturbing radio-frequency field at the nuclei be small if a net nuclear magnetic moment is to be preserved. The control of this r.f. field can be achieved in two ways:

(*a*) by altering the mutual inductance between the grid and plate coils; and

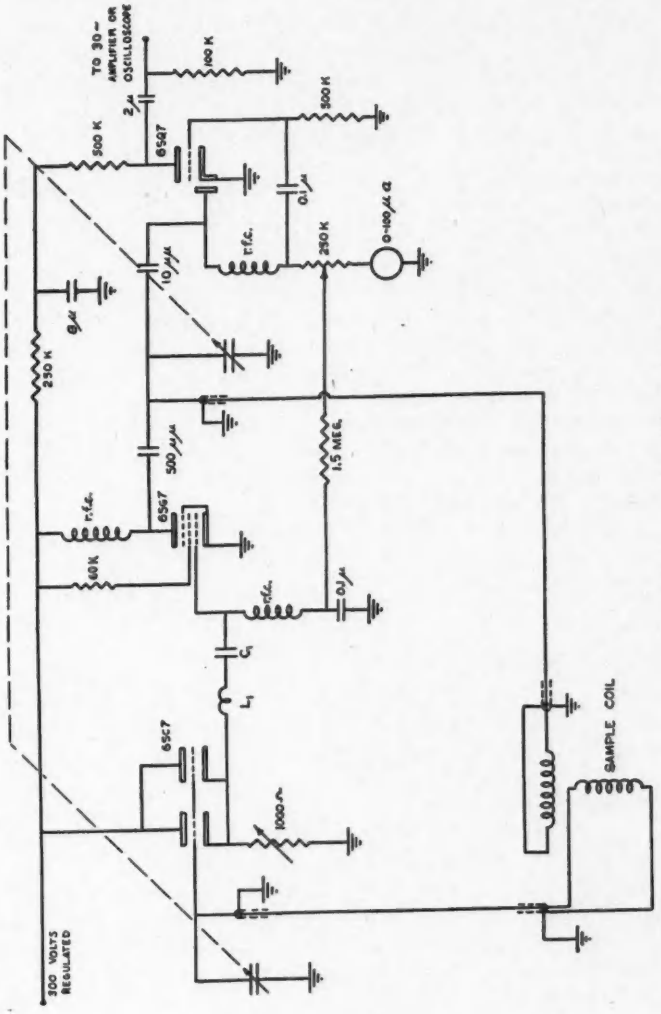

FIG. 2. *Circuit diagram of oscillator and detector.*

(*b*) by varying the grid bias of the semi-remote cutoff tube 6SG7 (Cf. Fig. 2). A point by point plot of the meter reading E against the mean magnetic field yields either the slope of the dispersion or the absorption curve or a superposition of both, depending upon the phase change suffered by the signal induced in the grid coil. In the apparatus as herein described the phase was adjusted by L_1 in Fig. 2 to give the slope of the dispersion curve. The shape of the line may also be altered (but to a lesser extent) by the resistor in the cathode circuit of the 6SC7.

Magnet

The magnetic field was provided by a one-ton magnet, the iron for which was presented to the University by the Steel Company of Canada. The ratio of pole face diameter (8 in.) to gap width (1 in.) was very close to that of the McGill cyclotron magnet, and the shimming was copied directly from it and machined into removable pole faces. It should be noted that the field requirements for our magnet are, strictly, not the same as for a cyclotron, the former requiring a field which is as homogeneous as is possible. However, the shimming adopted was satisfactory for fields below 5000 gauss. Fig. 4 shows a plot of the percentage change in the field versus radial distance from the center. The data for this curve was taken at 3800 gauss. In the present experiment only extremely small drifts in the magnetic field could be tolerated. It was, consequently, necessary to control the current electronically with the circuit shown in Fig. 3. This particular control is intended for a constant voltage source such as storage cells, and with it the drift in magnetic field could be kept as low as 2 or 3 parts in 10^5 over the period of an hour. The resistance of the magnet wire would change about 1% in a corresponding period.

Experimental Results

Hydrogen and Fluorine

A sample containing about 0.5 cc. of hydrofluoric acid was used for the hydrogen and fluorine measurements. The variation in magnetic field over the volume of the sample was about 5 parts in 10^5. It was assumed that this was comparable to the natural line width in this sample, since the actual line width was reduced very little by a further reduction of the volume. The signals from both the hydrogen and fluorine were large enough to be viewed directly on the screen of the oscilloscope when a 60 cycle modulation was applied to the magnetic field. The procedure was to adjust the frequency of oscillator A until the signals from the hydrogen nuclei were in the center of the oscilloscope trace. The frequency of the oscillator was then measured. A similar measurement was made for the fluorine nucleus, the only alteration in the equipment being the condensers controlling the frequency. Twenty-one measurements of ν_H/ν_F were obtained—12 at a field of 3500 gauss and 9 at 1000 gauss.

3500 gauss:	1.062916 ± 0.00001
1000 gauss:	1.062919 ± 0.00001
Average:	1.062917 ± 0.00001.

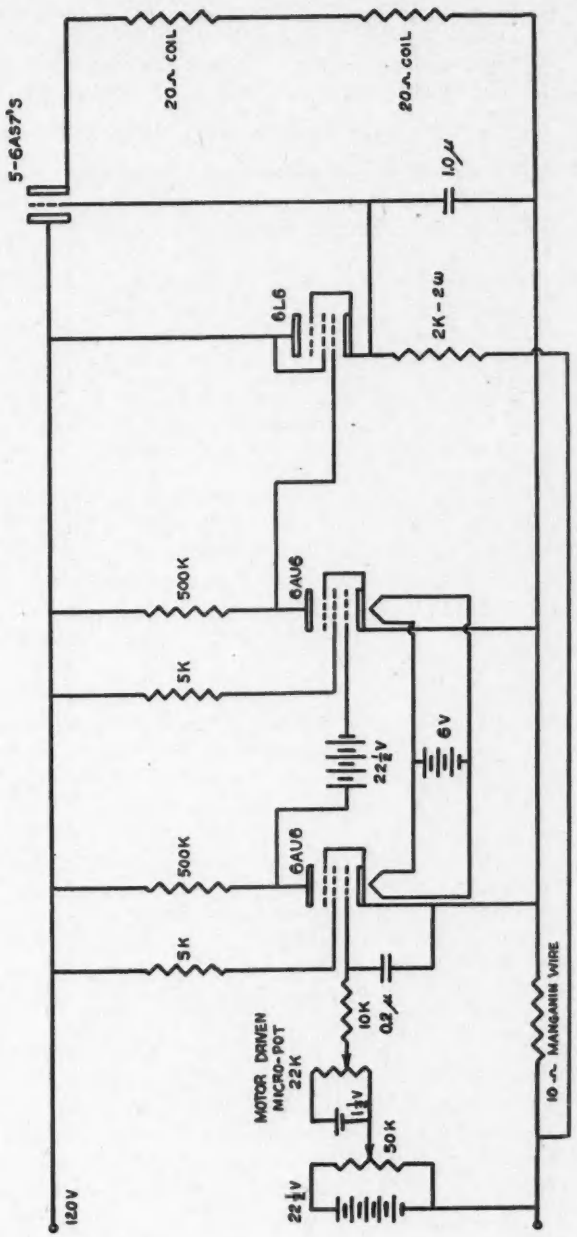

FIG. 3. *Control circuit for magnet.*

The second group of measurements was taken after altering as many variables as was possible, including the oscillator A and all its components. This was done in an effort to assess the magnitude of systematic errors. The estimated error (0.00001) is 1/5 of the line width and 4 times larger than that obtained by evaluating $\sqrt{\frac{\Sigma d^2}{N^2}}$, where N is the number of ratios and d the deviation from the mean. Seventy-five per cent of the ratios fell within the limits of the given error.

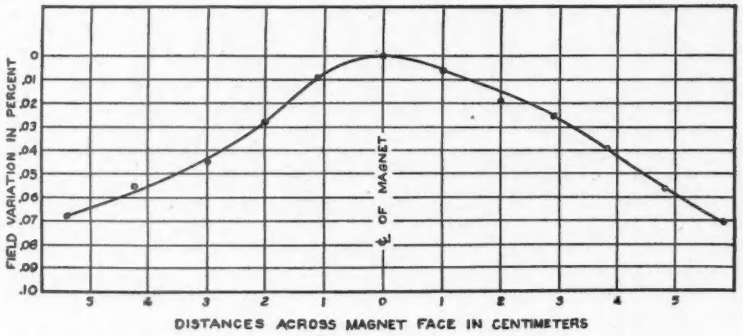

FIG. 4. *Graph showing the variation in magnetic field near the center of the magnet.*

Sodium and Aluminum

One-half a cubic centimeter of sodium aluminate was used for the measurements on Na and Al. As before, the line width was comparable to the field inhomogeneity; however, the signal-to-noise ratio was smaller, and it was necessary to use the 30 cycle modulation and the lock-in amplifier. Fig. 5 shows an Esterline–Angus plot of these lines as the magnetic field was slowly varied through resonance. A typical ratio was measured by first setting the oscillator frequency equal to the Larmour frequency of the magnetic moment. The criterion for the frequency adjustment was the maximum deflection of the Esterline–Angus meter. The frequency was then measured and similar data taken for the second magnetic moment. Thirty values of this ratio were obtained at a field of 3400 gauss:

$$\nu_{Na}/\nu_{Al} = 1.015081 \pm 0.00001$$

In this case the distribution was not gaussian but rather with one maximum each side of a central maximum in which 40% of the values occurred. The reason for this is not clearly understood, but there are good indications that it is a function of the apparatus. The mean of the 12 values occurring in the central region is 2 parts in 10^6 lower than the ratio given which is the mean of all values. The spread of the two subsiduary maxima was 3 parts in 10^5.

The frequency ratios above may be corrected to yield γ_H/γ_F and γ_{Na}/γ_{Al}, where the γ's are the nuclear gyromagnetic ratios. This diamagnetic correction has been calculated by Lamb (6):

$$H_1 = H_0 \frac{e}{3mc^2} \int_v \frac{f(r)}{r} dv,$$

where H_1 is the diamagnetic field at the nucleus, H_0 the magnetic field in which the charge density $f(r)$ is placed, e and m the charge and mass of the electron. The integral can be evaluated for any particular atom by the Hartree–Foch

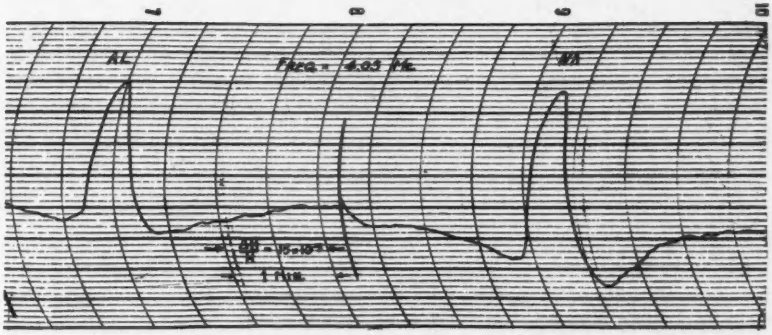

FIG. 5. *Esterline–Angus (recording milliammeter) plot of signals from aluminum and sodium in sodium aluminate. There is a discontinuity (1.5%) in the magnetic field at the center of the trace.*

method of the self-consistent field. In the case of the hydrogen atom $H_1/H_0 = 1/3\alpha^2 = 0.177 \times 10^{-4}$, where α is the fine structure constant. For the hydrogen in H_2O the factor would be almost twice this, or about three parts in 10^5.

The following values of H_1/H_0 were computed from the wave functions given by Kennard (Na) (5) and Hartree (Al and F) (4); Na 0.63×10^{-3}; Al 0.77×10^{-3}; and F 0.47×10^{-3}. These corrections, give for the *nuclear* gyromagnetic ratios,

$$\gamma_H/\gamma_F = 1.06245 \pm 0.00002$$
$$\gamma_{Na}/\gamma_{Al} = 1.01494 \pm 0.00002.$$

Acknowledgments

The authors wish to express their gratitude to the National Research Council of Canada, who supported this work with a grant-in-aid as well as a bursary, which was held by Mr. E. S. Warren. They are also indebted to Mr. J. W. Cullens who constructed some of the electronic equipment in addition to making all the drawings in this report.

References

1. BLOCH, F., HANSEN, W. W., and PACKARD, M. Phys. Rev. 70: 474. 1946.
2. BLOEMBERGEN, N., PURCELL, E. M., and POUND, R. V. Phys. Rev. 73: 679. 1948.
3. DICKIE, R. H. Rev. Sci. Instruments, 17: 268. 1946.
4. HARTREE, D. R. Proc. Roy. Soc. London, 151: 96. 1939.
5. KENNARD, E. H. and RAMBERG, E. Phys. Rev. 46: 1034. 1934.
6. LAMB, W. E. Phys. Rev. 60: 817. 1941.
7. PURCELL, E. M., TORREY, H. C., and POUND, R. V. Phys. Rev. 69: 37. 1946.
8. ZIMMERMAN, J. R. and WILLIAMS, D. Phys. Rev. 73: 94. 1948.

SPECIFIC HEATS OF CERTAIN SALTS OF IRON GROUP ELEMENTS FROM 65° TO 300°K.[1]

By H. D. Vasileff[2] and H. Grayson-Smith[3]

Abstract

Using a new low temperature calorimeter, which is briefly described in the paper, the specific heats have been measured from 65° to 300°K. for the following salts: chromium sulphate (hydrated and anhydrous), chromium nitrate, cobalt nitrate, and nickel nitrate (hydrated). Hydrated chromium sulphate was found to have a transition of the second order at 195°K., while the specific heat of the anhydrous salt was quite regular. The hydrated nitrates all showed second order transitions in the neighborhood of 150°K. The entropy changes associated with these transitions have been estimated approximately, and vary from about $0.4R$ for cobalt nitrate to $1.65R$ for chromium nitrate, where R is the gas constant. Pending further evidence, it is tentatively suggested that the transitions are due to the onset of partial rotation of the H_2O groups in the crystals.

Introduction

As part of a study of simple compounds of elements of the iron group, chromium to nickel, the specific heats have been measured from 65° to 300°K. for the salts listed in Table I. The same salts have been investigated magnetically by Johnson (8), using materials from the same lots. The two investigations were carried out at the same time because knowledge of either property may help in the interpretation of the other. However, the magnetic properties proved to be quite regular over the temperature range concerned, while the calorimetric study has revealed that all the hydrated salts pass through transitions of the second order. These are discussed in the present paper. They must be due to some cause other than magnetic, but cannot be definitely identified on the calorimetric evidence alone.

Materials Used

The salts were obtained from British Drug Houses (Canada) Ltd., and were specified as having impurity less than the amounts listed in Table I. The anhydrous chromium sulphate was prepared from the hydrate by heating at 400°C. until the weight was constant. The observed loss of weight was 1 to 2% greater than the amount accounted for by the removal of 18 H_2O. In a salt such as $Cr_2(SO_4)_3.18\ H_2O$ there is always some uncertainty concerning the amount of water of crystallization actually present. From the loss of weight in heating it was concluded that the amount of water in the sample used was close to the theoretical value.

[1] *Manuscript received February 7, 1950.*
Contribution from the Department of Physics, University of Toronto, Toronto, Ont.
[2] *Present address: Defense Research Board, Ottawa, Ont.*
[3] *Present address: Department of Physics, University of Alberta, Edmonton, Alberta.*

TABLE I

SPECIFICATIONS OF SALTS INVESTIGATED

Chromium sulphate, $Cr_2(SO_4)_3.18H_2O$
Chloride (Cl).....0.003%
Iron (Fe).....0.01%
Alkalis.....0.5%

Chromium sulphate anhydrous, $Cr_2(SO_4)_3$
Same as hydrated salt

Chromium nitrate, $Cr(NO_3)_3.9H_2O$
Chloride (Cl).....0.003%
Sulphate (SO_4).....0.01%
Iron (Fe).....0.01%
Alkalis.....0.5%

Cobalt nitrate, $Co(NO_3)_2.6H_2O$
Chloride (Cl).....0.001%
Sulphate (SO_4).....0.01%
Iron (Fe).....0.003%
Nickel (Ni).....0.002%
Alkalis and alkaline earths (Na).....0.03%
Ammonia.....No reaction.

Nickel nitrate, $Ni(NO_3)_2.6H_2O$
Chloride (Cl).....0.002%
Sulphate (SO_4).....0.01%
Cobalt (CO).....0.0005%
Iron (Fe).....0.001%
Alkalis and alkaline earths (Na).....0.03%

The Calorimeter

The low temperature calorimeter is shown in Fig. 1. It was of similar design to that used by Elson, Grayson-Smith, and Wilhelm (2), but was completely rebuilt. The powdered samples were compressed into the calorimeter chamber *E* by means of the plate *G* and nut *H*. The cover plate *J* was then soldered into place with Wood's metal, the calorimeter was exhausted, and filled with helium gas at a few centimeters pressure in order to improve the thermal

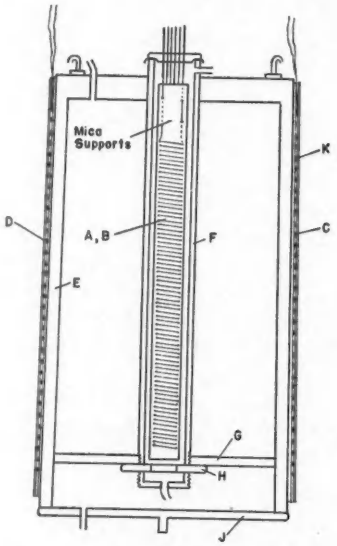

FIG. 1. *Low temperature calorimeter.*

contact at low temperatures. The calorimeter was heated from the outside surface by means of a constantan coil K, protected by a radiation shield D.

The temperatures were measured by means of resistance thermometers A, B, wound on a mica frame, and mounted in the central tube F, which was also filled with helium. The principal thermometer was of platinum, with a resistance at 0°C. of 8.4782 ohms. For temperatures down to 91°K. it was calibrated according to the specifications for the International temperature scale. At lower temperatures Henning's deviation method (6, 7) was used. Using a Mueller bridge, and a galvanometer with a sensitivity of 0.2 μv. per mm., resistances could be measured to 10^{-4} ohm, and temperature changes to 0.003°. The increases of temperature in the specific heat determinations were 0.5 to 1°, and could therefore be measured with a precision of 0.6 to 0.3%.

Auxiliary manganin thermometers were wound on the surface of the calorimeter at C, along with the heating coil, and on the inner mica frame, along with the platinum thermometer. The inner manganin thermometer was intended for extremely low temperatures, where the platinum thermometer becomes insensitive. It was not used in the measurements to be reported in this paper. That on the outer surface was used in tests of the rate at which temperature equilibrium was attained in the calorimeter.

The rate of heating was determined by measuring the potential difference across the constantan heater with a Leeds and Northrup type K2 potentiometer. The resistance of the heater was determined by comparing this potential drop with that across a standard resistance connected in series in the same circuit. This needed only to be checked occasionally, since the resistance of the constantan was nearly constant over a 1° temperature interval, and could be taken equal to the value at the middle of the interval. The time of heating, and the times at which temperature measurements were made, were recorded on a tape chronograph, and compared with time marks made by a 25 cycle electric clock motor.

The whole calorimeter assembly shown in Fig. 1 was suspended by threads inside a protecting jacket, which could be evacuated for insulation, or filled with a gas for thermal contact. Whenever possible, the jacket was kept at a constant temperature by immersing it in a cryostat of liquid nitrogen, liquid oxygen or liquid ethylene. For temperatures between 91° and 135°K., between the oxygen and ethylene ranges, the mean temperature of the jacket could be held sufficiently steady to enable measurements to be made by immersing it to different depths in liquid oxygen. For temperatures above the boiling point of ethylene (170°K.) the calorimeter jacket was suspended in the stream of cold air rising from liquid air boiling at a steady rate.

In low temperature calorimetry the influx of heat from parts of the apparatus at room temperature, by conduction along the electrical leads, and by radiation through the pumping tube, is usually greater than the loss of heat by radiation to the jacket, which is at the cryostat temperature. This source of error was

reduced by wrapping all the electrical leads around copper posts attached to the calorimeter jacket, and by placing a polished copper baffle over the outlet to the pumping tube.

Correction for Heat Exchange

When low temperature specific heat measurements have not been made in an adiabatic calorimeter it has been usual to correct for heat exchange with the surroundings by the graphical method developed by Keesom and Kok (9). This method involves three approximations, which may or may not be satisfactory for a particular calorimeter. It is assumed that the loss of heat to the immediate surroundings is proportional to the temperature difference, that the rate of gain from the more distant surroundings at room temperature is constant, and that the temperature of the calorimeter and sample is uniform. In preliminary tests the form of the temperature–time curve before and after a heating interval showed that the first two approximations were sufficiently accurate to be used in correction for heat exchange. However, during and immediately after a heating interval there was an appreciable difference of temperature between the center and the surface, such that, with heating intervals of two to four minutes, the maximum temperature at the center was not attained until 25 to 50 sec. after the surface heater was turned off.

In order to determine whether this time lag would cause an appreciable error in the temperature correction, a theoretical calculation was made, based on the well known equations for a cylinder with a radial temperature gradient. The conclusion was that the graphical method of Keesom and Kok would give too high values of the heat capacity when the time lag was appreciable. Correction for the time lag was not feasible on account of the uncertainty in the mean thermal conductivity within the calorimeter. However, any specific heat measurement involves the difference between the heat capacities with and without the sample. If these are both measured experimentally by the same procedure, the errors due to time lag should approximately cancel, and the specific heat values should not be seriously affected.

Heat Capacity of the Empty Calorimeter

The heat capacity of the calorimeter alone was measured directly, and was also deduced from a series of measurements with a copper sample, using the values given by Dockerty (1) for the specific heat of copper. The results are shown in Fig. 2, where the circles represent the direct values, and the triangles indirect values. The agreement between the two sets of values shows that the time lag has not seriously affected the differences, in spite of the large difference in thermal conductivity between copper and helium gas.

From the scattering of the points in Fig. 2 it was estimated that the random error in subsequent measurements of the specific heats of the salts studied should not exceed 0.001 cal.-gm.$^{-1}$-deg.$^{-1}$

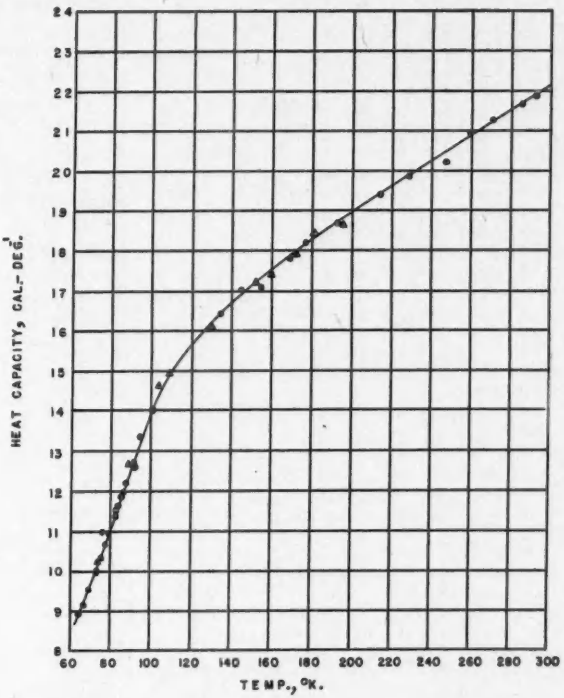

FIG. 2. *Heat capacity of calorimeter.* ○, *direct measurements;* Δ, *deduced from measurements with copper sample.*

Specific Heats of Iron Group Salts

Measurements of the specific heats of the salts listed in Table I are shown in Figs. 3 to 6. In each case the plotted points represent at least two distinct series of measurements. Values obtained from the smoothed graphs are collected in Table II.

The most interesting feature of these results is that all the hydrated salts show specific heat anomalies, while the specific heat of the anhydrous chromium sulphate is quite regular over the range of temperature investigated. From the shape of the specific heat curves it is evident that the anomalies are due to transitions of the second order.

The increase of entropy from 65° to 273°K. was determined by drawing smooth curves of the ratio (heat capacity per mole)/(absolute temperature) and integrating this function numerically, with the results given in Table III. It is not possible to extrapolate the entropies to 0°K. because these salts are all paramagnetic, and may be expected to have magnetic transitions of some kind

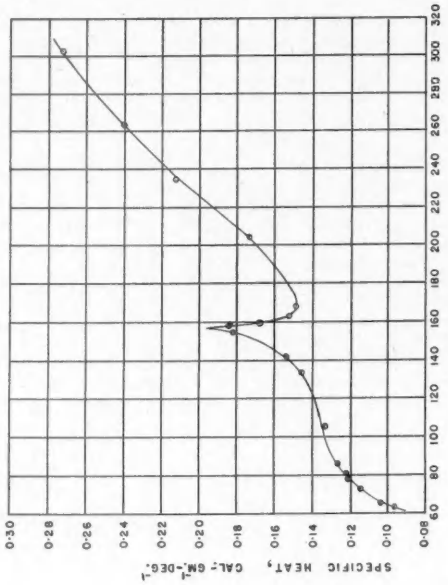

FIG. 4. *Specific heat of chromium nitrate, $Cr(NO_3)_3.9H_2O$.*

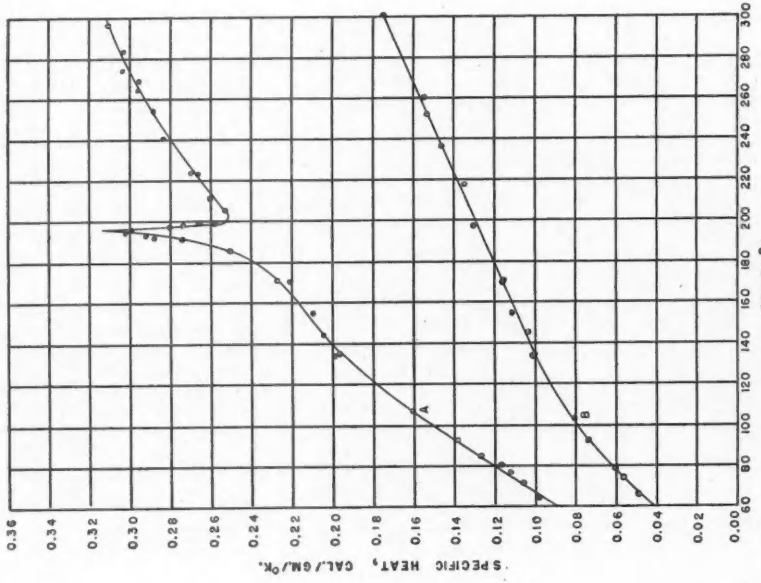

FIG. 3. *Specific heat of chromium sulphate. A, hydrated, $Cr_2(SO_4)_3.18H_2O$; B, anhydrous.*

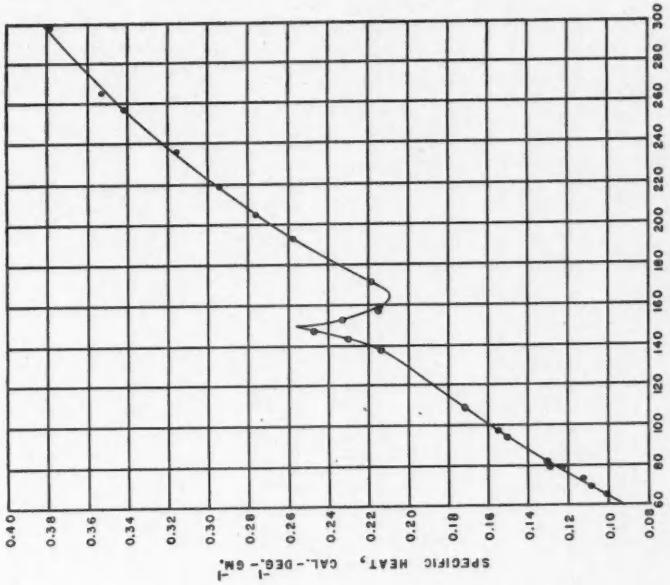

FIG. 6. *Specific heat of nickel nitrate,* $Ni(NO_3)_2.6H_2O$.

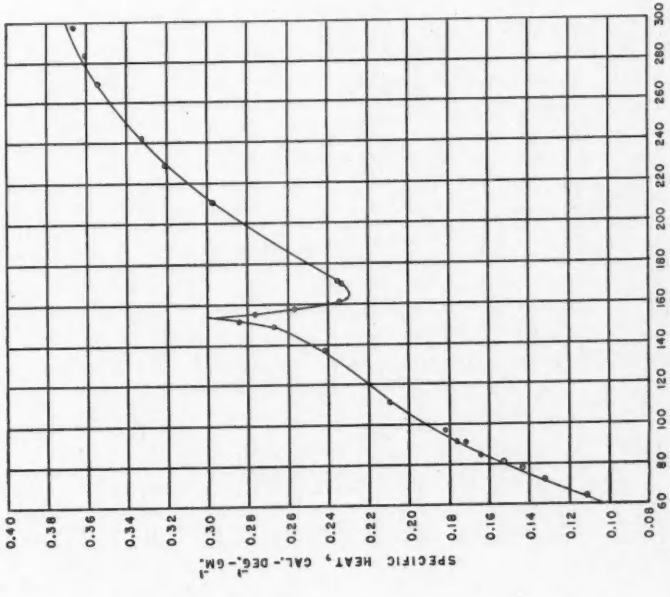

FIG. 5. *Specific heat of cobalt nitrate,* $Co(NO_3)_2.6H_2O$.

TABLE II

SPECIFIC HEATS DERIVED FROM SMOOTHED GRAPHS

Temperature, °K.	Specific heat, cal.-gm.$^{-1}$-deg.$^{-1}$				
	Chromium sulphate hydrate	Chromium sulphate anhydrous	Chromium nitrate	Cobalt nitrate	Nickel nitrate
300	0.312	0.172	0.273	0.371	0.382
280	0.304	0.163	0.255	0.363	0.365
260	0.293	0.154	0.237	0.350	0.345
240	0.280	0.146	0.216	0.333	0.323
220	0.265	0.137	0.193	0.311	0.297
200	0.252	0.128	0.169	0.283	0.269
195	0.312	–	–	–	–
190	0.273	–	–	–	–
185	0.251	–	–	–	–
180	0.239	0.120	0.151	0.250	0.235
170	0.224	–	0.149	0.234	0.217
160	0.214	0.111	0.168	0.240	0.212
155	–	–	0.182	0.270	0.222
150	–	–	0.167	0.275	0.244
145	–	–	0.156	0.256	0.237
140	0.201	0.102	0.150	0.248	0.220
130	–	–	0.143	0.236	0.201
120	0.181	0.092	0.139	0.224	0.188
100	0.151	0.080	0.133	0.192	0.160
90	0.136	0.072	0.129	0.172	0.144
80	0.120	0.064	0.122	0.150	0.128
70	0.104	0.053	0.110	0.125	0.110
65	0.095	0.046	0.100	0.112	0.102

TABLE III

ENTROPY CHANGES AND TRANSITION TEMPERATURES

Salt	Total entropy change $S_{273} - S_{65}$ cal.-mole.$^{-1}$-deg.$^{-1}$	Transition temperature, °K.	Estimated entropy due to the transition (as multiples of R)
$Cr_2(SO_4)_3.18H_2O$	202.5	195	$1.41R$
$Cr_2(SO_4)_3$	56.2	–	–
$Cr(NO_3)_3.9H_2O$	88.2	158	$1.65R$
$Co(NO_3)_2.6H_2O$	93.5	153	$0.4R$
$Ni(NO_3)_2.6H_2O$	87.1	149	$0.6R$

at lower temperatures. Table III gives also the transition temperatures, and the estimated increases of entropy due to the transition (as multiples of the gas constant R). For the cobalt and nickel nitrates the entropy change due to the transition can only be roughly estimated because the specific heat of the crystal lattice is also changing rapidly over the temperature range concerned, and seems to have a discontinuity at the transition temperature.

Evidence was obtained that supercooling effects might accompany any of these transitions. In most of the experiments it took several hours to cool the calorimeter and sample to the required initial temperature for a series of readings, using gas conduction only. Under these conditions the specific heat

curves in the neighborhood of the transitions were reproducible. However, if the salts were quenched rapidly to 90°K. before a series of measurements, abnormally high values of specific heat were obtained between 90° and the transition temperature. This indicates metastable forms of higher entropy, and so more or less "frozen-in disorder." After chromium sulphate hydrate had been quenched, it had to be annealed at room temperature for several days before the original curve could be reproduced.

Discussion

Second order transitions of the type described are well known, and may be due to any one of a number of causes. In pure substances they have been ascribed in different cases to ferromagnetism, to ferroelectric effects, or to the onset of partial rotation of one or more molecular groups within the crystal. Additional evidence must therefore be obtained in order to identify the cause in the salts investigated. It is known that they are not magnetic, since Johnson (8) has measured the paramagnetic susceptibilities of the same materials, and has found them to be quite regular down to 77°K. The possibilities remain of either dielectric transitions similar to that observed by Roberts (12) and by Harwood *et al.* (5) in barium titanate, or of rotational transitions similar to those observed in a number of ammonium salts (4).

Of these alternatives the onset of rotation seems the most likely. Since the anomaly occurs with hydrated chromium sulphate and not with the anhydrous salt, it must, in that case at least, be due to the water of crystallization. So far as the authors are aware, rotation within a crystal of H_2O groups has not hitherto been suggested as a cause of second order transitions. The nearest parallel case in the literature is a transition in $Ni(NO_3)_2.6NH_3$, which has been ascribed by Long and Toettcher (11) to the onset of rotation of both the NO_3 and NH_3 groups. Unexplained transitions have been observed in lanthanum magnesium nitrate (3) and hydrated magnesium chloride (10), and might be due to the same cause as those reported in the present paper.

Whether or not this suggestion is correct cannot be established on the calorimetric evidence alone. The obvious next step is a study of the dielectric properties. Apparatus for this study is now being constructed.

Acknowledgments

The authors wish to express their thanks to Prof. A. D. Misener for helpful suggestions and discussion, to Mr. J. C. Findlay for advice and assistance in constructing the apparatus, and to Mr. A. Owen for assistance in preparing pure cryostat liquids. They wish also to acknowledge the assistance of the the Research Council of Ontario, through the award of a scholarship to Mr. Vasileff, and the National Research Council, through a grant-in-aid which provided technical assistance for this and other projects.

References

1. DOCKERTY, S. M. Can. J. Research, A, 15: 59. 1937.
2. ELSON, R. G., GRAYSON-SMITH, H., and WILHELM, J. O. Can. J. Research, A, 18: 83. 1940.
3. FORNOFF, F., PITZER, K., and LATIMER, W. J. Am. Chem. Soc. 67: 1445. 1945.
4. FOWLER, R. H. Statistical mechanics, Chap. 21. Cambridge: The University Press. 1936.
5. HARWOOD, M. G., POPPER, P., and RUSHMAN, D. F. Nature, 160: 58. 1947.
6. HENNING, F. Naturwissenschaften, 16: 617. 1928.
7. HENNING, F. Die Physik, 2: 1. 1934.
8. JOHNSON, A. F. and GRAYSON-SMITH, H. Can. J. Research, A, 28: 229. 1950.
9. KEESOM, W. H. and KOK, J. A. Proc. Acad. Sci. Amsterdam, 35: 294. 1932.
10. KELLEY, K. and MOORE, G. E. J. Am. Chem. Soc. 65: 2340. 1943.
11. LONG, E. A. and TOETTCHER, F. J. Chem. Phys. 8: 504. 1940.
12. ROBERTS, S. Phys. Rev. 71: 890. 1947.

MATHEMATICAL ANALYSIS OF AN ACOUSTIC FILTER[1]

By N. Olson

Abstract

Equations have been derived for the frequency limits of the attenuation bands, the degree of attenuation, and the phase change of a specific type of filter which cannot be readily analyzed by the side branch method. The characteristics have been verified by measurements on experimental filters.

Introduction

A theory of acoustic filters has been developed by Stewart (3, 4) analogous to the theory of electrical filters, in which the series and shunt impedances of electrical filters are replaced by appropriate lumped acoustic impedances. In particular, a conduit with regularly spaced side branches may be represented thus, and the formulas for electrical filters can be used. In this theory, the assumption is made that the wave length of the sound is much greater than the dimensions of the filter section, so that the phase change in each section may be neglected.

A later theory developed by Mason (1, 2) considers the effect of the side branches on the transmission of a plane wave through a conduit. For the special case in which the wave length of the sound is much greater than the dimensions of the filter, this theory reduces to that of Stewart. Mason also extends his theory to include the case of a cylindrical side branch, coaxial with the main conduit and coupled to it via a gap in the conduit. The side branch impedance is determined by assuming that a radial piston acts in the opening.

This paper deals with a specific type of filter consisting of a conduit with a series of expansions at regular intervals. By considering the transmission of a plane wave through the conduit, equations will be derived for the limits of the attenuation bands, phase change, and attenuation. The assumption is here made that the transmitted wave is plane at all points along the filter, an assumption which is valid if the change in cross section is not excessively large. This type of filter can be considered as a special case of the one discussed by Mason, with the side branch opening extended until it includes the entire length of the side branch. However, Mason's approximations are not applicable to this case.

Filter Theory

The filter is taken to consist of an infinite series of sections as shown in Fig. 1, (*a*), or 1, (*b*), and in which the impedance is the same at all junctions

[1] *Manuscript received February 8, 1950.*
Contribution from the Electricity Section, Division of Physics, National Research Laboratories, Ottawa, Canada. Issued as N.R.C. No. 2160.

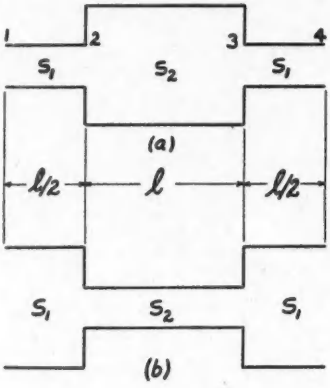

FIG. 1. *Filter sections.* (*a*) $m = S_1/S_2 < 1$. (*b*) $m = S_1/S_2 > 1$.

between sections. S_1 and S_2 are cross-sectional areas. The velocity potential in a plane wave is given by

$$\phi = Ae^{i(\omega t - kx)} + Be^{i(\omega t + kx)}, \tag{1}$$

from which the excess pressure and volume current are

$$p = -i\rho_0 kc(Ae^{-ikx} + Be^{ikx})e^{i\omega t} \tag{2}$$

$$\dot{X} = -ikS(Ae^{-ikx} - Be^{ikx})e^{i\omega t}, \tag{3}$$

where

ω = $2\pi \times$ frequency,
k = ω/c,
c = velocity of sound,
ρ_0 = equilibrium density of medium,
S = cross sectional area,
A and B are arbitrary constants,
$\dot{X} = S\dot{\xi}$, where $\dot{\xi}$ = velocity of particles in medium.

Omitting the exponential in t, and starting at position 1 in the filter section, Fig. 1:

$$\left.\begin{aligned} p_1 &= -i\rho_0 kc(A_1 + B_1) \\ \dot{X}_1 &= -ikS_1(A_1 - B_1) \end{aligned}\right\}. \tag{4}$$

At 2,

$$\left.\begin{aligned} p_2 &= -i\rho_0 kc(A_1 e^{-ikl/2} + B_1 e^{ikl/2}) \\ \dot{X}_2 &= -ikS_1(A_1 e^{-ikl/2} - B_1 e^{ikl/2}) \end{aligned}\right\}, \tag{5}$$

$$\left.\begin{aligned} p_2' &= -i\rho_0 kc(A_2 e^{-ikl/2} + B_2 e^{ikl/2}) \\ \dot{X}_2' &= -ikS_2(A_2 e^{-ikl/2} - B_2 e^{ikl/2}) \end{aligned}\right\}, \tag{6}$$

where unprimed quantities represent conditions to the left, and primed quan-

tities represent conditions to the right of the junction between the two cross sections.

At 3,

$$\left.\begin{aligned} p_3 &= -i\rho_0 kc(A_2 e^{-ikl/2} + B_2 e^{ikl/2}) \\ \dot{X}_3 &= -ikS_2(A_2 e^{-ikl/2} - B_2 e^{ikl/2}) \end{aligned}\right\}, \tag{7}$$

$$\left.\begin{aligned} p_3' &= -i\rho_0 kc(A_3 e^{-ikl/2} + B_3 e^{ikl/2}) \\ \dot{X}_3' &= -ikS_1(A_3 e^{-ikl/2} - B_3 e^{ikl/2}) \end{aligned}\right\}. \tag{8}$$

At 4,

$$\left.\begin{aligned} p_4 &= -i\rho_0 kc(A_3 e^{-ikl} + B_3 e^{ikl}) \\ \dot{X}_4 &= -ikS_1(A_3 e^{-ikl} - B_3 e^{ikl}) \end{aligned}\right\}. \tag{9}$$

Since there is continuity of pressure and volume current at the junctions, Equations (4) to (9) may be reduced to

$$\left.\begin{aligned} p_4 &= p_1/4m[\{(m+1)^2 \cos 2kl - (m-1)^2\} \\ &\quad -iZ_1/Z_0\{(m+1)^2 \sin 2kl + 2(m^2-1)\sin kl\}] \\ \dot{X}_4 &= \dot{X}_1/4m[\{(m+1)^2 \cos 2kl - (m-1)^2\} \\ &\quad -iZ_0/Z_1\{(m+1)^2 \sin 2kl - 2(m^2-1)\sin kl\}] \end{aligned}\right\}, \tag{10}$$

where $p_4/\dot{X}_4 = p_1/\dot{X}_1 = Z_0$. Z_0 is "characteristic impedance" of the filter.

$$Z_1 = \rho_0 c/S_1$$
$$m = S_1/S_2.$$

From Equation (10),

$$Z_0 = Z_1\sqrt{\frac{(m+1)\cos kl + (m-1)}{(m+1)\cos kl - (m-1)}}. \tag{11}$$

Eliminating Z_0/Z_1 from Equation (10),

$$\left.\begin{aligned} p_4 &= p_1\left[\frac{(m+1)^2 \cos 2kl - (m-1)^2}{4m}\right. \\ &\quad \left. -i\sqrt{\frac{(m+1)^4 \sin^2 2kl - 4(m^2-1)^2 \sin^2 kl}{16m^2}}\right] \\ \dot{X}_4 &= \dot{X}_1\left[\frac{(m+1)^2 \cos 2kl - (m-1)^2}{4m}\right. \\ &\quad \left. -i\sqrt{\frac{(m+1)^4 \sin^2 2kl - 4(m^2-1)^2 \sin^2 kl}{16m^2}}\right] \end{aligned}\right\}. \tag{12}$$

The two terms in each of the above expressions bear a simple relation to each other. If the first term is denoted by cos Y, then the second term will be sin Y. Thus,

$$\sin Y = \sqrt{\frac{(m+1)^4}{4m^2}\sin^2 kl\left[\cos^2 kl - \left(\frac{m-1}{m+1}\right)^2\right]}, \tag{13}$$

and

$$\left.\begin{aligned} p_4 &= p_1(\cos Y - i \sin Y) = p_1 e^{-iY} \\ \dot{X}_4 &= \dot{X}_1(\cos Y - i \sin Y) = \dot{X}_1 e^{-iY} \end{aligned}\right\}. \tag{14}$$

An examination of Equation (13) shows that sin Y, hence Y, may be real or imaginary. Let $Y = a + ib$, where a and b are real, and represent phase angle and attenuation factor respectively. Then

$$\sin Y = \sin a \cosh b + i \cos a \sinh b. \tag{15}$$

Equations (13) to (15) determine the characteristics of the filter. Consider briefly the following three cases:

(1) $$\text{Cos}^2 kl > \left(\frac{m-1}{m+1}\right)^2.$$

Sin Y is real, and Y is real. Hence $b = 0$, and sin $Y = \sin a$.

(2) $$\text{Cos}^2 kl < \left(\frac{m-1}{m+1}\right)^2.$$

Sin Y is imaginary. Hence sin $a = 0$, and sin $Y = i \sinh b$, from which $Y = ib$. Then from Equation (13)

$$\sinh b = \sqrt{\frac{(m+1)^4}{4m^2} \sin^2 kl \left[\left(\frac{m-1}{m+1}\right)^2 - \cos^2 kl\right]}. \tag{16}$$

For attenuation, the negative value of b must be chosen.

(3) $$\text{Cos}^2 kl = \left(\frac{m-1}{m+1}\right)^2, \text{ or } \sin kl = 0.$$

Sin $Y = 0$, and sin $a = 0$, $b = 0$.

Fig. 2 shows the manner in which the terms of the expression for sin Y vary with kl, hence frequency. The characteristics of the filter may be studied with reference to this, and Equation (14). As the frequency increases from zero to the first frequency for which $\cos^2 kl = \left(\frac{m-1}{m+1}\right)^2$, the attenuation factor remains zero, and the phase angle a increases from 0 to π. This is the first transmission band. At frequencies for which $+\left(\frac{m-1}{m+1}\right) > \cos kl > -\left(\frac{m-1}{m+1}\right)$, there is attenuation, and a remains constant at π. The attenuation factor b is determined from Equation (16). In the second transmission band, attenuation is again zero, and the phase angle a increases from π at the lower frequency limit, to 2π at the center, for which sin $kl = 0$, to 3π at the high frequency limit of the band.

It is seen that there will be an infinite series of successive transmission and attenuation bands. The band widths are determined by the value of m, and

the cutoff frequencies by the expression $\cos^2 kl = \left(\frac{m-1}{m+1}\right)^2$. Maximum attenuation occurs at $\cos^2 kl = 0$. It will be noted that

$$\frac{m-1}{m+1} = -\left(\frac{g-1}{g+1}\right), \text{ where } g = 1/m.$$

Hence the filters of Fig. 1, (*a*), and 1, (*b*), will have the same characteristics, except for the characteristic impedance Z_0, Equation (11).

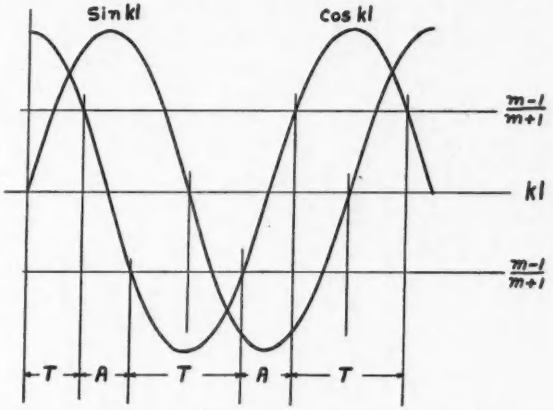

FIG. 2. *Graphical representation of filter characteristics. T, transmission bands; A, attenuation bands.*

Characteristic Impedance

The value of Z_0 may be investigated in the same fashion as the transmission characteristics. Rearranging terms in Equation (11),

$$Z_0 = Z_1 \sqrt{\frac{\cos kl + \left(\frac{m-1}{m+1}\right)}{\cos kl - \left(\frac{m-1}{m+1}\right)}}. \tag{17}$$

In the transmission bands, $\cos^2 kl > \left(\frac{m-1}{m+1}\right)^2$, Z_0 is real, a pure resistance, and therefore positive. Hence the positive root must be taken. In the attenuation bands, Z_0 is a pure reactance, and may be positive or negative. At zero frequency, $\cos kl = 1$, and

$$Z_0 = \sqrt{m}\, Z_1. \tag{18}$$

At cutoff frequencies, $\cos^2 kl = \left(\frac{m-1}{m+1}\right)^2$. Therefore, if $m < 1$, Fig. 1, (*a*),

$\left(\frac{m-1}{m+1}\right)$ is negative, and $Z_0 = 0$ at the first cutoff frequency, and increases to infinity at the upper limit of the attenuation band. On the other hand, if $m > 1$, Fig. 1, (*b*), $\left(\frac{m-1}{m+1}\right)$ is positive, and the zeros and infinities of Z_0 are interchanged. Hence Z_0 can be traced through successive transmission and attenuation bands. The two cases are shown graphically in Fig. 3 for the actual

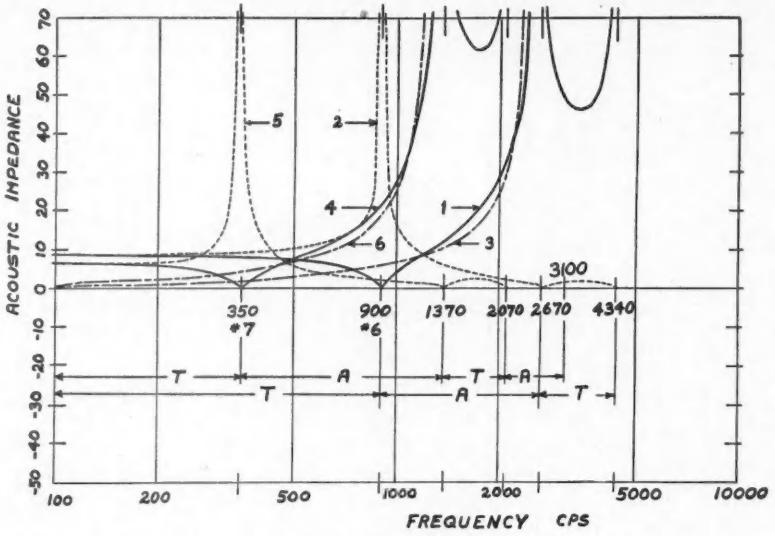

FIG. 3. *Impedance curves. T, transmission; A, attenuation.*
1. *Characteristic impedance Z_0, filter #6a, $m < 1$.*
2. *Characteristic impedance Z_0, filter #6b, $m > 1$.*
3. *Output coupling impedance Z_{02}, filters #6a and #6b, $l_2 = 3.3$ cm., $Z = \rho_0 c/S = 9.3$.*
4. *Characteristic impedance Z_0, filter #7a, $m < 1$.*
5. *Characteristic impedance Z_0, filter #7b, $m > 1$.*
6. *Output coupling impedance Z_{02}, filters #7a and #7b, $l_2 = 6.7$ cm., $Z = \rho_0 c/S = 9.3$.*

filters used in the measurements. The reactances are shown positive. In electrical filter theory, the section under examination may lie between successive "mid-series" or "mid-shunt" points in the infinite line on which the theory is based. The acoustic equivalents lie between successive "mid-contraction" or "mid-expansion" points in the infinite acoustic line. In both systems, the frequencies of infinite impedance for one section are frequencies of zero impedance for the other, and vice versa.

Impedance Matching

The preceding theory applies to an infinite series of filter sections; i.e., each section is perfectly terminated. In the practical filter, with a finite number of

sections, the ends must be terminated in devices with impedances equal to Z_0. As with electrical filters, exact impedance matching can be achieved only at certain frequencies. In electrical filters, the usual procedure is to terminate the filter in a pure resistance, equal to the characteristic impedance in the transmission band. In the present case, this could be achieved by terminating the filter in an infinite conduit, of cross section S, such that $\rho_0 c/S$ is equal to Z_0 in the transmission band. In practice, however, terminating elements of finite dimensions must be used. Since the application of the present development was simply to attenuate noise, a simple system was desirable. Hence, the effect of terminating the filter in short conduits was investigated.

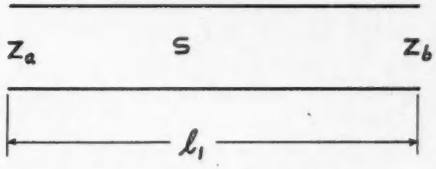

FIG. 4. *Filter terminating conduit.*

Consider a short conduit of length l_1, and cross section S, Fig. 4. The impedance Z_a at the input end can be expressed in terms of Z_b at the output end. Thus

$$Z_a = Z\left[\frac{Z_b + iZ \tan kl_1}{Z + iZ_b \tan kl_1}\right], \tag{19}$$

where $Z = \rho_0 c/S$. Note that if $Z_b = Z$, then $Z_a = Z$ also. The sections comprising the filter are inserted between two conduits, Fig. 5, of lengths l_1 and l_2 and of cross section S, such that $Z = Z_0$ approximately, for the first transmission band. If the output conduit opens into free space, the impedance will be

$$Z_{b2} = \frac{\rho_0 \omega k}{2\pi} + \frac{i\rho_0 \omega}{C_0}, \tag{20}$$

where C_0 is the conductivity of the orifice. The first term represents radiation resistance, and will be small for wave lengths large compared to the dimensions

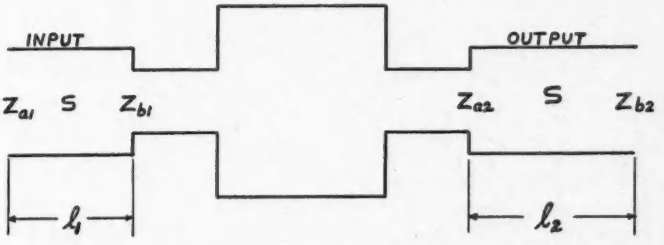

FIG. 5. *Single filter section with terminating conduits.*

of the filter sections. The second term is the inertance of the air in and around the opening, and at low frequencies this will also be small compared to Z. Therefore, as a first approximation, let $Z_{b2} = 0$. Then from Equation (19),

$$Z_{a2} = iZ \tan kl_2. \tag{21}$$

If now $Z_{a2} = Z_0$, then $Z_{b1} = Z_0 = iZ \tan kl_2$.
Substituting Z_{b1} into Equation (19),

$$Z_{a1} = iZ \tan k(l_1 + l_2) . \tag{22}$$

This equation also gives the impedance Z_a at the input end of a simple conduit of length $(l_1 + l_2)$, assuming $Z_b = 0$ as before. From these considerations, it may be concluded that the filter system, with terminal conduits of length l_1 and l_2 should be as closely matched to free space as a simple conduit of length $(l_1 + l_2)$, and that comparison with such a simple conduit ought to provide a useful measure of filter performance. It appears that the value of l_1 is not critical for such a comparison.

A comparison of Equations (19) and (21) shows that in the first attenuation region, the curve for Z_{a2} versus frequency can be made to coincide closely with the curve for Z_0, for the case of the filter section of Fig. 1, (*a*), by a suitable choice of l_2. For the filter section of Fig. 1, (*b*), the curves for Z_{a2} and Z_0 intersect near the center of the attenuation band. Hence, in this region, it ought to be possible to obtain impedance matching. The curves of Z_{a2} for the terminal conduits used here are included in Fig. 3.

To connect two filters of different characteristics in series, a coupling conduit may be required. If the filters have the same cross sections, they will have the same characteristic impedance over a large part of the first transmission band, and therefore they may well be connected directly.

Experimental Method

A method of measuring filter characteristics has already been suggested in the theory. The experimental arrangement is shown in Fig. 6. Readings of

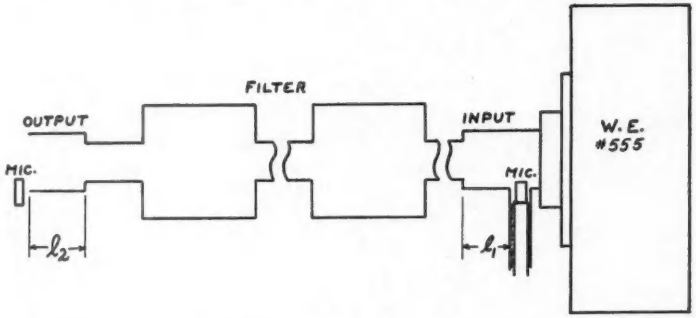

FIG. 6. *Experimental arrangement. Sound source, Western Electric #555 receiver.*

input and output sound levels were taken with the filter terminated in conduits of length l_1 and l_2, and with the filter replaced by a simple conduit of length $(l_1 + l_2)$. The difference in attenuation in the two cases is the attenuation due to the filter.

Experimental Results

Measurements have been carried out on several filters, of both circular and rectangular cross section. Two triple section filters, made up of cylindrical brass

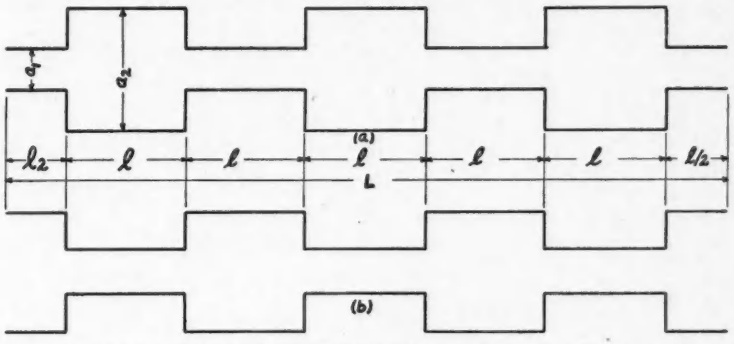

Filter	l, cm.	L, cm.	a_1, cm.	a_2, cm.	$m - 1/m + 1$	$Z = \rho_0 c/S$
#6*a*	5.0	30.0	1.65	3.8	−0.685	19.9
#7*a*	10.0	60.0	1.65	5.0	−0.805	19.9
#6*b*	5.0	30.0	3.8	1.65	+0.685	3.70
#7*b*	10.0	60.0	5.0	1.65	+0.805	2.14

FIG. 7. *Triple section filter.* (*a*) $m < 1$. (*b*) $m > 1$.

tubing, and designated #6*a*, #6*b*, and #7*a*, #7*b*, are shown in Fig. 7. If $b = -\beta$, then the attenuation characteristic of a three section filter is given by

$$P_{out} = P_{in} e^{-3\beta}, \tag{23}$$

where, of course, β varies with frequency, Equation (16), and is a maximum at the center of the attenuation band. The terminal conduits are made of tubing 2.4 cm. in diameter, for which $Z = \rho_0 c/S = 9.3$ acoustic ohms. Curves for the characteristic impedance Z_0 are shown in Fig. 3. Also shown are the output conduit impedances Z_{a2}. The theoretical frequency limits of the attenuation bands of each filter are indicated. The lengths of output conduit corresponding to the impedance curves of Fig. 3 are 3.3 cm. and 6.7 cm. for filters #6 and #7 respectively. Measurements were carried out using several lengths of output conduit, and the above values were found to be optimum. The attenuation curves obtained are shown in Figs. 8 and 9. The two filters were also connected in series, with #7 at the input end. The attenuation curve is shown in Fig. 10.

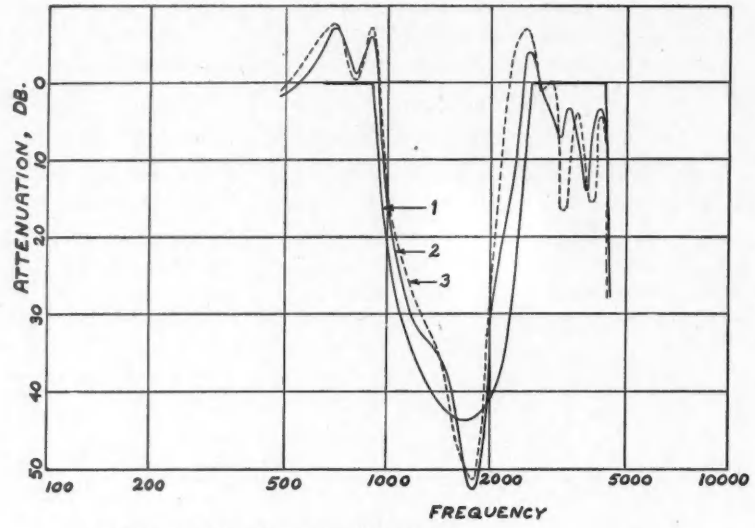

FIG. 8. *Attenuation, filters #6a and #6b.*
1. *Theoretical attenuation.*
2. *Experimental attenuation,* $l_1 = 3.3$ *cm.,* $l_2 = 1.5$ *cm.*
3. *Experimental attenuation,* $l_1 = 3.3$ *cm.,* $l_2 = 3.3$ *cm.*

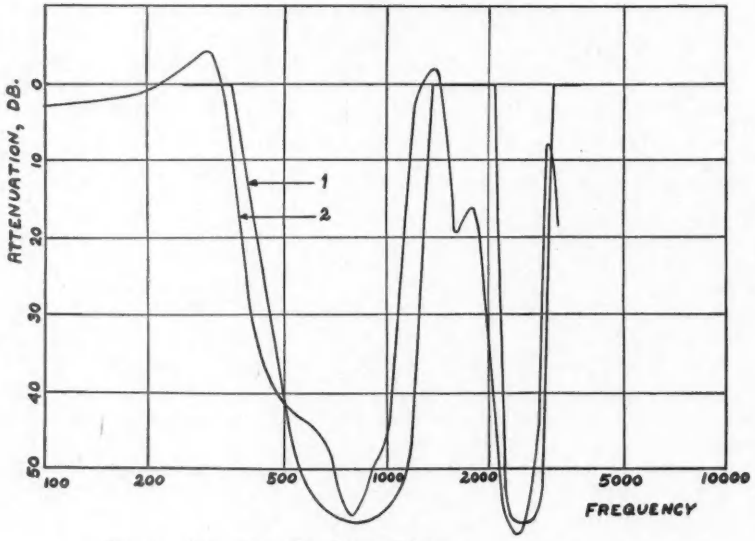

FIG. 9. *Attenuation, filters #7a and #7b.*
1. *Theoretical attenuation.*
2. *Experimental attenuation,* $l_1 = 6.7$ *cm.,* $l_2 = 6.7$ *cm.*

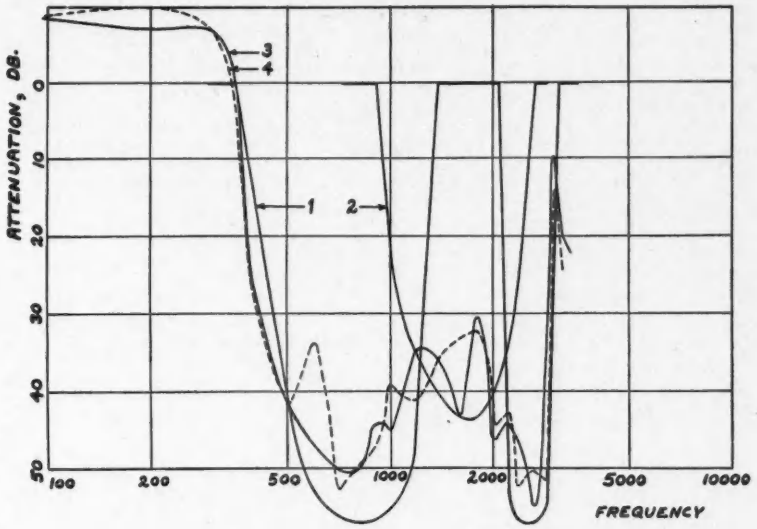

FIG. 10. *Attenuation, filters #6a and #7a, #6b and #7b in series, #7 at input end.*
1. *Theoretical attenuation, #7a, #7b.*
2. *Theoretical attenuation, #6a, #6b.*
3. *Experimental attenuation,* $l_1 = 6.7$ *cm.,* $l_2 = 1.5$ *cm.*
4. *Experimental attenuation,* $l_1 = 6.7$ *cm.,* $l_2 = 3.3$ *cm.*

Attenuation measurements were carried out on a series of filters of rectangular cross section, made up of both types of section shown in Fig. 1, and, as before, agreement with theory was satisfactory. In these filters, the expansions and contractions were confined to only one transverse dimension, the other remaining constant over the entire length of the filter.

Conclusions

It may be concluded from experimental measurements on filters designed according to the preceding theory that, up to frequencies to which measurements were carried, agreement with theory was satisfactory.

The filters of rectangular cross section are particularly suitable for the construction of a filter unit of large cross section, since the two types of section can be placed side by side, with a single partition forming one boundary of both.

Acknowledgment

The writer wishes to thank Mr. T. D. Northwood for his suggestions and constructive criticism of the results of this investigation.

References

1. MASON, W. P. Bell System Tech. J. 6: 258. 1927.
2. MASON, W. P. Electromechanical transducers and wave filters, 2nd ed. D. Van Nostrand Company, Inc., New York. 1948.
3. STEWART, G. W. Phys. Rev. 20: 528. 1922.
4. STEWART, G. W. and LINDSAY, R. B. Acoustics. D. Van Nostrand Company, Inc., New York. 1930.

ON THE FLOW OF GASES AND WATER VAPOR THROUGH WOOD[1]

By P. M. Pfalzner

Abstract

The quantities of water vapor passing through wood have been measured under the conditions of hydrodynamic flow and of kinetic diffusion. Air and oxygen pass through wood under hydrodynamic flow conditions in accordance with the Knudsen–Poiseuille law. Water vapor passes through wood under hydrodynamic flow conditions in much larger quantities than those predicted by the law. The rate of passage of water vapor under diffusion conditions follows the Fick diffusion law but with a diffusion coefficient that increases with relative humidity. The distinct features of the diffusion and hydrodynamic flow processes are pointed out. Porous, hygroscopic media permit the transfer of water vapor either by diffusion or by hydrodynamic flow, as determined by two distinct sets of conditions, while compact, hygroscopic media permit the transfer of water vapor by diffusion only, regardless of the external conditions.

1. Introduction

In recent years it has become increasingly evident that the movement of water vapor through hygroscopic media is a complex phenomenon. Water vapor can move through such media more readily than can permanent gases such as oxygen, nitrogen, or even hydrogen. Any simple theory of the mechanism by which the passage of gases and vapors takes place leads one to expect that small and light molecules will penetrate a porous body more easily than large and heavy molecules. The ease of penetration of porous hygroscopic media by water vapor points to some special mechanism facilitating the movement of water molecules. This mechanism must be sought in the fact that water vapor and other vapors are strongly sorbed by porous, hygroscopic bodies while the permanent gases are sorbed in negligible quantities only.

Several mechanisms by which water molecules might be enabled to move more readily through porous, hygroscopic media have been suggested by a number of investigators. So far these have answered the problem in a qualitative way only; the precise laws governing the movement of water vapor through porous bodies remain to be formulated.

The simplest considerations suggest at least three mechanisms by a combination of which water vapor may move through a hygroscopic medium:
(1) Since water vapor is a gas (close to its condensation point) it should pass through porous bodies in the same manner in which permanent gases do. The laws of kinetic diffusion of gases through porous interfaces have been well established; knowing the coefficient of diffusion for one permanent gas, one readily calculates the coefficients for other gases and, in particular, that for water vapor. Likewise, there exists a semi-empirical law of Knudsen–Poiseuille for the hydrodynamic or pressure flow of gases through porous bodies; again,

[1] *Manuscript received January 20, 1950.*
Contribution from the Division of Physics, National Research Laboratories, Ottawa, Canada. Issued as N.R.C. No. 2158.

one may calculate the coefficients for the flow of water vapor from the coefficients found for a permanent gas. In this way, one obtains the amount of water vapor that would be transported through a medium either by kinetic diffusion or by hydrodynamic flow, on the assumption that water vapor behaves—at least in part—as any other permanent gas. As pointed out already, this calculated amount is much less than the actually observed transfer of water vapor, and hence, to account for this excess transfer, there must exist additional mechanisms based on the hygroscopicity of the medium.

(2) Water vapor can move through a porous body by capillary action. If the capillaries become filled, the water will tend to rise in accordance with well known laws. Water is certainly drawn into porous bodies in this way, but in general such movement is confined to conditions in which the moisture content of the medium is quite close to the saturation value. It is known from experimental evidence, however, that an excess transfer of water vapor takes place even at the very lowest moisture contents, and hence capillary action cannot wholly explain the observed facts.

(3) Evidence from a variety of experiments has indicated that adsorbed water molecules are not static but are free to move over the surface of the adsorbing medium. This suggests that water vapor may move through the medium as an adsorbed layer on the internal surfaces. It is this mechanism that presents the greatest interest to research.

The experiments to be described below are a first attempt at separating the contributions of mechanisms (1) and (3) to the vapor flow. In these experiments, the transfer of gases has been studied under hydrodynamic flow conditions rather than diffusion. Diffusion experiments with permanent gases present considerable difficulties while hydrodynamic flow measurements are relatively simple.

It should be pointed out here that there exists a good deal of confusion in the literature in the use of the term "diffusion" (which is often applied where the term "hydrodynamic flow" is more appropriate). The term "hydrodynamic flow" is here used to describe fluid flow under a pressure head, while the term "diffusion" of gases should be restricted to describe the exchange of gases from opposite sides of a barrier (real or imaginary) or a porous interface, where there is a partial pressure gradient but where the total pressure on both sides remains constant throughout. Such exchange of gases will occur, for instance, in the walls of a building where the total pressure is atmospheric both inside and outside but where there is a difference in water vapor pressure between the exterior and interior of the walls. The water vapor will accordingly diffuse through the wall until equilibrium is established. At first sight, it would appear that such a process should obey the same laws as hydrodynamic flow, since it is known from kinetic gas theory that within certain limits in a mixture of gases each gas behaves as if it alone were present. Consequently, one might expect that the presence of air on both sides of an interface ought not to influence the movement of water vapor across this interface. This is not so, however. Not

only does there also take place a counter movement of an air mass equal to the mass of the diffusing vapor, but the vapor also has to diffuse through the air towards and away from the interface. The counter movement of air will be very small since the mass of water vapor in the air at normal temperatures is quite small—at 20°C., 100% relative humidity, the absolute humidity is 17.5 gm. of water vapor per cubic meter of air, or the mole fraction of water vapor is 0.0218. Such a counter movement of the air, however, does not take place when the vapor diffuses from one side of an interface to the other and condenses there. No air will then flow in a direction opposite to that of the vapor flow since the condensing vapor does not increase the total pressure.

The fundamental law of diffusion of two gases is, according to Stefan (16),

$$\rho_1 u_1 = -\frac{k_1 k_2}{CP}\frac{d\rho_1}{dx} \tag{1}$$

and

$$\rho_2 u_2 = -\frac{k_1 k_2}{CP}\frac{d\rho_2}{dx} \tag{2}$$

where ρ = density of the gas

u = velocity of the gas

$k = \frac{RT}{M}$ = a constant for any given temperature and gas

P = total pressure

$= p_1 + p_2$

p = partial pressure

C = coefficient of resistance.

The subscripts refer to the two diffusing gases.

If only one gas is diffusing, the equation governing this movement is

$$\rho_1 u_1 = -\frac{k_1 k_2}{C(P - p_1)}\frac{d\rho_1}{dx}. \tag{3}$$

The hydrodynamic flow of a gas through a circular tube is given by Poiseuille's law

$$Gp = K(p_1 - p_2)\frac{p_1 + p_2}{2}, \tag{4}$$

where G = volume of gas flowing in unit time,

$K = \frac{\pi r^4}{8\eta d}$ = the Poiseuille constant for a circular tube, of radius r, length d, and gas of viscosity η

p_1 and p_2 = the pressures at the two ends of the tube, and

p = pressure at which the volume G is measured.

In the experiments described below, the procedure was:

(*a*) To measure the flow of a permanent gas through a porous body,

(*b*) To calculate the flow to be expected for water vapor under the same conditions,

(*c*) To measure the flow of water vapor and compare with the calculated value as obtained from (*b*).

As a simple concept, it is then assumed that any excess of observed over calculated amount of water vapor flow is due to either or both of the mechanisms (2) and (3) described above.

In addition to the hydrodynamic flow measurements with both water vapor and permanent gases (oxygen and air were used), diffusion experiments were also made with water vapor only. These will illustrate the difference between hydrodynamic flow and diffusion of water vapor.

The hygroscopic medium chosen for these experiments was wood. This was done for a number of practical reasons. Wood has a fairly uniform pore structure with capillaries ranging from coarse to very fine (14). It adsorbs water vapor strongly but does not sorb air or oxygen to any extent. Much work has already been done by various investigators on the diffusion of water vapor through wood and charcoal but not on the hydrodynamic flow of water vapor.

2. Experiments with Hydrodynamic Flow of Air, Oxygen, and Water Vapor

(*a*) *Apparatus*

The apparatus was designed to permit observations to be made at constant pressures so that a stationary concentration gradient would be maintained throughout the disk of wood. As shown in Fig. 1, there are two absolute mercury manometers M_1 and M_2 with attached movable mercury reservoirs R_1 and R_2 on each side of the cell A in which the disk is clamped. In the figure, gas flow takes place from M_2, the high pressure or inflow side, towards M_1 the low pressure or outflow side, either upwards or downwards through the disk, as determined by the position of the threeway stopcocks G, G. The mercury level in M_2 is held just below the tungsten contact F; whenever the pressure falls owing to the flow of gas across the disk, contact is made at F and a relay closes a circuit which causes gas to be generated electrolytically in the bulb B_2 filled with water containing a little sulphuric acid. The pressure increase in B_2 causes the mercury column in the burette D_2 to rise until an amount equal to the volume of gas flowing through the disk has been displaced, and the circuit is once more opened at F. The rise of the mercury column in D_2, measured with a cathetometer, serves as a measure of the rate of flow of gas across the disk. At the low pressure side a similar relay is actuated by the tungsten contact S sealed into manometer M_1 and starts a pump acting on the bulb B_1 which causes the mercury in D_1 to fall. As soon as the contact S opens, the pump stops and air is permitted to leak back through the tap H into the bulb B_1. This ensures continual opening and closing of the circuit. The pull of the pump may be suitably throttled by adjusting taps H and J. At the lowest

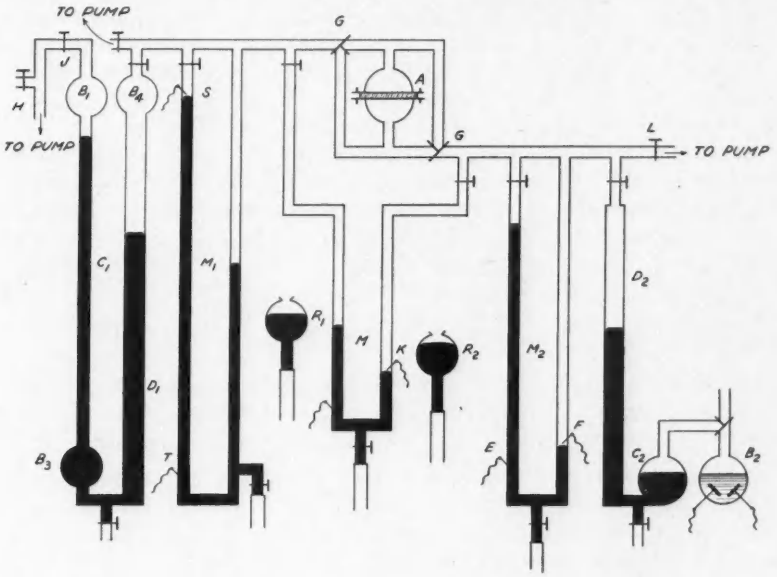

FIG. 1. *Schematic drawing of apparatus for measuring the flow of gases through wood.*

pressures, when the flow takes place into vacuum, the pump can be switched to act directly on the outflow side of the disk.

A differential manometer M was added during the course of the experiments to obtain direct readings of the pressure difference maintained across the disk. It was then unnecessary to read manometer M_1, as the absolute pressure was read on M_2 and the pressure head on M; the latter carried the tungsten contacts controlling the manostat pump. The same pressure head could be obtained accurately at all mean pressures as long as the amount of mercury in M was kept unchanged.

The disk of wood was sealed at its edge with several coats of varnish and beeswax, the latter applied while the disk was clamped in position with the apparatus under vacuum. The metal flanges holding the disk were faced with rubber washers and sealed to the glass tubing with de Khotinsky wax.

(*b*) *Method of Taking Readings*

The apparatus was exhausted with a mercury diffusion pump and tested for leaks. Gas was admitted through L until the desired pressure was obtained at M_1. The stopcocks G were then adjusted for upward or downward flow, and additional gas was admitted until the desired pressure head was reached. The mercury levels in M_1 and M_2 were adjusted so as to be just below the contacts

S and F respectively. (After the manometer M had been installed, the pressure was increased by adding more gas until the mercury in M was just below the contact K.) No measurements were taken during the first minutes of flow, in order to permit establishment of a stationary pressure gradient inside the wood. The time was then measured for a volume of from 30 to 50 cc. of gas to pass through the disk as indicated by the rise of the mercury column in the calibrated burette D_2, the volume readings being taken with a cathetometer, the time with a stopwatch. The room temperature, which did not vary more than 1°C. during any one setting of the pressure head and mean pressure, and not more than 2°C. over a complete set of measurements for one gas, was read at the beginning and end of each observation. (See Appendix II for effect of temperature changes.) For each mean pressure two readings were taken, the first with the flow upwards through the disk, the second downwards.

Both the air and the oxygen were dried over magnesium perchlorate before being admitted into the apparatus. The oxygen was taken from a pressure tank of the Dominion Oxygen Co.

The same circular disk of wood was used throughout the experiment. It was a piece of spruce wood cut from a radial section, i.e., the flow took place in a direction tangential to the yearly rings. Size and other characteristics as determined by methods described in Appendix I were as follows:

Thickness of disk at 0% humidity	0.629 cm.
Diameter of disk	3.39 cm.
Area of disk available for flow	9.02 sq. cm.
Void fraction when dry, W_0	0.78 cc. per cc.
Dry bulk density, ρ_D	0.33 gm. per cc.
Density of wood substance, ρ	1.48 gm. per cc.

(*c*) *Theory*

(1) *The Streamline Flow of Gases Through a Single Capillary*

Poiseuille's law is, as stated above,

$$Gp = K(p_1 - p_2)\frac{p_1 + p_2}{2}, \tag{4}$$

with the symbols defined as before.

(2) *The Flow of Rarefied Gases*

At pressures where the mean free path of the gas molecules is of the same order of magnitude, or larger, than the diameter of the capillary, the flow no longer obeys Poiseuille's law. At these pressures the flow becomes much larger than that law indicates. Knudsen (10), on the basis of kinetic theory and with the added assumption that a gas molecule may be reflected in any direction from the wall of a capillary regardless of the angle of incidence, developed an equation of the form

$$Gp = b(p_1 - p_2), \tag{5}$$

where $b = 4/3\sqrt{2\pi}\sqrt{\frac{RT}{M}}\frac{r^3}{d}$,

R = gas constant,
T = absolute temperature,
M = molecular weight of gas,
r = radius of capillary,
d = length of capillary.

This equation has been shown to be valid at very low pressures (7), the volume flowing being inversely proportional to the square root of the molecular weight and directly proportional to the third power of the radius. The type of flow occurring under these low pressures has been termed "molecular flow" to distinguish it from Poiseuille or "streamline flow".

In the pressure region intermediate to molecular and Poiseuille flow, Knudsen combined Equations (4) and (5) with a variable factor γ obtaining

$$Gp = K\frac{p_1 + p_2}{2}(p_1 - p_2) + \gamma b(p_1 - p_2). \tag{6}$$

$$\text{Knudsen found that } \gamma = \frac{1 + C_1\bar{P}}{1 + C_2\bar{P}} \tag{7}$$

$$\text{where } C_1 = 2.00\sqrt{\frac{RT}{M}}\frac{r}{\eta},\ C_2 = 2.47\sqrt{\frac{RT}{M}}\frac{r}{\eta} \tag{8}$$

$\bar{P}$ = mean pressure.

Equation (6) is valid for a wide pressure range; at low pressures $\gamma \to 1$, and the first term in (6) becomes negligible, thus giving Knudsen's law of molecular flow, while at high pressures $\gamma \to \frac{C_1}{C_2}$, and the equation reduces to the Poiseuille law of streamline flow with an added constant. The curve of $\frac{Gp}{p_1 - p_2}$, the specific flow, against mean pressure $\frac{p_1 + p_2}{2}$ has a minimum at a pressure where the mean free path of the gas molecules is approximately five times the capillary radius.

It must be emphasized that Equation (6) takes no account of sorption, and in fact Knudsen's derivation assumes a uniform concentration of the gas molecules in any cross-section of the capillary.

(3) *The Flow of Gases Through Porous Systems*

When a gas flows through capillaries whose radii are of the order of magnitude of the mean free path of the gas molecules at normal pressures, the conditions are formally the same as for rarefied gases flowing through coarse capillaries as described under (2) above. While Knudsen developed his Equation (6) for rarefied gases, Adzumi (2) has shown that an equation of the same

form, with γ replaced by a constant, is applicable to gases flowing through a porous system. Any complex system of capillaries will be made up of capillaries of a wide range of radii, some so narrow as to fall in the region where molecular flow occurs at normal pressures, and others wide enough to permit streamline flow. On the basis of his experiments, Adzumi replaced γ by a constant = 0.9, and wrote the equation

$$Gp = \left(\frac{\pi}{8\eta} E\bar{P} + 0.9 \times 4/3 \times \sqrt{2\pi} \sqrt{\frac{\overline{RT}}{M}} F\right)(p_1 - p_2), \tag{9}$$

where E and F are functions of the radii and lengths of the capillaries. The form of these functions is, of course, unknown owing to the complex structure of most capillary systems. The values of E and F, however, may be obtained from a graph of specific flow $Gp/(p_1 - p_2)$ against mean pressure $\bar{P}$ which will be a straight line (if the equation correctly describes the flow) having a slope of $\pi E/8\eta$ and an intercept of $0.9 \times 4/3 \times \sqrt{2\pi} \sqrt{\frac{\overline{RT}}{M}} F$.

(4) *Comparison of Flow of Different Gases Through the Same Porous System*

If two gases of molecular weights M_1 and M_2, and viscosities η_1 and η_2 flow through the same capillary system under the same conditions, then from (9)

$$G_1 p = (A_1\bar{P} + B_1)(p_1 - p_2), \tag{10}$$

and

$$G_2 p = (A_2\bar{P} + B_2)(p_1 - p_2), \tag{11}$$

where

$$A = \frac{\pi E}{8\eta} \tag{12}$$

$$B = 0.9 \times 4/3 \times \sqrt{2\pi} \sqrt{\frac{\overline{RT}}{M}} F, \tag{13}$$

and hence

$$\frac{A_1}{A_2} = \frac{\eta_2}{\eta_1} \tag{14}$$

and

$$\frac{B_1}{B_2} = \sqrt{\frac{M_2}{M_1}}. \tag{15}$$

Thus if A and B are found for any one gas, the corresponding constants for any other gas may be computed from Equations (14) and (15).

(*d*) *Results for Hydrodynamic Flow of Air and Oxygen*

(1) *Air*

The volume of dry air flowing at mean pressures from 4.4 cm. to 80.0 cm. of mercury with a constant pressure head of 5.50 cm. of mercury was measured. In Fig. 2 values of the specific flow $Gp/(p_1 - p_2)$ are plotted against the mean pressure $(p_1 + p_2)/2$. The slopes and intercepts taken from the graph are given in Table I.

(2) *Oxygen*

The flow of oxygen was similarly measured, and the slope and intercept obtained from the graph for oxygen (Fig. 2) are also given in Table I, together

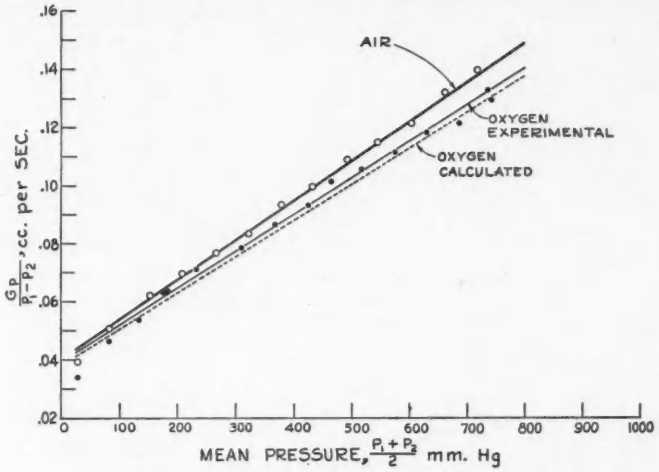

FIG. 2. *Flow rates of air and oxygen through wood at 20.8°C.*

with the values calculated from the measured air flow by use of Equations (14) and (15). The calculated and observed figures for oxygen flow based on air-flow data are within 3% of each other. Other investigators, such as Tomlinson and Flood (17), have recently confirmed that the Knudsen–Poiseuille equation accurately predicts the flow rates of permanent gases. They used a method similar to the one described here, except that their medium of flow was activated carbon. Taking the flow of nitrogen as basis, they found good agreement between calculated and observed flow rates of carbon dioxide and helium. For hydrogen they found a somewhat lower observed rate than that calculated from the equation.

The values for the viscosities and molecular weights of air, oxygen, and water vapor at 20.8°C. which were used in the calculations were calculated from values given in Landolt–Börnstein Tabellen (10). These figures are given in Table II, together with the viscosity of air containing water vapor corres-

TABLE I

HYDRODYNAMIC FLOW OF AIR AND OXYGEN

	A (slope)	*B* (intercept)
	Cc./sec./mm. Hg	Cc./sec.
Air	0.000139	0.0400
Oxygen	0.000126	0.0393
Oxygen (calc.)	0.000123	0.0380
% Difference	3%	3%

ponding to 75% relative humidity at 20.8°C., calculated from a relation for the viscosity of gas mixtures given by Adzumi (1).

TABLE II

VISCOSITY AND MOLECULAR WEIGHT OF AIR, OXYGEN, AND WATER VAPOR

	Viscosity $\times 10^4$ c.g.s. units	Molecular weight
Air (dry)	1.814	29
Air (75% R.H.)	1.806	29
Oxygen	2.054	32
Water vapor	0.949	18

(3) *Air at 75% R.H.*

The flow of air containing water vapor corresponding to 75% relative humidity at 20.8°C. was measured in order to discover whether the presence of water vapor in the air had any influence on the rate at which the air passed through the wood. The presence of water vapor has only a slight influence on the viscosity of the mixture. As seen from Table II, for air at 20.8°C., 75% R.H. the change is 0.45%. Hence, there should be no noticeable change in the measured air volume if water vapor behaves just like any permanent gas. However, owing to adsorption and swelling of the wood, changes in the flow rate might be expected.

In order to obtain 75% relative humidity, air was bubbled through saturated sodium chloride solution and circulated through the apparatus by means of a reciprocating pump, past wet and dry bulb thermometers sealed into the system, and back to the saturated salt solution. After the thermometers had been registering a steady relative humidity of 75% for several hours, the circulation was halted, and the flow through the wood was measured in the manner described above for air and oxygen. It was found that the flow was not measurably different from that at 0% humidity. Measurements with the same negative result were obtained after the wood had been exposed to the humid atmosphere for more than a week.

The reason—apart from the negligible change in viscosity as pointed out above—is that the volume of moisture contained in the air and in the wood under the conditions of the experiment is small. The absolute humidity at 75% R.H., 20.8°C. is 12.5 gm. per cu. m., or 0.0156 mole fraction H_2O in air; the moisture content of the wood at 20°C. is approximately 14% of the dry weight (9, p. 57), and for wood of a bulk density of 0.3 gm. per cc. there will be approximately 0.04 gm. of water content per cubic centimeter. Hence, if the density of the sorbed water is not less than that of free water (the opposite, higher density of the sorbed water than that of free water, has been found by various investigators, see Stamm, 15, p. 58), about 4% or less of the volume of the wood will be occupied by water, and the void fraction will be reduced

by this amount. A 4% reduction in the void fraction will not appreciably reduce the volume available for flow, especially since any condensation of the water will occur initially in the narrowest capillaries which do not contribute measurably to the flow.

(e) *The Hydrodynamic Flow of Water Vapor*

(1) *Method*

In order to measure the flow of water vapor through the wood a gravimetric method was adopted for the following reasons. The flow takes place at very low pressures (the saturation pressure of water vapor at 20°C. is 17.54 mm. of mercury) and the volume flowing is therefore very small. Hence, it is more convenient to measure the weight of water vapor passing through the disk. To obtain a given vapor pressure, a flask containing a suitable saturated salt solution (see Table IV) was sealed to the apparatus and kept in a water bath thermostatically controlled at 20°C. Distilled water was used to make up the saturated salt solutions, and distilled water alone was used to give the highest relative humidity, 100%, at 20°C. It must be realized, however, that the relative humidity at the disk of wood was at all times slightly lower than that given by the saturated salt solution at 20°C. since the temperature of the apparatus and wood was always slightly above 20°C. to avoid condensation of the water vapor. To ensure saturation of the salt solutions at all times, they were agitated by means of a magnetic stirrer. The air was exhausted from the apparatus. The flow then took place through the disk into vacuum maintained by continuous pumping. Between the pump and a Schwartz drying tube containing magnesium perchlorate which served to collect the outflowing water vapor, a calcium chloride drying tower was inserted to prevent moisture from the pump rising into the Schwartz tube. The vapor pressure was read directly on the mercury manometer M (Fig. 1) with a cathetometer. The Schwartz tube was taken down and weighed at intervals of about 20 hrs. The readings were repeated at the same vapor pressure at least four times, or longer, if necessary, until the change in weights recorded remained constant.

(2) *Results*

From the increase in weight of the Schwartz tube, the following values (Table III) were calculated: amount of water vapor passing through the disk in

(*a*) grams per hour, W_0,

(*b*) grams per hour per millimeter mercury pressure head, W_1,

(*c*) specific flow, $Gp/(p_1 - p_2)$.

In Fig. 3, the specific flow of water vapor as measured is plotted against the mean pressure. In addition, the curve predicted by the Knudsen–Poiseuille equation for gas flow has been calculated for water vapor from the air-flow

data and drawn on the same plot. The slope A and intercept B of this curve were calculated by use of Equations (14) and (15) and are

A = 0.000265 cc. per sec. per mm. mercury

B = 0.0507 cc. per sec.

TABLE III

HYDRODYNAMIC FLOW OF WATER VAPOR

$(p_1 - p_2)$ mm. Hg	$\frac{p_1 + p_2}{2}$ mm. Hg	(*a*) W_0 gm./hr. $\times 10^4$	(*b*) W_1 gm./hr./mm. Hg $\times 10^4$	(*c*) $Gp/(p_1 - p_2)$ cc./sec. $\times 10^2$
2.20	1.10	10.60	4.82	13.60
5.58	2.79	16.08	2.88	8.13
7.14	3.57	19.64	2.75	7.76
8.13	4.06	22.35	2.75	7.76
9.43	4.72	23.12	2.45	6.91
11.58	5.79	25.63	2.21	6.23
13.83	6.92	29.42	2.13	6.01
14.91	7.46	32.37	2.17	6.12
16.00	8.00	50.75	3.17	8.94
17.83	8.92	47.31	2.65	7.48

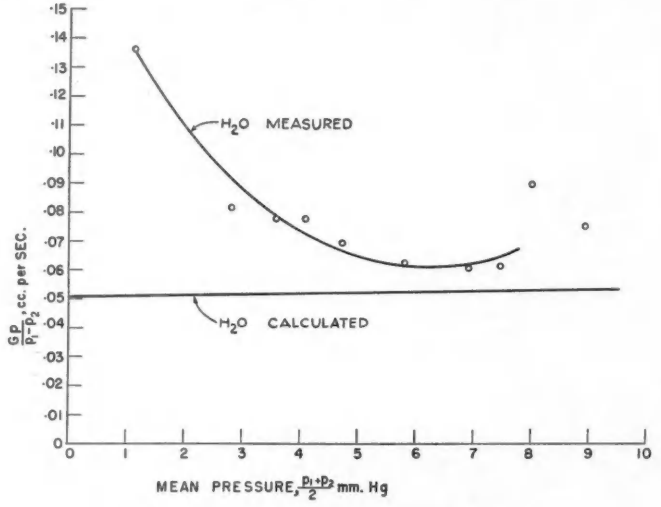

FIG. 3. *Flow rates of water vapor through wood at 20°C.*

It will be seen that the experimental curve is totally different from the calculated curve. At the lowest mean pressures, the observed value of the specific flow is almost three times that given by the Knudsen–Poiseuille equation. The specific flow decreases rapidly to a minimum at a mean pressure of about 6.5 mm. of mercury, and then rises once more as saturation pressure is

approached. The Knudsen–Poiseuille curve, which lies below the experimental values is, of course, a straight line. It must be noted that the experimental curve was obtained from the average flow rates over the range extending from zero pressure to that given by the saturated salt solutions, corrected for unit pressure difference (integrated flow rate). The Knudsen–Poiseuille curves for air and oxygen were obtained as average flow rates over a constant range of pressure difference for varying mean pressures, and were also corrected for unit pressure difference (differential flow rate). Since the Knudsen–Poiseuille curves are straight lines, a straight line should always be obtained for gases or vapors obeying the Knudsen–Poiseuille flow relation regardless of whether the integrated or differential flow rates are plotted. The differential flow rates for water vapor would yield a curve of a shape different from that of the integrated curve plotted in Fig. 3, but it would certainly not be a straight line. It probably has a more pronounced minimum than the curve drawn in Fig. 3.

Tomlinson and Flood (17) have measured the flow rates for the vapors diethyl ether and ethyl chloride through activated carbon rods. They found that the flow rates of these vapors, which are adsorbed, are considerably larger than the Knudsen–Poiseuille relation predicts, and their flow rates for diethyl ether show a minimum at low pressures similar to that obtained here for water vapor. The suggestion has been made by Tomlinson and Flood that the molecules in the adsorbed layer are mobile and that the excess flow is determined by the concentration gradient in the adsorbed layer. Owing to the S-shape of the adsorption isotherm of water vapor on wood, the concentration gradient for equal pressure differences will be large at very low pressures and near saturation and, hence, the flow will be large in these regions. The curve of Fig. 3, which is that of the integrated flow reduced to unit pressure difference, supports this view. If the differential curve had been obtained, the minimum would be more pronounced, as pointed out above.

According to Pollard and Present (12), the expression for the interdiffusion of two gases in long capillary tubes reduces to the Knudsen equation for mean free paths much greater than the capillary radius; according to these same investigators, the curve of specific flow against mean pressure will show a minimum at low pressures only if the flow takes place through uniform capillaries; in porous media, owing to the effect produced by the range of capillary radii, there will be no minimum. This seems to hold true for nonadsorbed gases such as oxygen and air investigated here, and hydrogen, helium, carbon dioxide, and nitrogen as measured by Tomlinson and Flood. It does not hold for water vapor as shown here, or diethyl ether as pointed out above.

3. Experiments on Diffusion of Water Vapour

(*a*) *Method*

In order to measure the rate of diffusion of water vapor through wood, a dry-cell method similar to that employed by Babbitt (3) in measuring the per-

meability of building papers was adopted. Circular disks of spruce wood of three different thicknesses (0.376, 0.624, and 1.276 cm.) with an area of 37 sq. cm. were sealed across the mouth of aluminum dishes containing calcium chloride. The wood was taken from the same board from which the disk used in the hydrodynamic flow measurements had been cut. The aluminum dishes were exposed to humid air in a constant humidity chamber kept at 91°F. (32.8°C.). This temperature, rather than 20°C. as in the hydrodynamic flow experiments, was chosen here because it was simpler to control thermostatically a closed chamber at a temperature above room temperature than below it. Salt solutions were used as before to establish constant relative humidities. These are given in Table IV for both 20°C. and 32.8°C.

TABLE IV

SATURATED SALT SOLUTIONS TO ESTABLISH DEFINITE WATER VAPOR PRESSURES

Salt	20°C.*		32.8°C.†	
	Vapor pressure, mm. Hg.	R.H. %	Vapor pressure, mm. Hg.	R.H. %
Na_2CO_3	16.0	91	—	–
KCl	14.9	85	32.8	88
NaCl	13.8	79	28.0	75
$NaNO_2$	11.6	66	—	–
$Ca(NO_3)_2$	9.4	54	—	–
K_2CO_3	8.1	46	—	–
$MgCl_2$	7.1	41	12.3	32
CH_3COOK	5.6	32	—	–
$ZnCl_2$	2.2	12.5	—	–

** The vapor pressures at 20°C. were measured directly on manometer M for each flow experiment and averaged, and the corresponding relative humidities calculated. These are not in every case identical with the ones given in Landolt–Börnstein Tables.*

† The vapor pressures at 32.8°C. were obtained by plotting data given by O'Brien (11). The corresponding relative humidities were calculated.

(*b*) *Theory*

The diffusion equation of Stefan has been given above. For only one gas diffusing, it is

$$\rho_1 u_1 = - \frac{k_1 k_2}{C(P - p_1)} \frac{d\rho_1}{dx}, \tag{3}$$

where the symbols have been defined previously. This equation can be integrated as follows: Substituting $k_1\rho_1 = p_1$, we obtain

$$u_1\rho_1 dx = - \frac{k_2}{C} \frac{dp_1}{(P - p_1)},$$

which gives, on integration with respect to x and p_1

$$u_1\rho_1 d = \frac{k_2}{C} \log (P - p_1) + A,$$

where d = thickness of the medium,
and A = a constant of integration.

Now for $p_1 = 0$, the condition is that $u_1 = 0$, hence

$$A = -\frac{k_2}{C} \log P$$

$$\therefore\ u_1 \rho_1 d = \frac{k_2}{C} \log \frac{P - p_1}{P};$$

now $u_1 \rho_1$ = velocity times density,

= mass flow per unit time per unit area of cross section,

$$= \frac{W}{At}$$

where W = mass flowing in time t across an area A;
i.e., the equation can be written

$$\frac{Wd}{At} = \frac{k_2}{C} \log \frac{P - p_1}{P} = \overline{D} \log \frac{P - p_1}{P}. \tag{16}$$

The common form of Fick's diffusion law is

$$\frac{Wd}{At} = D\Delta p,$$

where $\Delta p = p_1 - p_2$, the partial pressure gradient. (17)

If $p_2 = 0$ at all times, $\Delta p = p_1$,

i.e., $$\frac{Wd}{At} = Dp_1. \tag{18}$$

Equation (16) can be expanded into

$$\frac{Wd}{At} = -\frac{k_2}{C}\left[\frac{p_1}{P} + \frac{1}{2}\left(\frac{p_1}{P}\right)^2 - \frac{1}{3}\left(\frac{p_1}{P}\right)^3 + \frac{1}{4}\left(\frac{p_1}{P}\right)^4 - \ldots\right]$$

which is, on a first approximation,

$$\frac{Wd}{At} = -\frac{k_2}{C}\frac{p_1}{P}. \tag{19}$$

Hence D, the diffusion coefficient in (18), is equal to $-\frac{k_2}{CP}$ approximately,

while the value of the true diffusion coefficient is given by

$$\frac{Wd}{At} = \overline{D} \log \frac{P - p_1}{P}, \tag{16}$$

where $$\overline{D} = \frac{k_2}{C}. \tag{20}$$

(*c*) *Results*

The ratio $\frac{D}{d}$ in Equation (18) was calculated from the steady rate of increase in weight of the aluminum dishes. It is given in Table V in grams per 24 hr. per square meter per mm. of mercury and is plotted against mean relative humidity in Fig. 4. It is seen that the permeability increases rapidly with mean humidity and that it depends on the thickness of the medium. The permeability decreases steadily at decreasing humidity, as has also been shown by Babbitt (4) and King (6). The curve is again that of the integrated water vapor transfer, i.e., the mean rate of diffusion over the range of pressures extending from zero to

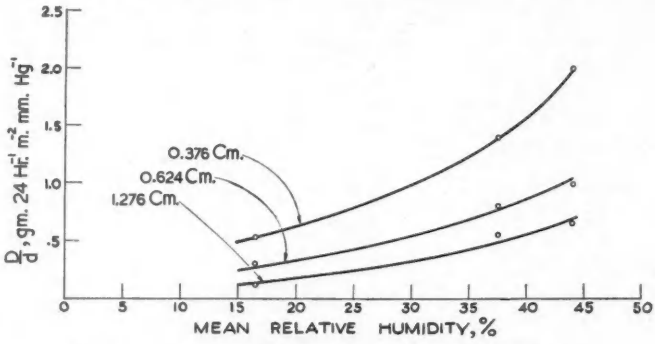

FIG. 4. *Diffusion rates of water vapor through wood at 32.8°C.*

that maintained in the constant humidity chamber. The coefficients are plotted against the mean relative humidity rather than the mean vapor pressure, since the moisture content is a function of the relative rather than absolute humidity and since media of the same moisture content rather than at the same mean vapor pressure are comparable with regard to permeability. The specific permeability or coefficient of diffusion, D, is also given in Table V,

TABLE V

DIFFUSION OF WATER VAPOR

p_1, mm. Hg.	Mean R.H., %	Thickness, cm.						D, av.
		0.376	0.624	1.276	0.376	0.624	1.276	
		$D/d = W/tAp_1$, gm./24 hr./sq. m./mm. Hg.			$D = \frac{Wd}{tAp_1}$, gm. cm./24 hr./sq. m./mm.Hg.			
12.3	16.5	0.53	0.31	0.13	0.20	0.20	0.17	0.19
28.0	37.5	1.39	0.80	0.55	0.52	0.50	0.70	0.57
32.8	44.0	1.98	0.98	0.64	0.74	0.61	0.81	0.72

and it will be noted that for the same humidity this value is independent of the thickness of the medium, within the experimental errors.

The true coefficient of diffusion, $\bar{D}$, has been calculated in Table VI and is plotted against mean relative humidity in Fig. 5. The ratio $\bar{D}/D$ is given in

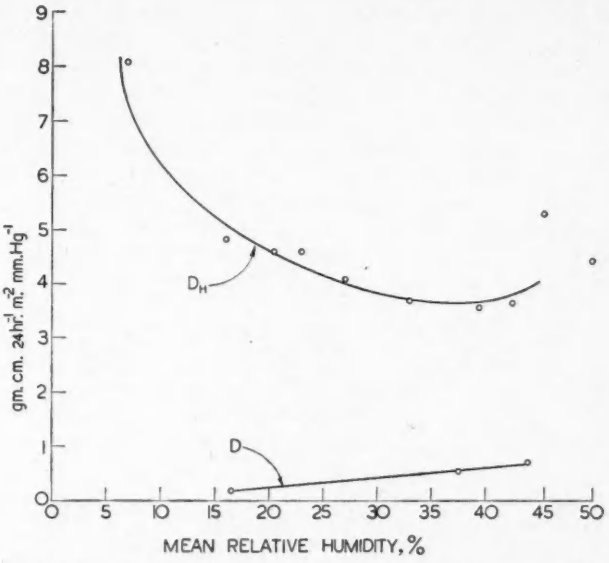

FIG. 5. *Diffusion rates of water vapor through wood. D_H from hydrodynamic flow; D from diffusion.*

the table; it is seen to be nearly constant and has an average value of 75.6; this should follow also from the fact that $\bar{D} = k_2/C$ while $D = k_2/CP$ approximately, and $P = 76.0$ cm. of mercury. The approximation made in Equation (19) is seen to be justified, i.e., Equation (18) may be used to calculate relative values of the diffusion coefficients.

It is not possible to obtain a value corresponding to $\bar{D}$ from hydrodynamic flow experiments since there is no equivalent for P, the total pressure. It is

TABLE VI

THE DIFFUSION COEFFICIENT $\bar{D}$ FOR WATER VAPOR

p_1 mm. Hg.	mean R.H. %	$P - p_1$ mm. Hg.	$\bar{D} = \frac{Wd}{ta} \Big/ \log \frac{P - p_1}{P}$	$\bar{D}/D$
12.3	16.5	747.7	14.5	76.3
28.0	37.5	732.0	42.6	74.7
32.8	44.0	727.8	54.5	75.7

possible, however, to calculate a value which is here called D_H corresponding to D from these data. This has been done in Table VII where D_H has been calculated from the W_1 values of Table III. In Fig. 5 the average value of D from diffusion experiments (Table V) has been plotted against mean relative humidity together with the values of D_H from hydrodynamic flow experiments (Table VII). The two curves, both of which represent integrated vapor transfer, are entirely different. Quantitatively, the D_H values are about 10 times as large as the D values. D gradually approaches zero at low humidities while D_H passes through a minimum and then rises sharply. Thus besides the quantitative differences there are outstanding qualitative ones. The absence of air probably facilitates the passage of vapor through the medium and this may partly account for the quantitative difference, but there must be additional mechanisms at work to account for the qualitative phenomenon of increased transfer of vapor under hydrodynamic flow conditions at low humidities as compared to the gradual approach to zero transfer under diffusion conditions.

TABLE VII

THE DIFFUSION COEFFICIENT D_H FOR WATER VAPOR FROM HYDRODYNAMIC FLOW MEASUREMENTS

$p_1 - p_2$, mm. Hg.	Corresponding mean R.H., %	$D_H = \frac{W_1 d}{A} \times 24 \times 10^4$ gm. cm./24 hr./sq. m./mm. Hg
2.20	6.8	8.08
5.58	16	4.83
7.14	20.5	4.62
8.13	23	4.62
9.43	27	4.10
11.58	33	3.70
13.83	39.5	3.57
14.91	42.5	3.63
16.00	45.5	5.31
17.83	50	4.44

King (6) has measured the diffusion of water vapor through horn keratin and obtains a curve showing the variation of the integrated mass transfer with relative humidity. His curves and those of Fig. 4 (which represent the integrated mass transfer of water vapor through the wooden disks of varying thicknesses plotted against mean relative humidity) have the same shape when reduced to the same conditions. King's original curves represent values which have not been reduced to unit vapor pressure difference, and his abscissae are the relative humidities on the high pressure side in place of the mean relative humidity of the medium. Recalculating King's figures, it is found that his values of D range from 0.03 at about 30% mean R.H. to 0.45 gm. cm. per 24 hr. per sq. m. per mm. of mercury at about 45% mean R.H. This compares with our values from about 0.40 at 30% mean R.H. to 0.72 gm. cm. per 24 hr. per sq. m. per mm. of mercury at about 44% mean R.H.; it is seen that our values are higher throughout but do not rise as sharply as King's at higher humidities.

It follows that the diffusion coefficient for keratin changes more rapidly than that for wood as the humidity approaches saturation.

It is interesting to note the conditions of King's experiment. He excluded all air from both sides of a thin (5×10^{-3} cm.) keratin membrane and kept one side at zero pressure while the other was exposed to water vapor. These are the conditions we have so far termed those of hydrodynamic flow; nevertheless King applies the ordinary diffusion equation and obtains curves which as stated above are identical with our curves of Fig. 4 where the mass transfer due to what we have so far termed kinetic diffusion through a porous medium is plotted. In Fig. 5 we plotted data from hydrodynamic flow measurements using the diffusion equation to calculate D_H and we noted that the upper curve of Fig. 5 is totally different from the true diffusion curve. The reasons are to be sought in the structure of the flow medium. Keratin is not porous in the same sense as wood. Keratin may have a void fraction of the same order of total magnitude as some woods, but the voids are those of intermolecular spaces and not parts of a connected system of pores. Permanent gases will move through keratin—which may be termed a compact medium—at very low rates, if at all. Water vapor, however, is sorbed by keratin, swelling takes place, and the characteristic hysteresis loop of the absorption isotherm is observed exactly as for a porous medium such as wood. Water vapor will accordingly move in the adsorbed film by a kinetic process—but there will of course be no flow through capillaries.

We can now elaborate the distinction previously drawn between diffusion and hydrodynamic flow. Diffusion of water vapor or any other adsorbable vapor takes place according to Equation (16), through either porous or compact media when there is an equal total pressure at the two faces of the medium with partial pressure gradients across the medium; or when there is a hydrodynamic pressure gradient of a single vapor across a compact medium which sorbs the vapor. Hydrodynamic flow of a gas or a vapor takes place only through a porous medium, when there is a hydrodynamic pressure gradient of a single gas or vapor across the medium. The flow of nonadsorbable gases obeys Equation (9) while the flow of adsorbable vapors takes place in excess of the amount given by this equation.

In other words, vapor transfer through a compact medium will take place under the conditions of true diffusion (i.e., in the presence of air with equal total pressure on both sides) as well as under the hydrodynamic conditions which King actually employed; in both cases the diffusion equation (16) is applicable, and similar curves will be obtained for the variation of the diffusion coefficient with relative humidity. King found that the presence of small amounts of air reduced the mass transfer of water vapor but he was able to account for this by the reduction in vapor pressure at the inflowing face of the keratin membrane which is caused by the resistance of the air through which the vapor had to diffuse when passing from the source to the medium.

King has successfully applied an analysis of the diffusion process given by Cassie (5) for wool to his experiments with keratin. We hope to discuss at a later date the application of the same analysis to a porous medium such as wood.

Acknowledgment

The author wishes to record his indebtedness to Dr. J. D. Babbitt for many helpful suggestions and valuable discussions.

References

1. ADZUMI, H. Bull. Chem. Soc. Japan, 12: 199. 1937.
2. ADZUMI, H. Bull. Chem. Soc. Japan, 12: 304. 1937.
3. BABBITT, J. D. Can. J. Research, A, 17: 15. 1939.
4. BABBITT, J. D. Pulp & Paper Mag. Can. 49: 83. 1948.
5. CASSIE, A. B. D. Trans. Faraday Soc. 41: 458. 1945.
6. KING, G. Trans. Faraday Soc. 41: 479. 1945.
7. KLOSE, W. Ann. Phys. 11: 73. 1931.
8. KNUDSEN, M. Ann. Phys. 28: 75. 1909.
9. KOLLMANN, F. Technologie des Holzes. Verlag von Julius Springer, Berlin. 1936.
10. LANDOLT–BÖRNSTEIN. Physikalisch-chemische Tabellen. 5th ed. Verlag von Julius Springer, Berlin. 1923.
11. O'BRIEN, F. E. M. J. Sci. Instruments, 25: 73. 1948.
12. POLLARD, W. G. and PRESENT, R. D. Phys. Rev. 73: 762. 1948.
13. SCHUGAJEW (SHUGAYEV), W. Physik. Z. Sowjetunion, 5: 645. 1934.
14. STAMM, A. J. J. Agr. Research, 38: 23. 1929.
15. STAMM, A. J. Passage of liquids, vapors and dissolved materials through softwoods. U.S. Dept. of Agriculture, Tech. Bull. No. 929. Oct. 1946.
16. STEFAN, J. Sitzber, Akad. Wiss. Wien, Math.-naturw. Klasse. Abt. IIa: 83. 1881.
17. TOMLINSON, R. H. and FLOOD, E. A. Can. J. Research, B, 26: 38. 1948.

APPENDIX

I. Preliminary Experiments

The void fraction, density of wood substance, bulk density, and percentage swelling of the wood were determined. Small blocks of wood were dried to constant weight G in a vacuum desiccator at 104°C., then saturated under vacuum with water to weight G_H, weighed while immersed in water, G_{HH}, and while immersed in benzene, G_{HB}. The density ρ is then computed from

$$\rho = \frac{G\rho_H}{G - G_{HH}},$$

where ρ_H is the density of water at the temperature of the experiment. The void fraction W of the swollen wood is given by

$$W = \frac{G_{HH} + V\rho_H - G}{V\rho_H}$$

$$= 1 - \frac{G}{V\rho},$$

where V is the volume of the swollen wood and may be measured or calculated from

$$V = \frac{G_{HH} - G_{HB}}{\rho_B - \rho_H},$$

where ρ_B is the density of benzene. The bulk density ρ_w of the swollen wood is given by

$$\rho_w = (1 - W)\rho.$$

The figures for percentage swelling of the wood when taking up water from the oven-dry to the water-logged state were 0.8%, 1.5%, and 8.3% respectively for longitudinal, radial, and tangential swelling; the volumetric change was therefore about 10%.

The bulk density ρ_D of the dry wood is therefore given by

$$\rho_D = \frac{\rho_w}{0.9},$$

and the void fraction W_0 of the dry wood by

$$W_0 = 1 - \frac{G}{0.9V\rho}.$$

The calculations gave the following results:

$$\begin{aligned} W &= 0.80 \text{ cc. per cc.} \\ W_0 &= 0.78 \text{ cc. per cc.} \\ \rho &= 1.48 \text{ gm. per cc.} \\ \rho_w &= 0.30 \text{ gm. per cc.} \\ \rho_D &= 0.33 \text{ gm. per cc.} \end{aligned}$$

II. The Effect of Small Temperature Changes on the Constants of the Knudsen–Poiseuille Equation

Equation (9) may be written

$$\frac{Gp}{p_1 - p_2} = \frac{A}{\eta}\overline{P} + B\sqrt{T}.$$

The fractional change in slope $\frac{A}{\eta}$, for a change δt in temperature, is given by

$$\frac{\delta(A/\eta)}{A/\eta} = -\frac{1}{\eta}\frac{d\eta}{dt}\delta t,$$

and similarly, the fractional change in intercept $B\sqrt{T}$, for a change δt in temperature, is

$$\frac{\delta(B\sqrt{T})}{B\sqrt{T}} = \frac{1}{2}\frac{\delta T}{T}.$$

Now, the temperature dependence of the viscosity is given by the following laws:

(*a*) For air: $\eta = \eta_0 - a(23° - t)$ (10)

(*b*) For oxygen: $\eta = \eta_0(1 + bt)^a$ (10)

(*c*) For water vapor: $\eta = \eta_0 + a(t - 100)$ (13).

For air, therefore, $$\frac{\delta(A/\eta)}{A/\eta} = -\frac{a\delta t}{\eta_0 - a(23° - t)},$$

and $\eta_0 = 1.824 \times 10^{-4}$,

$a = 4.93 \times 10^{-7}$,

hence $\frac{\delta(A/\eta)}{A/\eta} = -0.27\%$ per degree C. for air at 20°C.

For oxygen, $$\frac{\delta(A/\eta)}{A/\eta} = -\frac{ab\delta t}{1 + bt},$$

and $a = 0.82$,

$b = 3.665 \times 10^{-3}$;

hence $\frac{\delta(A/\eta)}{A/\eta} = -0.33\%$ per degree C. for oxygen at 20°C.

For water vapor, $$\frac{\delta(A/\eta)}{A/\eta} = -\frac{a\delta t}{\eta_0 + a(t - 100)},$$

and $a = 3.86 \times 10^{-7}$,

$\eta_0 = 1.255 \times 10^{-11}$;

hence $\frac{\delta(A/\eta)}{A/\eta} = +1.25\%$ per degree C. for water vapor at 20°C.

The fractional change in intercept is

$$\frac{\delta(B\sqrt{T})}{B\sqrt{T}} = \frac{1}{2}\frac{\delta T}{T} = +0.18\% \text{ per degree at } 20°\text{C}.$$

A SPECTROPHOTOMETRIC DETERMINATION OF EXHAUST GAS TEMPERATURES IN THE PULSE-JET ENGINE[1]

By H. F. Quinn

Abstract

This paper describes a spectrophotometric method whereby instantaneous values of a variable flame temperature, in the particular case of nonluminous flames, may be determined and continuously recorded.

This new technique, which depends upon the establishment of monochromatic black-body radiation conditions in the flame for a small region in the visible spectrum, involves the continuous measurement of radiation intensity in the above region, the intensity being, thereafter, correlated with the temperature of the flame.

The problem of temperature measurement in the general case of nonluminous flames (flames which do not contain an appreciable amount of free carbon in the form of soot) is considered and a brief review of previous techniques employed for this purpose over the past 50 years is given. The basic theory and preliminary experimental justification of the present method are discussed.

A description of the apparatus and the experimental arrangement used by the author in a specific application of the present method in the determination of the time variation of temperature in the exhaust flame of a pulse-jet engine is given. This includes details of a special type of spectrophotometer which employs a multiplier photocell as the radiation detecting and measuring element and, also, a "black-body" cavity constructed as a standard radiation source for the calibration of the former instrument. An original technique used to investigate the emissivity of flames colored by alkali metal vapors is described and its application to the present problem shown.

Finally, the measurable temperature range of the present apparatus is considered together with the inherent limitations of the new method.

Introduction

Developments in the field of jet propulsion over the past 10 years have emphasized the necessity for the development of suitable techniques for the measurement and recording of instantaneous values of thrust, fuel flow, gas pressure, and temperature in typical jet propulsion motors. This process of instrumentation development has proceeded with great rapidity both in Great Britain and in the U.S.A. It is desired, in this paper, to report on one particular phase of the general development, namely the technique of measuring and recording continuously and rapidly varying temperatures in the exhaust gas stream of jet propulsion motors. To simplify the discussion, the paper has been divided into two parts, Part I of which deals with the basic physical principles and underlying theory of a new technique in flame temperature measurement, while Part II describes the application of the developed method in the case of a specific jet engine, the pulse-jet.

The present problem, as originally assigned to the author (then engaged as a Research Associate of the University of New York) by the late Prof. J. K. L. MacDonald, Technical Director of a jet propulsion project (Project "Squid")

[1] *Manuscript received in original form September 26, 1949, and, as revised, February 28, 1950.*

Contribution from the Canadian Armament Research and Development Establishment, Valcartier, Que.

in the above University, may be summarized as follows:—"It was desired to design and construct an instrument capable of providing an accurate record of varying flame temperatures at any specified point in a jet motor. This instrument was required to record these temperature variations up to a fundamental frequency of 250 engine cycles per second and was to be fully responsive to harmonic frequency components up to the limit of 2500 cycles per second. The instrument was not to be subject to destructive action by the hot gases of the jet and was to be free from radiation or other sources of error. Finally, the insertion of any part of the instrument (if insertion were necessary) into the gas stream was not to lead to any additional perturbation of its mode of flow". The above requirements were originally postulated with specific reference to one particular type of motor, the pulse-jet and, following some preliminary investigations, it was decided to limit the application of the instrument to the practically nonluminous gas stream at the exhaust end of one of the above engines.

Part I

A thorough search of the existing literature in the field of gas temperature measurements was made in the hope of finding an existing method of dealing with the problem or, at least, one which could be conveniently modified so to do. Of the mass of literature on the subject, dating from 1890 onwards, only one article gave promise of a method which might be employed after considerable modification to meet the above stated requirements. A brief outline of the survey has been included here in so far as it is indicative of the many problems which are encountered in the temperature measurement of nonluminous flames. The very earliest methods of temperature measurement applicable to nonluminous flames required the introduction of thermocouples into the body of a stationary flame such as that of a Bunsen burner: many elaborate techniques were evolved to compensate for losses due both to radiation from the couple itself and to conduction along the leads. Typical experimental arrangements are described by Waggener (20), by Burkenbusch (2) and by Nicols (15). It is obvious that the time-lag due to the thermal capacity of any practical thermocouple element completely eliminated the use of such a device as far as the present problem was concerned.

An original optical method of flame temperature determination was devised by Kurlbaum (9) for the luminous, carbonaceous type of flame but served as the basis for the method of spectral line reversal due to Fery (3) and independently to Kurlbaum and Schulze (10). An excellent description and theoretical explanation of the latter method has been given by Lewis (11). While this method, which applies strictly to a nonluminous flame, has been used with considerable success by Awbery and Griffiths (5) and by Loomis and Periott (12) for the determination of static flame temperatures, it is essentially a static method in so far as it requires a visual matching of brightness by the experimenter and is, therefore, completely unsuitable for the determination of rapidly varying temperatures. It is noteworthy, however, that this method

has been extended in its application to the special case of nonluminous flames in an Otto cycle engine cylinder by the use of a stroboscopic arrangement whereby the brightness matching is effected at a specific point in the cycle of the engine; this is achieved by the use of a stroboscopic disk driven synchronously from the engine crankshaft, a set of holes cut into the disk allowing light from a comparison radiator to pass through the flame during a very short time interval at some specific point in the engine cycle. Procedures devised for this point-to-point temperature measurement are described by Hershey and Patton (6), and also by Rassweiler and Withrow (16). This modified line reversal technique is unfortunately inapplicable to the pulse-jet owing to the fact that not only are the individual cycles of the engine remarkably dissimilar but also because there is no rotating mechanical part of the engine with which to effect the synchronization of a stroboscopic disk.

A further optical means of determining temperatures in the case of nonluminous flames depends upon the measurement of emission and absorption of radiation by the flame in the infrared region of the spectrum between the limits of 2 and 6 microns: this method was extensively investigated by Schmidt (18) for the particular case of the Bunsen flame. Schmidt was able to show conclusively that the Planck Radiation Law applied to certain molecular band radiation in the above region. In order to apply this method to the flame of the pulse-jet exhaust, it would first be necessary to examine the complete infrared spectrum from a gasoline flame burning in air under conditions which closely simulated those in the actual pulse-jet engine in the hope of finding some particular band radiation for which the above law applied: facilities for such a study were not available. No attempt was made, therefore, to explore this method any further.

The experimental procedure finally adopted was first suggested by MacDonald following consideration of an original report by Graff (4) in which a description was given of another radiation method of temperature measurement applicable to the flames in an Otto cycle engine. Graff considered that, as the radiation properties of the intermediate and final products of combustion in the combustion chamber of such an engine were not sufficiently well defined and were, in part, unknown, it would be feasible to make exact temperature measurements using the radiation due to certain additive substances purposely introduced into the combustion chamber. Suitable additives were found to be the alkali metals introduced with the fuel in the form of organic salts reasonably soluble in gasoline. Graff quotes some preliminary investigations of Yosida (a reference which cannot be traced), wherein it was apparently shown that the above additives (when present in sufficient concentration in the flame) emit, within the limits of their resonance lines, radiation which is a function of temperature only, as given by the Planck formula: that is to say, monochromatic black-body conditions could be established in the flame for the spectral regions of the resonance lines. It is at once apparent that, in general, the above condition is not attained, the radiation intensity due to the additive depending

not only upon the temperature but also upon the concentration of the additive in the particular portion of the flame examined. No mention is made by Graff of any investigations pertaining to the minimum amount of additive required to effect black-body conditions in the flames which he examined.

The apparatus used by the above author in the application of his method to the Otto cycle engine flame consisted of a photoelectric cell used as a radiation detector, a color filter placed in front of the detector to eliminate band or continuous spectral radiation from the flame, and an amplifier to amplify the output voltage of the photocell up to the level necessary to operate a cathode ray tube on the screen of which the intensity versus time record was presented. No mention is made of the calibration procedure employed or of the means of recording the deflection of the oscilloscope beam. In order to apply this method to the case of the pulse-jet exhaust flame, it was first necessary to examine whether or not the concentration of the additive which it would be possible to inject into this engine could be increased beyond the minimum level required to provide monochromatic black-body conditions in the exhaust flame.

Theoretical

The concept of temperature as applied to the particular case of the completely or partially burned gases which comprise a flame is defined as corresponding to a particular state of complete statistical equilibrium in these gases. Such a state is described thus: collisions between the atoms or molecules and interaction with the radiation of the system, although changing continually the energy state of every individual particle, maintain, on the average, the randomness of direction of motion and the constancy of (*a*) the percentage of atoms or molecules possessing a specific velocity, (*b*) the quantity of molecules or atoms possessing a given quantum state of rotation, vibration and of electronic excitation, and, finally, (*c*) the concentration of the dissociation products. It is here assumed, following Lewis (11), that, in the present case of the exhaust flame, the equilibrium (*a*) is completely established owing to the rapidity of the molecular collision sequences. An additional factor in the statistical equilibrium must be postulated in the case of the present problem where an additive, sodium, is present in the exhaust gases, namely the constancy of the percentage of atoms of the additive possessing a given degree of electronic excitation. In this connection, it has been shown by Bauer (1) and by Awbery and Griffiths (5) that identical temperatures are obtained in practice in the case of a specific flame by means of the line reversal technique irrespective of the particular alkali metal used as the additive, that is, irrespective of the excitation potentials of the atoms. This experimental fact admits of no other interpretation than that a complete thermal equilibrium existed between the translational degrees of freedom of the gas molecules and the electronic degrees of freedom (excitation states) of the alkali metal atoms. Since the radiation intensities due to the atoms of the additive is intimately connected with the number of these atoms in the several excited states, it is possible to

associate a measured radiation intensity from a given concentration of these atoms with a specific temperature. In the case of the jet exhaust flame specifically considered here, this temperature will be defined to correspond to a state of statistical equilibrium between the translational degrees of freedom of the gas molecules and the electronic degree of freedom of the additive atoms. No attempt has been made to investigate the establishment of the (*b*) and (*c*) equilibria: such an attempt would be unnecessary in so far as modern gas dynamical calculations as applied to jet engines include the simplifying assumption that the gases are "perfect". Hence, only a temperature corresponding to a statistical equilibrium in the translational degrees of freedom is of useful significance in such calculations.

The intensity–temperature relation for the additive has been seen to alter, in general, with the concentration of the latter in the flame. Two limiting cases of the thermal excitation of atomic spectra may, however, be distinguished to which the terms "Planck radiation" and "Boltzmann radiation" have been applied by Smit (19). Thus, consider a perfect black-body cavity, the walls of which are maintained at a temperature T: let some means be provided whereby a controlled amount of some alkali additive (sodium, for example) can be admitted in the form of a gas. If now two small holes are bored axially into the cavity as shown in Fig. 1, it will be observed that the radiation emerging

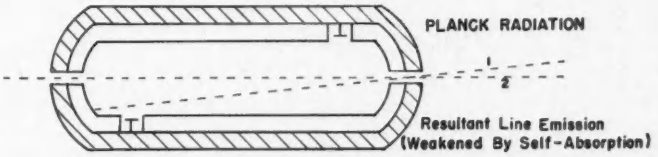

FIG. 1. *Theoretical black-body cavity containing a discrete line emitter.*

from the wall (direction 1 in the figure) will obey the Planck formula, whereas the radiation observed in the axial direction joining the two holes will give the line spectrum of the sodium gas, the intensities of the spectral lines depending upon the populations of the excitation levels according to the Boltzmann formula. This situation is represented in Fig. 2 where the nearly horizontal line represents the spectral energy distribution of the radiation proceeding from the wall, while the lower curve represents the energy distribution in the line spectrum observed along the axis. As the concentration of the additive is increased, so will the intensities of the several lines increase, being finally limited by self-absorption to the "ceiling" represented by the Planck curve: that is to say, monochromatic black-body conditions will have been established for the axial direction of observation for each of the spectral lines.

It is possible, by means of a simple experiment, to show that monochromatic black-body conditions can likewise be established in the case of the "D" line resonance radiation from sodium atoms thermally excited in a flame. The experimental arrangement is as follows. A saturated solution of common salt is

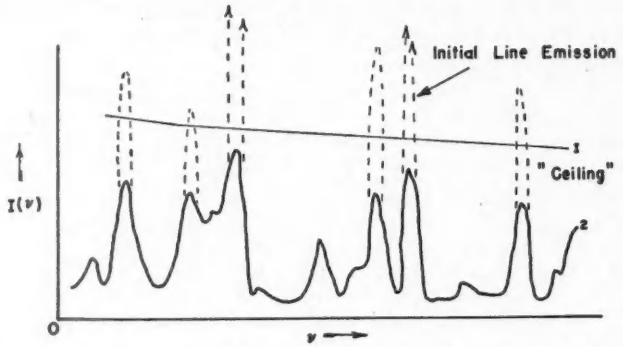

FIG. 2. *Distribution in intensity for Planck radiation from the cavity walls and Boltzmann radiation from the thermally excited line emitter.*

Planck Radiation

$$I(\nu) = \frac{2h\nu^3}{C^2} \cdot \frac{1}{(e^{h\nu/KT} - 1)} \quad \frac{erg}{cm.^2\ sec.\ sterad.\ sec.^{-1}}$$

aspirated under some 25 lb. air pressure into a Bunsen type burner of rectangular cross section together with ordinary coal gas used as fuel. A photocell used as a radiation detector receives "D" line radiation emanating from a 1 cm. square area of the flame at the front of the burner. Once steady burning of the flame has been established, an opaque barrier consisting of a sheet of "transite" is moved into several positions along the length of the burner, effectively reducing the thickness of the flame as seen by the detector as it moves towards the front of the burner. Fig. 3 shows a plot of typical results obtained in practice,

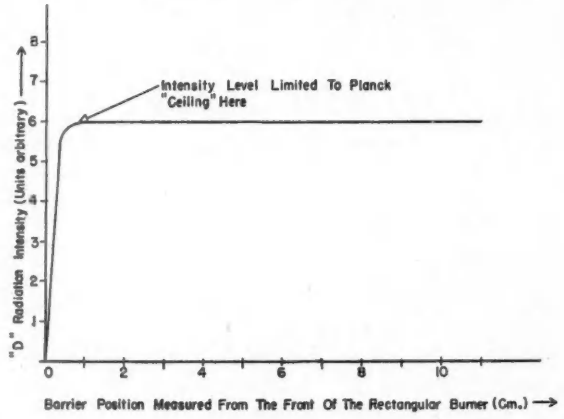

FIG. 3. *Results of a preliminary test for monochromatic black-body conditions in a static flame.*

intensity as measured by the detector being plotted against the distance of the barrier from the front of the burner. It is concluded from these results that, in the above case, monochromatic black-body conditions were established for the "D" line radiation in a 1 cm. thickness of the flame, the requisite amount of additive being obtained by the injection of the salt solution. Theoretically, the above conditions could be established in a lesser flame thickness but, in practice, it would be difficult to provide the necessary high concentration of additive.

In any specific case of flame temperature measurement in terms of the radiation intensity of an alkali metal additive, it remains, therefore, to be determined whether or not a sufficient amount of the additive can be injected to establish a monochromatic black-body condition in the flame for the resonance radiation. This, in turn, presupposes some means whereby the establishment of the condition may be verified. If the condition can be shown to exist, then the intensity of the resonance radiation will follow the Planck law, and the calibration of a suitable spectrophotometer in terms of temperature against radiation intensity will readily be obtained by sighting the instrument into a standard black-body cavity. In particular, the case of the exhaust flame of a pulse-jet motor will now be considered, this flame, in the specific case of the small motor employed in these investigations, having a thickness of 4.14 cm. at the extreme end of the tail pipe.

Part II

Application of the Spectrophotometric Method in the Particular Case of a Pulse-jet Engine

Details of the operation of the pulsating jet engine, together with a comprehensive review of the history of its development, have been described by Miller (14); consequently a description of the engine and its properties is omitted here. According to the above author, satisfactory instrumentation techniques for measuring the time average of the thrust, fuel flow, and body temperature of the engine were developed after minor modification of existing methods but, as of the summer of 1946, development of satisfactory instruments to measure and to record instantaneous values of thrust, pressure, and temperature had proved to be a slow and difficult process primarily owing to the high operating rate of the engine (up to some 250 complete engine cycles per second).

Great impetus was given to the development of adequate instrumentation not only by the pressing requirements for such devices in the empirical development of these engines at several laboratories in the U.S.A. but also by the need for actual numerical values of instantaneous pressure, temperature, gas density, and gas velocity for substitution in the theoretically derived hydrothermodynamical equations for the pulse-jet which had been developed by MacDonald and his school (13) in their one dimensional mathematical treat-

ment of pulse-jet operation. At this time, therefore, among the other instrumentation requirements, it became imperative to develop some method of measuring and recording the rapid cyclic temperature variations at several points in the main combustion chamber, the transition cone, the tail pipe, and finally in the exhaust flame itself.

Information received from the Naval Research Station at Annapolis, where continuous performance tests of pulse-jet engines were being carried out at this time, indicated that the flames in all portions of the particular types tested there were nonluminous (as opposed to the luminous, soot-containing type of flame). Accordingly, the instrument requirements were initially limited to a device which would meet the previously stated specification in the case of nonluminous flames only. It was not until the construction and testing of a glass-walled pulse jet had finally been accomplished at New York that the flames both in the combustion chamber and in the tail pipe were revealed to be brightly luminous, only the exhaust flame being nonluminous (a faint bluish flame). At this point, the research program diverged, a group at New York commenced investigation of methods of temperature measurement for luminous flames while the author, having at this time returned to McGill University, continued the original research as applied to the case of the nonluminous exhaust flames.

Method

The general arrangement of the apparatus as employed in the pulse-jet application is illustrated in Fig. 4. The sodium additive was, at all times, injected with the air stream through the intake valves of the motor in the form of a finely powdered inorganic salt by the use of a small blower located some distance away from the intake valve bank. This method of additive injection was considered far superior to the water-spray injection technique used by other investigators, as there is less probability of the operation of the engine being adversely affected by the addition of a dry powder than by the considerable amount of water required to effect adequate aqueous injection of the additive; cooling of the flame due to the absorption of the heat of vaporization of the water is also eliminated.

The arrangement of the optical and electrical components of the simple type of spectrophotometer employed is shown in Figs. 5 and 6 respectively. An image of the source (a small hole of 13/64 in. diameter pierced into the blast and radiation screen directly opposite the extremity of the tail pipe of the motor) is formed by an auxiliary biconvex lens on the spectrometer slit. The prism P is set in the position of minimum deviation for the "D" line image which is formed by the lens L_2 at the knife-edge jaws of a second adjustable slit, A_2. The latter opening is adjusted until the bright image of the "D" lines just disappears through it, the light in the spectral region so selected being received by the lens L_3 whose focal plane is at the second slit. Finally, the light emerges to uniformly flood the photo-cathode of the detector element, a

FIG. 4. *General arrangement of the apparatus in the pulse-jet application.*

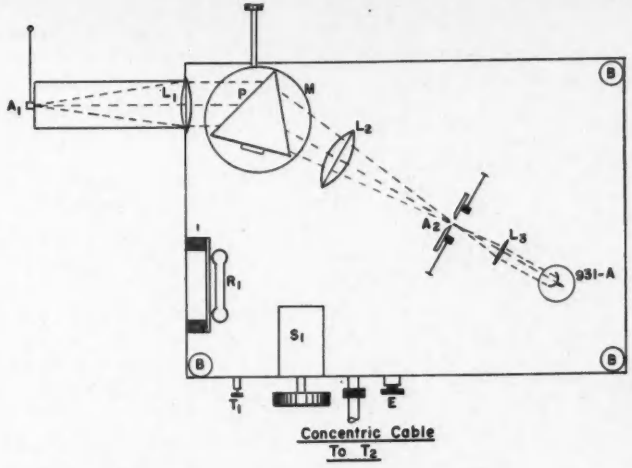

FIG. 5. *Optical system of the spectrophotometer.*

L_1— Collimator lens; focal length, 7.525 in.
L_2— Objective lens; focal length, 1.746 in.
A_2— Selector slit.
L_3— Telescope lens; focal length, 7.525 in.
A_1— Spectrometer slit.
P — 60° crown glass prism.

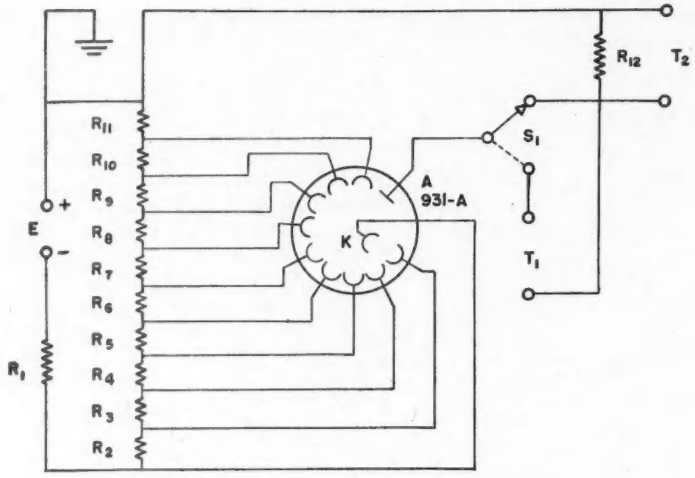

FIG. 6. *Electrical circuit of the spectrophotometer.*

R_1— *1.05 M ohms*
R_2 *to* R_{10}— *100 K ohms*
R_{11}— *50 K ohms*
R_{12}— *200 K ohms*
T_1— *To microammeter*
T_2— *To d-c. amplifier*
S_1— *Change-over switch.*
E — *Supply voltage, 2000 v. d-c. regulated.*

standard electron multiplier photocell (R.C.A. type 931-A). The requisite voltages for the several dynodes of the tube are obtained as shown from a potentiometer, R_1 to R_{11}, placed across the output of a 2000 v. regulated d-c. power supply, E. The entire spectrophotometer is housed in a light-tight metal box, the latter also protecting the detector from the considerable blast and vibration from the jet engine. Further protection from these effects is also obtained by mounting the instrument on a separate heavy table.

A check on both the optical filtering efficiency of the above system and also on the linearity of the photocell was obtained by the use of a calibrated broad-filament tungsten lamp as a light source: the phototube currents corresponding to a series of different lamp currents were recorded. The tungsten lamp had been previously calibrated in another experiment and the relation between its apparent black-body temperature and heating current was known. Provided the filtering was adequate and the tube response linear, a plot of the natural logarithm of the measured intensity in the immediate spectral region of the "D" lines against the reciprocal of the absolute temperature should yield a straight line, that is, the Wien law equation should hold. This plot is shown in Fig. 7: taking the "mean wave length" of 5893 Angstrom units and the accepted values for the Planck and Boltzmann constants, the theoretical slope of the straight line was computed, giving the figure -2.48. The experimental value obtained from the above graph was -2.57, leading to an error of just under 4% which, considering the roughness of the measurements, was taken to con-

firm both a satisfactory filtering of the incident light and a satisfactory linear response of the tube.

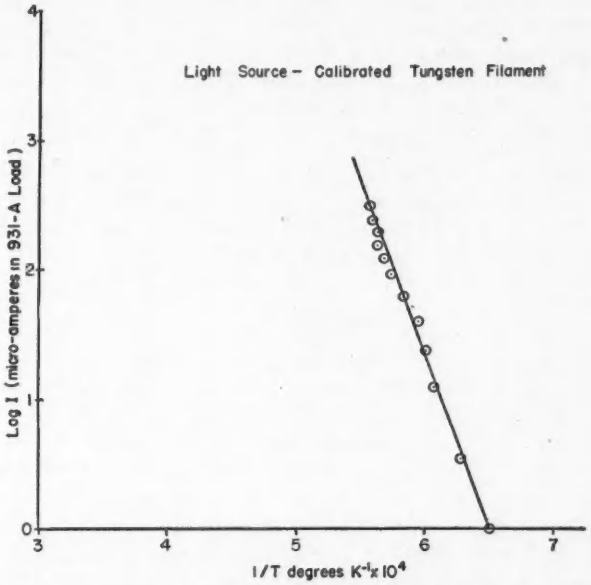

FIG. 7. *Results of a preliminary test of the spectrophotometer (application of the Wien law in the form—*

$$\log_e I = \log_e C_1 - \frac{h}{K} \cdot \frac{1}{T}).$$

A single stage of push-pull d–c. amplification was used between the photocell and the cathode-ray oscilloscope. It was experimentally determined that, by increasing the level of the light incident upon the multiplier tube and by the use of a 200,000 ohm resistor as a load, it was possible to obtain an output voltage adequate to operate the push-pull single stage d-c. amplifier which is employed as a fourth stage in a Dumont type 208-B oscilloscope. This amplifier stage has a frequency response flat from 0 to 100,000 c.p.s. and has its output terminals directly connected to the deflection plates of the cathode ray tube. Frequent tests demonstrated the excellent stability of this system, and its operation was completely adequate in all respects.

A procedure for determining the existence of monochromatic black-body conditions in the case of a static, steadily burning flame has already been described: in so far as this method requires the insertion of a barrier into the flame, it is inapplicable to the jet exhaust flame—nothing must be inserted into the latter which might perturb the normal mode of flow of the exhaust gases. To overcome this difficulty, it was decided to assume the applicability of the

Kirchhoff law for the "D" line radiation (17) and to test the flame for unity monochromatic absorptivity. This was arranged as follows. Radiation from a small area of the flame diametrically opposite the source hole in the screen was received by a small plane mirror and reflected back into the flame towards the spectrophotometer. If the flame possessed unity absorptivity for the "D" line radiation, it was considered that identical intensity values would be recorded by the photometer whether the mirror was exposed to the radiation or not. Preliminary tests on static flames demonstrated the effectiveness of the method.

In the application of this test to the exhaust flame, it was decided to provide a satisfactory basis for comparison of intensities measured both with the mirror exposed and screened in the following manner. A rotating metal disk having four open sectors cut into it was arranged to spin in front of the mirror, thereby alternately exposing and screening the latter during a period corresponding to four complete engine cycles. It was, thereby, anticipated that all cycles would show approximately the same maximum amplitude of intensity and general intensity–time relation if unity absorptivity were established, while alternate sets of four cycles would show marked differences if this condition were not attained. A provision was made whereby the exact period during which the mirror was screened could be indicated on the final intensity–time record by the use of a cam fitted to the drive shaft of the disk: this cam was arranged to

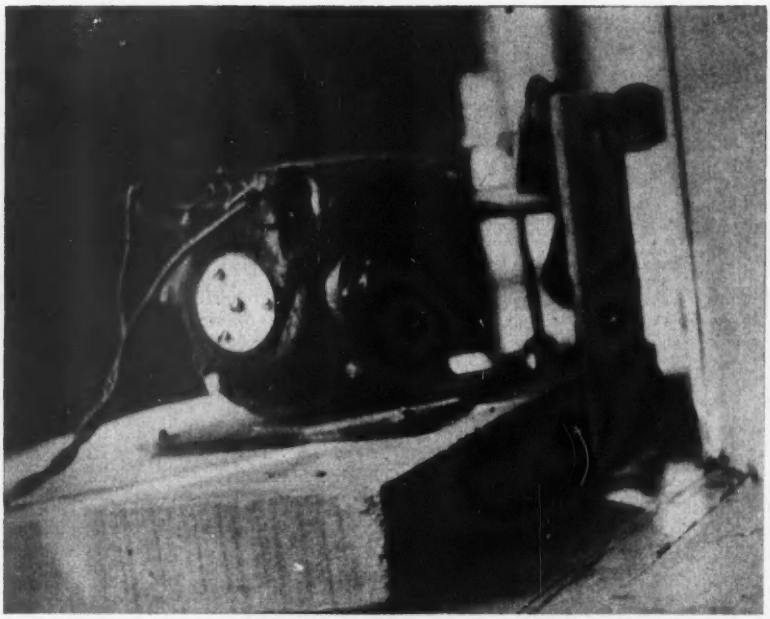

FIG. 8. *Emissivity test arrangement.*

close a sensitive microswitch whenever a segment of the disk completely screened the mirror. The switch itself was connected to the external contactor terminals of a General Radio "Strobotac" which provided a brilliant flash of light each time complete screening of the mirror was accomplished. These light flashes fell on the face of the cathode ray tube screen and were recorded simultaneously with the deflection of the beam. The sector disk, the driving motor (operated at 3150 r.p.m.) and the plane mirror are fully illustrated in Fig. 8.

The calibration method employed a cylindrical black-body cavity heated electrically to incandescence by a concentric graphite heating resistor as a standard radiation source. The complete unit is shown in Fig. 9. The cavity

FIG. 9—*A*

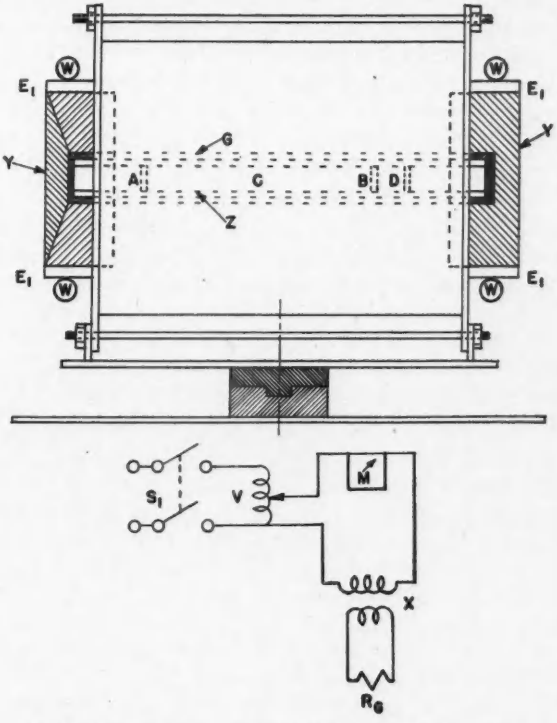

FIG. 9—*B*

FIGS. 9–A AND 9–B. *The black-body cavity and furnace.*

Fig. 9–A.
W — *Water cooling pipes*
Y — *Carbon end sections*
G — *Graphite tube*
B — *Cavity end insert*
V — *Variable transformer*
E$_1$ — *High-current clamp electrodes*
C — *Black-body cavity*
Z — *Zirconium oxide tube*
D — *Radiation breaker*

Fig. 9–B.
M — *0-15 amp. a-c. meter*
X — *High-current transformer*
R$_G$ — *Resistance (Tube G)*

itself was constructed by core-drilling out of a block of solid zirconium oxide, this refractory material having a melting point in the vicinity of 2500°C. A central pivot arrangement together with the provision of flexible leads allowed the entire furnace to be swung from one fixed position where it could be viewed by the spectrophotometer through an angle of 30 degrees into another position where it could be viewed by a Leeds and Northrup type 8622 optical pyrometer. Thus a measured radiation intensity could be rapidly correlated with a specific black-body temperature of the cavity.

The circular aperture of the cavity was chosen to be identical with the source hole in the blast screen; hence the images formed on the spectrometer slit both from the flame itself and from the cavity were of equal size. It is fully realized that perfect black-body conditions were not attained in the cavity owing to the nonuniform electrical heating system employed and to the extremely poor thermal conductivity of the zirconium oxide which introduced large temperature gradients in the walls. In the absence of a tungsten cavity, however, the above arrangement was the most satisfactory; apart from the necessity for frequent replacement of the heating element the entire unit gave trouble-free service throughout its period of use.

Recording of the intensity–time variations was achieved throughout the entire period of research by the use of the conventional cathode ray oscilloscope – continuous film camera arrangement, the output signal of the amplifier being presented in the form of an "X" deflection of the electron beam. The oscilloscope was a standard Dumont type 208-B model, the camera a General Radio type 651-A-E incorporating an $f/1.5$ lens. Timing marks were impressed on the film by the Strobotac arrangement as previously described.

The procedure adopted during a single test run on the engine was as follows. A period of one-half hour was allowed in order for the electronic circuits to become stabilized: during this waiting period, the camera was loaded with 50 ft. of film, the a-c. mains voltage checked and recorded, the main optical chain of the spectrophotometer aligned and the additive injection blower loaded with finely powdered sodium chloride and set in position facing the intake valves of the jet. Owing to the extreme sensitivity of the multiplier photocell, all the tests were run in complete darkness, apart from the small, flashing light of the Strobotac. As soon as the room was darkened, the high voltage supply to the cell was switched on, together with the "Beam" switch of the oscilloscope, and the disk motor was started. As the entire film length was run through the camera in approximately 1 1/2 sec., it was imperative that the switching on of the camera be effected by one operator who carefully observed the deflection on the oscilloscope screen while another operator assumed responsibility for both the starting of the engine and the injection of the additive. At the start of the test run, the latter operator switched on the starting spark and aspirated fuel into the engine combustion chamber, using an auxiliary starting compressed air supply. Once stable operation of the jet had been attained over a five-second period of time, the jet operator threw on the blower-

injector switch, forcing a stream of salt dust into the valve bank of the engine. Meanwhile the camera operator observed the oscilloscope screen and, when the single spot on the latter expanded into a trace some three inches long consequent upon the injection of the additive, made the main switch to the camera motors. The entire procedure from the initial starting of the engine to the final switching off of the camera occupied just under 15 sec.

Completion of this recording was followed by a calibration of the photometer as follows. The engine, the emissivity test apparatus, and the blast screen were removed and the furnace placed in position. The latter was slowly raised through a series of temperatures from 800 to 1500°C. (these temperatures being measured by the optical pyrometer) and the deflections corresponding to specific cavity temperatures were recorded. The results of a typical calibration run appear in Table I. This data enabled the curve of Fig. 10 to be con-

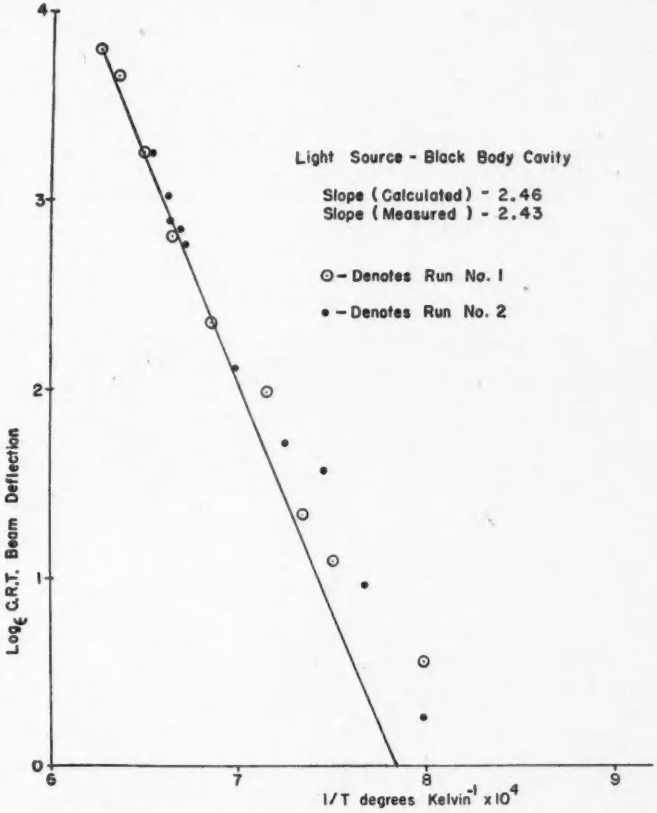

FIG. 10. *Spectrophotometer calibration curves (application of the Wien law).*

TABLE I

Cavity temperature			Oscilloscope deflection, in.
°F.	°C.	°K.	
2300	1262	1535	2.3_3
2262	1240	1513	1.9_6
2242	1230	1503	1.6_6
2230	1223	1496	1.6_3
2220	1219	1492	1.4_9
2110	1157	1430	0.8_0
2020	1105	1378	0.5_4
1965	1072	1345	0.4_7
1880	1028	1301	0.2_6
1790	976	1249	0.1_3
1760	959	1232	0.0_7

NOTE: *The practical limit of "cutoff" of the thermally excited "D" line radiatiation was estimated to occur at 950°C.*

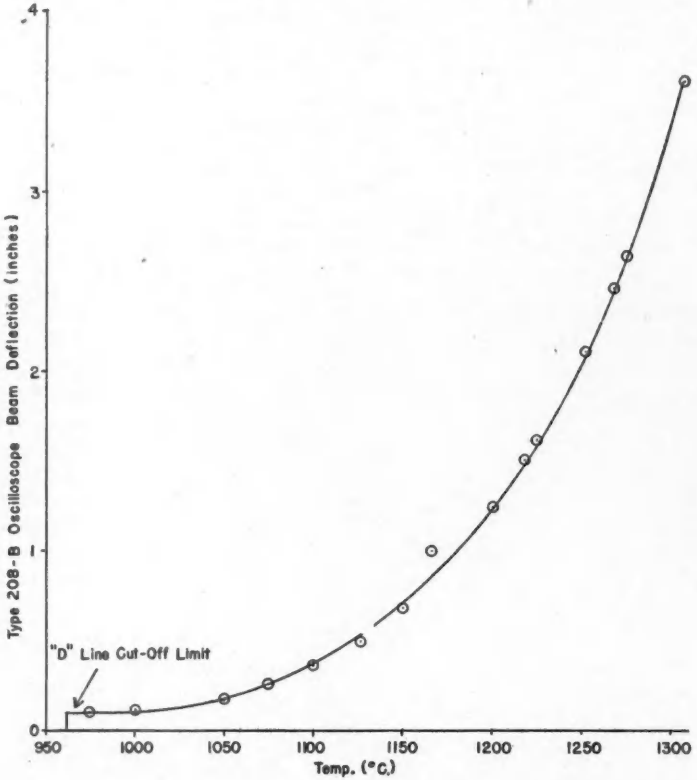

FIG. 11. *Corrected calibration curve for the recording oscilloscope.*

structed where it is to be particularly noted that the measured slope of the curve differs by only 1.2% from the theoretically calculated value, thus indicating the satisfactory achievement of black-body conditions in the cavity. The final calibration curve for the spectrophotometer–oscilloscope combination appears in Fig. 11. It will be noted that the thermally excited "D" line radiation, as detected by the present apparatus, tends to a practical cutoff in the vicinity of 950°C.

The conversion from the intensity–time record on the film to the final temperature–time results was effected as follows. Two marks were provided on the face of the cathode ray tube, the distance between these being carefully measured, using dividers and a steel rule. Finally the two marks were photographed and the negatives obtained placed in a Kodak Precision Enlarger which was then adjusted until the distance between the images of the two marks projected on a plane white surface equalled the distance originally measured on the face of the tube. Having made this adjustment of the enlarger, it was locked in this position: thereafter it was simply necessary to project any particular film record onto the white surface and, by the use of the calibration curve of Fig. 11 to read off the temperature–time results.

Results

The following results have been derived from a study of some 600 ft. of film constituting the intensity–time records for 12 separate test runs of the jet engine. First, it was immediately apparent on examining the records that a general dissimilarity existed in the intensity–time wave forms from one cycle of the engine to another. This is exemplified in Fig. 12 where several cycles are

FIG. 12. *Representative set of successive intensity-time cycles obtained in the pulse-jet application.*

shown, these being recorded before the camera reached its maximum operating speed of 25 f.p.s. Indeed, when all the factors which influence the operation of this type of engine are reviewed particularly the nature of the fuel injection system, it was considered remarkable that any consistency among the wave forms would be obtained: some definite consistency has, however, been definitely established in this research.

In examining the film records, a search was made for two particular points of similarity in the cycles: (1) equality of the intensity maxima and, (2) similarity of the general configuration of the wave forms. It was discovered that

one special configuration occurred at irregular intervals throughout the records: this configuration is illustrated in the rough sketch below.

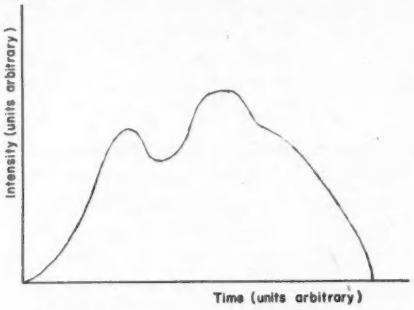

It is to be noted that the test for the establishment of black-body conditions in the exhaust flame did not give positive results in that no alternate sets of four large and four small intensity–time wave forms were ever observed, the maximum intensity and general configuration varying widely from cycle to cycle. It is interesting to note, however, that the records show that the above-mentioned scattered similar cycles were recorded at times when the mirror was screened and also when it was exposed.

The existence of these recurrent similar cyles admits of two separate interpretations: (1) there is a fairly definite and consistent temperature–time variation in the exhaust gases and, in the case of the above cycles, black-body conditions were established in the flame or, (2) the temperature–time relation varies widely from cycle to cycle, black-body conditions were never established at any time in the flame and the above similarity results only from fortuitous combination of several factors. These factors are (*a*) the particular temperature–time variation for a given cycle, (*b*) the particular concentrations of the additive present in the exhaust flame at all times during the cycle and, (*c*) the effect of additional light received by the spectrophotometer in those cases where the mirror was exposed. The former interpretation, being the most probable, has been accepted here.

While an interpretation of the consistent cycles has been given, the wide dissimilarity observed from cycle to cycle remains to be explained. Studies of the behavior of the engine, particularly in the cases where an especially finely powdered additive was injected, indicated that the normal combustion processes in the engine could be adversely affected by the addition of an excess of salt powder: such a disturbance would explain the widespread variations from one cycle to the next. It is considered, however, that at some particular intervals during the recording periods, the concentration of the additive present in the engine was adequate to effect the requisite conditions in the exhaust flame without seriously perturbing the main combustion process and that the above consistent cycles were recorded at such times.

The return of the intensity–time wave forms to the zero level over a large part of the operating cycle is due to two separate factors. The present apparatus is unable to detect thermally excited "D" line radiation emitted by a source whose temperature is less than 950°C. In the absence of evidence from other investigations revealing a more surprising reason, it might be reasonably assumed that, at the periods of zero intensity, the exhaust gases simply fell to temperatures below the above limit. It has, however, been definitely established by Hudson and Hett (7) in their investigations of the pulse-jet exhaust flame by means of high-speed photographic techniques that, following the initial outflow of the exhaust gases shortly after the beginning of a particular engine cycle, a period of flow reversal occurs wherein the exhaust flame appears to contract in diameter and then to vanish backwards into the tail pipe of the engine—there is a reversal of mass-flow. It is considered that both of the above effects operated to give the wave forms observed in this research; the exhaust gases probably fell first to a much lower temperature than 950°C. and then were effectively swept out of the field of view of the spectrophotometer, being replaced by atmospheric air at room temperature.

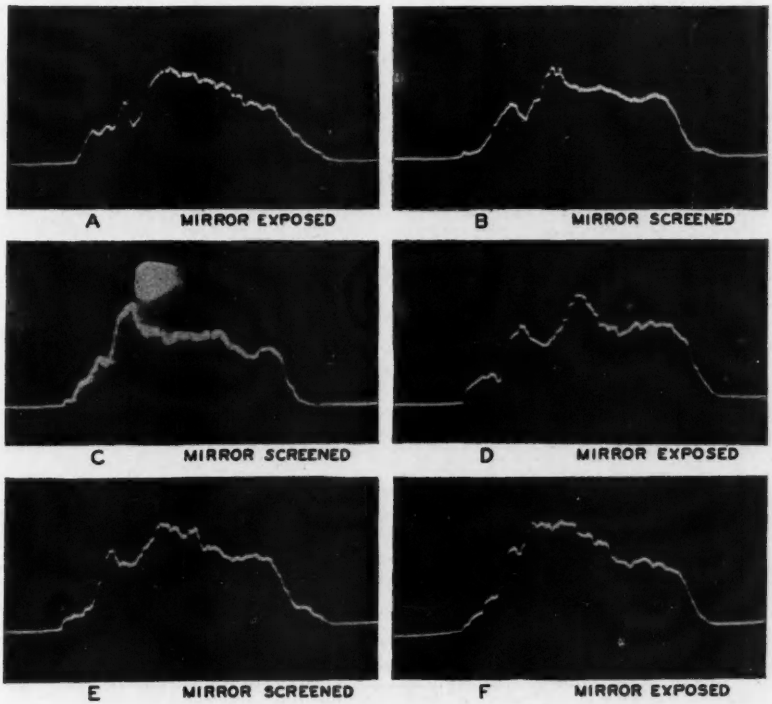

FIG. 13. *Selected similar cycles obtained from records in the pulse-jet application.*

While the lower limit of temperature which the present apparatus can measure has been seen to be 950°C., there is no theoretical upper limit to the measurable temperature range in so far as the maximum temperature which can be recorded is controlled only by the saturation current of the particular photocell employed, the ability of the amplifier to handle a large input voltage signal and, finally, the size of the cathode ray tube required to present the deflection corresponding to the maximum temperature. The apparatus here was limited in practice to an upper temperature limit of 1350°C.

The appearance of the "secondary maxima" near the start of the intensity–time curves was initially regarded as being extremely peculiar in so far as it was difficult to understand why a sudden drop in temperature of the exhaust gases should occur shortly after the initial outflow. This peculiar phenomenon has, however, been strikingly correlated with some early high-speed photographic results of Hudson and Hett (8). These investigators showed that the flame propagation in the pulse-jet takes place in the following manner:—upon ignition of the air–fuel mixture in the combustion chamber, a small knot of flame (termed a "flambeau" by Hett) is rapidly propagated throughout the length of the engine, finally emerging at the end of the tail pipe; this preliminary

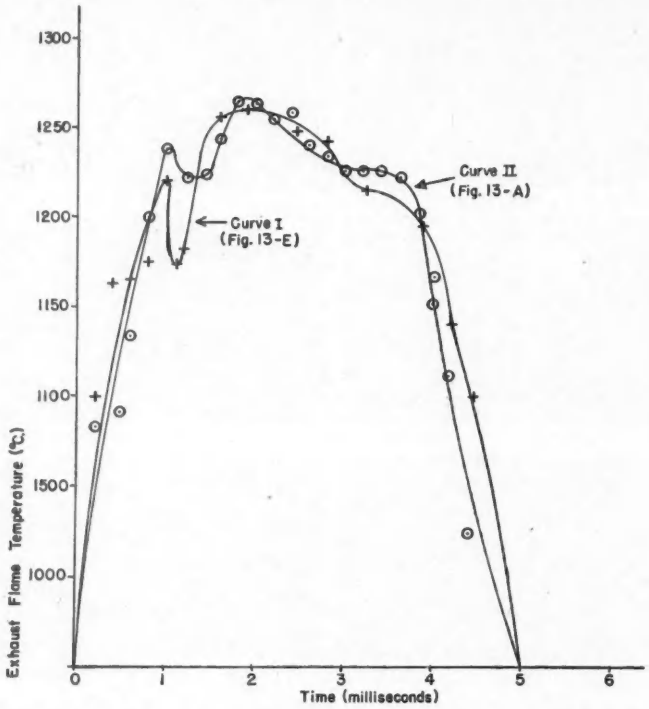

FIG. 14. *Temperature-time relations for the particular cycles 13-A and 13-E.*

"flambeau" is followed after an interval of no visible burning, by a marked bank of flame traveling some four inches behind the flambeau. The occurrence of the above secondary maximum is, therefore, interpreted to correspond to the arrival at the extremity of the tail pipe of the high temperature section of the flambeau, while the succeeding upward rise to the main maximum is taken to correspond to the arrival of the main body of flame.

When the several consistent cycles which are shown in Figs. 13–A to 13–F are considered, the logarithmic relation between the recorded intensity and the actual temperature must be borne in mind: in particular, it must be realized that, at the higher temperatures, a small change in temperature results in a very disproportionate change in intensity. To further illustrate this point, the temperature–time graphs obtained from the particular cycles of Figs. 13–A and 13–E are shown in Fig. 14. Both curves indicate a secondary maximum occurring 1.0 msec. after the beginning of the initial upward temperature gradient; moreover, the general configuration of the curves and their maximum temperatures are strikingly similar. Fig. 15 shows similar temperature–time curves for the cycles of Figs. 13–B and 13–C. As minor differences still exist

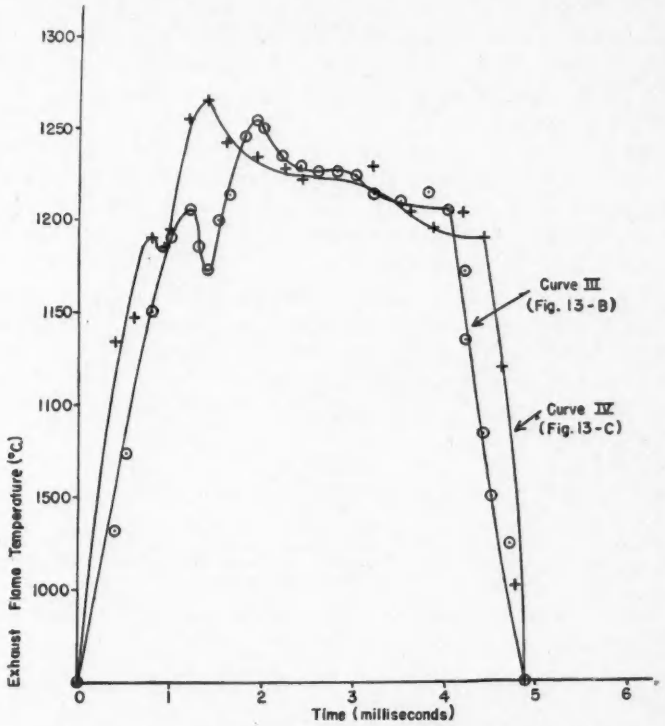

FIG. 15. *Temperature-time relation for the particular cycles 13-B and 13-C.*

between the above curves, it has been decided to select Curve 1 of Fig. 14 as representing an average relation, and this particular curve has been taken to represent the considered temperature–time relation for the exhaust flame.

Acknowledgments

The author wishes to gratefully acknowledge the considerable assistance received from the Staff of the Department of Physics and the Staff of the Department of Mechanical Engineering of McGill University during the period of this investigation.

Particular thanks are due to Prof. C. A. Robb, Chairman of the Department of Mechanical Engineering, for making available to the author the facilities of that Department. Prof. D. L. Mordell gave invaluable advice concerning the engineering and thermodynamical aspects of the problem, while the late Professor Patton assisted in the design and construction of the black-body furnace. Mr. Charles Damacour, Graduate Student in this Department, assisted in all the experimental tests on the engine: without this considerable aid the project could not have been carried to its final conclusion.

Dr. A. Norman Shaw, Chairman of the Department of Physics, provided much appreciated constructive criticism of the author's methods and results, while all members of the Physics Staff contributed advice concerning the optical and electronic phases of the project and assisted greatly in the procurement of apparatus.

Finally, special thanks are due to the Defence Research Board of Canada for the grant of one thousand dollars ($1,000.00) to cover the purchase of equipment and to meet operating costs. Mr. A. K. Wickson of the Board kindly made available the high-speed camera.

References

1. Bauer, E. Recherches sur le rayonnement, These, Gauthier-Villars, Paris. 1912.
2. Burkenbusch, O. Wied. Ann. 67: 649. 1895.
3. Fery, C. Compt. Rend. 137: 909. 1903.
4. Graff, I. Z. Ver. deut. Ing. 86: 29. 1942.
5. Griffiths, E. and Awbery, J. H. Proc. Roy. Soc. (London), A, 123: 401. 1929.
6. Hershey, A. E. and Patton, R. F. Univ. Illinois Bull. Eng. Exp. Sta. Bull. Ser. No. 262. 1933.
7. Hett, J. United States Navy Project "Squid", Semi-annual Progress Report. Jan. 1. 1947.
8. Hett, J. United States Navy Project "Squid", Semi-annual Progress Report. Oct. 1. 1947.
9. Kurlbaum, F. Physik. Z. 3: 187, 332. 1902.
10. Kurlbaum, F. and Schulze, G. Verhandl. deut. physik Ges. 5: 428. 1903.
11. Lewis, B. and Von Elbe, G. Combustion, flames and explosions of gases, Text.
12. Loomis, A. J. and Periott, L. B. J. Ind. Eng. Chem. 30: 1004. 1928.
13. MacDonald, J. K. L. A gas dynamical formulation for waves and combustion in pulse-jets, Report of the Applied Mathematics Group, New York University. 1946.
14. Miller, P. S. S.A.E. Bull. 222, April, 1947.
15. Nicols, J. Phys. Rev. 10: 234. 1900.
16. Rassweiler, G. and Withrow, L. S.A.E. Journal, 36: 125. 1935.
17. Ruark, A. E. and Urey, H. C. Atoms, molecules and quanta, Text.
18. Schmidt, H. Verhandl. deut. physik Ges. 90: 238. 1909.
19. Smit, C. Physica Proc. zeeman conference, 12: 476. 1946.
20. Waggener, H. Verhandl. deut. physik Ges. 14: 78. 1895.

FAST NEUTRONS FROM THE T + D AND T + Li REACTIONS[1]

By E. Almqvist

Abstract

The fast neutrons produced by the triton bombardment of LiF, Li_2CO_3, $LiOH.H_2O$, LiOD, and $LiOD.D_2O + D_2O$ have been detected, and the thick target yields and their slowing down lengths in graphite measured. The tritons were produced by irradiating the compounds in the high thermal neutron flux of the thermal column of the NRX pile. The spatial distributions of the fast neutrons from the T + D and T + Li reactions were measured in the graphite with indium resonance detectors. The numbers of fast neutrons emitted per second were obtained by comparing the space integrals of the indium activity with that measured when a standard Ra-α-Be source of neutrons was in the position of the lithium compounds. The number of incident tritons was estimated from the measured flux of thermal neutrons at the lithium compound and the total capture cross section of the lithium. The thick target yields were thereby derived. The average cross sections for neutron production by 2.6 Mev. tritons are 1.5×10^{-24}cm.^{2} per atom of lithium and 0.41×10^{-24}cm.^{2} per atom of deuterium. The slowing down lengths in graphite of density 1.64 gm. per cc. are 19.2 and 23.4 cm. for the neutrons from the lithium and deuterium respectively. The smallness of the latter indicates that inelastic scattering of these 14 Mev. neutrons occurs in graphite.

Introduction

The bombardment of light nuclei with tritons is expected to yield very energetic neutrons owing to the large positive energy balance of (T, n) reactions with most light elements. The reaction T(d, α)n has been studied at low energy (5) and the excitation function and cross section measured up to 2.5 Mev. deuteron energy (4, 17) by detecting the α-particles. Even at low bombarding energies this reaction has a prolific yield, and it is expected that triton reactions with other light elements will be useful sources of fast neutrons when tritium becomes available in sufficient quantities to be used in accelerators.

Another means of obtaining fast tritons is offered by the high neutron flux in the NRX pile. The tritons are released in the reaction $Li^6(n, \alpha)T$ for which the cross section for thermal neutrons is 870 barns. It has been possible to study the secondary reactions due to the tritons producing fast neutrons in the graphite thermal column of the pile. Here the naturally occurring level of fast neutrons is very low.

This report describes an experiment to measure the thick target yields and slowing down lengths in graphite of the fast neutrons produced by triton bombardment of lithium compounds, some containing deuterium. In addition to the fast neutrons from the T + D reaction, neutrons from a T + Li reaction were detected and studied. The latter appears not to have been reported previously in the literature.

When a lithium compound is irradiated with thermal neutrons, tritons of

[1] *Manuscript received March 20, 1950.*
Contribution from the Nuclear Physics Branch, Atomic Energy Project, National Research Council of Canada, Chalk River, Ontario, Canada. Issued as N.R.C. No. 2162.

2.65 Mev. energy and α-particles of 2.00 Mev. energy are produced by the reaction Li(n, α)T (6, 7). These particles bombard the nuclei of the lithium compound and may produce reactions of the types:

$$T + Z^A \longrightarrow (Z+1)^{A+2} + n_0^1 + Q, \qquad (a)$$

and

$$\alpha + Z^A \longrightarrow (Z+2)^{A+3} + n_0^1 + Q, \qquad (b)$$

which give fast neutrons if the energy balance Q is positive. For the common isotopes of the light elements, except boron and beryllium, reactions of type (b) are endothermic (see Table II) and will not occur with α-particles of 2.0 Mev. energy, or if they are energetically possible the yield is small (13) owing to the short range of the α-particle in the material of the target and the effect of the potential barrier of the nucleus. Therefore, the fast neutrons produced can be assigned to triton reactions of type (a), and the data obtained give the thick target yields for 2.6 Mev. tritons on the compounds used. By using a detector which is insensitive to slow neutrons, these fast neutrons can be detected and information about their yield and energy obtained in the presence of a high thermal neutron flux.

In this experiment calibrated indium resonance detectors were used to detect the fast neutrons after they had been slowed down to indium resonance energy, and the number of fast neutrons emitted per second by the source obtained by graphical evaluation of the space integral of the indium activity (1, 2). The number of incident tritons was calculated from the thermal neutron flux at the surface of the source, the amount of lithium in the source, and the thermal neutron capture cross section of lithium.

Experimental Arrangement

The thermal column of the Chalk River pile was used as a large block of scattering material with a high flux of thermal neutrons, as shown in Fig. 1. The lithium compound was loaded into a spherical shell container, 12 cm. in outside diameter, which was placed on the central line of the column 152 cm. from the front face. Each container consisted of two concentric shells made of 1/32 in. stainless steel with 1 cm. space between them to hold the lithium compound, and a solid graphite sphere to fill the central space. With the pile operating, the thermal neutron flux at the surface of the shell was measured with four calibrated manganese foils fastened with cellulose tape to the graphite blocks in contact with the container. The thermal neutron flux was also monitored at the front face of the thermal column by indium and manganese detectors and the pile power monitored at an experimental hole so that separate runs could be normalized. The central string of graphite blocks were slotted to hold the indium resonance detectors, which were indium foils 3.3 by 5.7 cm. in area and 113 mgm. per cm.^{2} thick contained in disk-shaped cadmium boxes. These were made in two halves each that screwed together so as to have a wall thickness 2 mm. of cadmium on all sides. The detectors were

calibrated by putting a Ra-α-Be source of known neutron emission in place of the shell during a shutdown period of the pile and obtaining the space integral of the activity as described below.

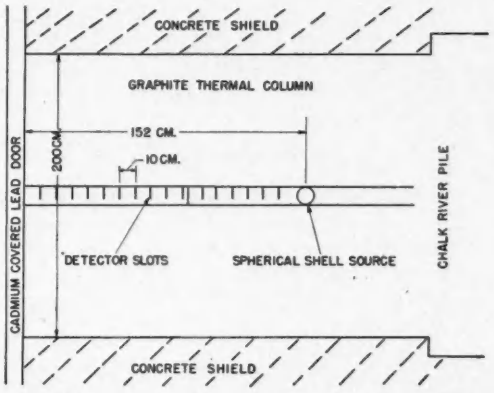

FIG. 1. *Experimental arrangement in thermal column of NRX pile.*

To minimize the effect of one indium detector on the adjacent ones they were loaded in alternate slots for each run, taking care always to place them with the same side facing the source and filling the remaining slots with graphite disks. After the activation these detectors were wrapped around a thin-walled aluminum β-counter and counted, first with one side facing the counter and then the other to minimize the orientation effect caused by the gradient of the neutron density. The background counting rate was subtracted and the readings corrected to zero decay and to saturation irradiation, taking 54.5 min. as the half-period of the indium activity. To calibrate the counters for sensitivity, six identical indium foils were irradiated in fixed positions in a paraffin wax box containing a 1.2 gm. Ra-α-Be source of neutrons and their activities measured on the counters each day. The counting losses at high counting rates were estimated from the measured decay of actinium active deposit, the half-period of which is known accurately as 36.1 min. (14), and corrections applied where necessary.

Calibration of Indium Resonance Detectors

If a point source of fast neutrons is surrounded by a large volume of a slowing down medium in which there is no capture of neutrons above thermal energy, then

$$Q_s = 4\pi \int_0^\infty q(E, r) r^2 dr,$$

where Q_s = emission from the point source in neutrons per second,
r = radial distance from the source,
and $q(E, r)$ = number of neutrons per second passing through the energy E per cc. at distance r from the source.

If a detector, sensitive only to neutrons of essentially one energy E_0 is used, e.g., an indium resonance detector, then its saturation activity $A(r)$ is proportional to the number of neutrons per second that pass through the energy E_0 per cc. at the detector:

i.e., $$q(E_0, r) = kA(r).$$

Therefore $$Q_s = 4\pi k \int_0^\infty A(r)r^2dr = k_0 \int_0^\infty A(r)r^2dr,$$

where $k_0 = 4\pi k$,

and $A(r)$ = activity of the detector placed at a distance r from the source.

For any given source, $A(r)$ can be measured by experiment at various values of r and the integral evaluated graphically in arbitrary units. To obtain the constant k_0 it is necessary to use a source of known neutron emission Q_s and of sufficient strength to give the required statistical accuracy in the counting rates $A(r)$ at large values of r. Once k_0 is known, the foils can be used to measure the emission of fast neutrons from another source.

Two sources for which the absolute neutron emission had been determined were available. Source No. 1 consisted of 600 mgm. of radium surrounded by a beryllium capsule weighing about 8 gm. By means of the spatial integration method (1, 2) in water the neutron emission of this source had been compared with that of the same radium surrounded by a similar beryllium capsule. Gluckaüf (9) by a method developed by Paneth and Gluckaüf (10) then measured the amount of helium produced by the (γ, n) reaction on the beryllium in the latter capsule. This measurement, combined with the comparison of the emissions from the two beryllium capsules, gave an emission of 3.03×10^5 neutrons per sec. from source No. 1 with an error estimated at $\pm 3\%$. Source No. 2 was a 200 mgm. Ra-α-Be source that had been calibrated in terms of the standard source at the Argonne National Laboratory, Chicago. The absolute neutron emission of the standard source had been obtained by Seidl and Harris (16). The emission of source No. 2 was given as 2.8×10^6 neutrons per second, $\pm 7\%$.

As these standards were too weak to give good counting rates at large distances from the source in the graphite, a 1.2 gm. Ra-α-Be source was calibrated in terms of the standards by comparing the activities induced in a tank of manganese sulphate solution (3, 19) irradiated by each of the three sources in turn. The tank was 60 cm. in diameter and filled to a level of 60 cm. depth with a nearly saturated solution of manganese sulphate (density of solution = 1.37 gm. per cc.). Each neutron source was suspended by a string in the center of the liquid overnight. After removing the source from the tank the manganese γ-ray activity was measured by observing the rate of deflection of a quartz-fiber electroscope connected to a large ion chamber filled to a pressure of 20 atm. with argon and immersed in the solution. A correction of 5% for loss of neutrons through the wall of the tank was applied in the case of the Ra-α-Be sources. Owing to the shorter slowing down length of the neutrons from the Ra-γ-Be

source [2.5 cm. in water as compared with 6.8 cm. for Ra-α-Be neutrons (12)] no correction to the readings obtained with the photo-neutron source was required.

The results obtained were

1.2 gm. source = $64(\pm 4\%) \times$ No. 1 = $64 \times 3.03 \times 10^5 = 19.4 \times 10^6$ neutrons per sec.

1.2 gm. source = $6.42(\pm 2\%) \times$ No. 2 = $6.42 \times 2.8 \times 10^6 = 18.0 \times 10^6$ neutrons per sec.

Mean value of 1.2 gm. Ra-α-Be emission = $\underline{18.7 \times 10^6}$ neutrons per sec.

Using the 1.2 gm. neutron source in the chosen position in the thermal column with the pile shut down, the value

$$\int_0^\infty A(r) r^2 dr = 2.35 \times 10^8 \text{ counts per min.} \times \text{cm.}^3 \text{ was obtained.}$$

Hence the detector constant

$$k_0 = \frac{18.7 \times 10^6}{2.35 \times 10^8} = 7.96 \times 10^{-2} \frac{\text{neutrons per second}}{\text{counts per minute} \times \text{cm.}^3}.$$

Calibration of Manganese Monitors of Thermal Neutron Flux

There were available manganese foils, 1 cm. square, that had been calibrated by irradiating them in a thermal neutron flux the absolute value of which had been determined by means of a small, BF_3-filled, pulse ion chamber of known counting volume and boron content (8). The activity of the foils was measured by counting with a Geiger–Müller counter in standard geometry, and calibrated for sensitivity by a standard uranium foil.

The calibrated foils were not suitable for measuring the strong neutron fluxes encountered in the thermal column, as they became too active for the available measuring equipment. Instead, small disks of manganese foil, 1/8 in. in diameter, were stamped out and pressed into small 1 cm. squares of 3/64 in. aluminum sheet, which could be mounted in the standard foil holders. The small foils were calibrated for flux measurement by irradiating them simultaneously with the standard foils in a paraffin box with a 1.2 gm. Ra-α-Be source of neutrons and counting them on the standard counters. This was repeated until every foil had been irradiated in each position in the box, and the mean counting rate was associated with the average flux of thermal neutrons. This comparison showed a variation of $\pm 4\%$ in sensitivity among the small foils.

When used in the thermal column the small foils could be measured conveniently on a TQQ electroscope* but were too active to count in the standard geometry, and it was therefore necessary to obtain the conversion factor to change rate of deflection in divisions per minute on the electroscope to counts per minute on a standard counter. This was done by following the decay of a

* *This type of electroscope was designed by Dr. H. Carmichael of this laboratory.*

foil initially on the electroscope, then on an ion chamber connected to a vibrating reed electrometer, and when the activity had decayed sufficiently to count it on three of the standard counters. It was found that 1 div. per min. on the electroscope = 186 mv. per min. on the ion chamber and that 1 mv. per min. on the ion chamber = 259.5 counts per min. A blank aluminum mount was irradiated and counted simultaneously and its activity subtracted to get the activity of the manganese without a holder. The readings, converted to divisions per minute on the electroscope, are plotted on a logarithmic scale against time in Fig. 2. The slope yields a half-period of 2.60 ± 0.01 hr., in good agreement with the accepted value of 2.59 hr. (15) for Mn^{56}.

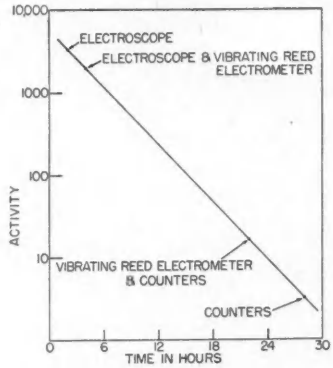

FIG. 2. *Decay of activity of manganese foils used to monitor thermal neutron flux. Half-period = 2.60 ± 0.01 hr.*

From the above intercomparisons the small manganese foils were calibrated to measure high thermal neutron fluxes with the aid of a TQQ electroscope.

Results

The following lithium compounds were irradiated: lithium fluoride, lithium carbonate, lithium hydroxide, lithium deuteroxide paste ($LiOD.D_2O + D_2O$), and lithium deuteroxide.* In order to determine the background due to epi-cadmium neutrons from the pile, runs were made with a mixture of boric acid and graphite, adjusted to give about the same total capture cross section as the lithium compounds (all approximately 300 $cm.^2$). To check the yield of photo-neutrons from the deuterium in the deuteroxide a run was made with $Ca(OD)_2$. The counting rates normalized as described in the following paragraph are plotted against the distance from the center of the source in Fig. 3.

* *The lithium fluoride and lithium carbonate were N. F. grade chemicals supplied by Mallinckrodt Co. and the lithium hydroxide C.P. grade. The lithium deuteroxide was made by the Chemical Control Branch and analyzed as 84.4% LiOD, 5% moisture (mostly D_2O), 2.3% $CaCO_3$ and 8% insoluble. The $LiOD.D_2O + D_2O$ was obtained by adding D_2O to this. Analysis showed the LiOD to be 72 atom %D. The D_2O added to form the $LiOD.D_2O + D_2O$ was better than 98 atom %D.*

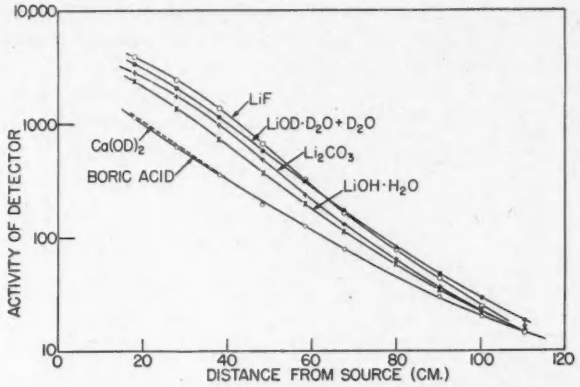

FIG. 3. *Detector activity, $A(r)$, vs. distance, r, from the source. The curve for boric acid represents the activity due to the background of epicadmium neutrons in the thermal column. The increase of the detector activity with the lithium compounds shows that fast neutrons are produced by the lithium compounds.*

With each lithium compound two runs were made with the detectors in alternate slots. To correct for the different effects of the cadmium-covered detectors on the thermal neutron flux at the source the results for the two positions were plotted as shown for lithium fluoride in Fig. 4. Here the activities have been normalized to the same pile power, corrected to saturation and zero decay, and the background from fast pile neutrons subtracted. The points for the two runs fall on two curves, whose corresponding ordinates have a constant ratio, which is the normalization factor required to bring the curves into coincidence with each other.

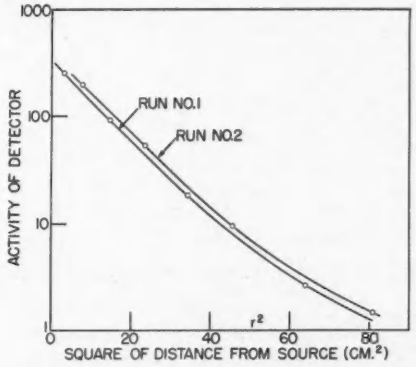

FIG. 4. *Detector activity vs. r^2 for LiF. Note—abscissas shown should be multiplied by 100.*
Run No. 1—Nearest detector is 17.9 cm. from the source.
Run No. 2—Nearest detector is 28.0 cm. from the source.
Ratio of ordinates gives normalization factor to bring the curves into coincidence.

In Figs. 5 and 6 are plotted the normalized values of Ar^2 vs. r after subtraction of the background due to epicadmium pile neutrons and the background due to photo-neutrons from the deuterium. The fast neutron emissions from the samples were obtained from the areas under the curves and the indium detector constant previously measured. Table I lists the compounds

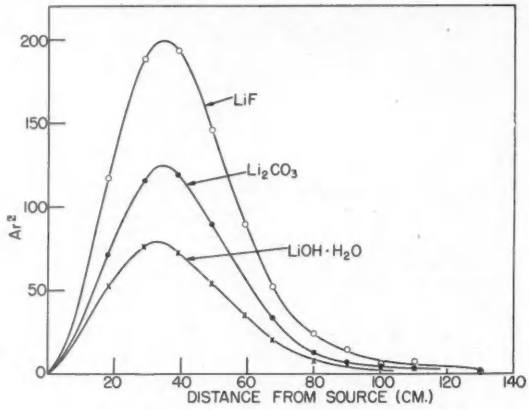

FIG. 5. *Plot of Ar^2 vs. r for the compounds not containing deuterium. The area under each curve is proportional to the neutron emission from the sample.*

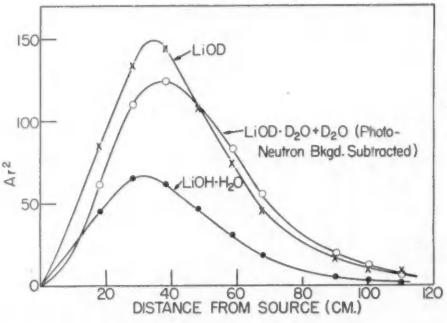

FIG. 6. *Plot of Ar^2 vs. r for deuteroxides and the hydroxide. The area under each curve is proportional to the neutron emission from the sample.*

used and the neutron emission observed together with the number of incident tritons as calculated from the thermal neutron flux measured at the surface of the shells and the amount of lithium in the samples, using 65×10^{-24} cm.^{2} per atom of natural lithium for the cross section of the Li(n, α)T reaction. In the case of lithium hydroxide the calculation of the number of thermal neutrons captured per second involves the scattering cross section of hydrogen atoms bound in lithium hydroxide molecules. This is not known exactly as it depends on the

chemical binding energy of the molecule and its mass. A value of 50×10^{-24} cm.^{2} per atom was used, which is intermediate between those of pure water (46×10^{-24} cm.^{2}) and paraffin (58×10^{-24} cm.^{2}) (21). The last three columns of Table I show the relative yields calculated on the following assumptions:

(1) The fast neutrons are produced only by (T, n) reactions on lithium and deuterium; i.e., neutron yields from the oxygen, carbon, and fluorine are assumed negligible in comparison.

(2) The thick target yield of neutrons is inversely proportional to the stopping power of the compound for 2.6 Mev. tritons.

TABLE I

THICK TARGET YIELDS FOR (T, n) REACTIONS

Substance	No. of tritons per second, $\times 10^{-10}$	Fast neutrons per second, $\times 10^{-6}$	Neutrons per 10^6 tritons	Observed relative yield	Calculated relative yield		
					T + Li	T + D	Total
LiF	43.9	118	26.8	100	100	0	100*
Li_2CO_3	41.6	71.7	17.2	64.1	64.6	0	64.6
$LiOH.H_2O$	31.0	47.1	15.2	56.5	50	0	50
$LiOD.D_2O + D_2O$	40.8	87.4	21.4	79.8	33.8	46†	79.8
LiOD	41.7	98.8	23.7	88.4	73.6	17.5	91.1

* *Calculated value normalized to 100 for LiF.*
† *Calculated value normalized to 46 for $LiOD.D_2O$.*

The atomic stopping powers of the light elements relative to air were taken from Livingston and Bethe's review article (11) and the values interpolated for the elements not listed.

Table II shows the neutron yields obtained by Roberts (13) for the bombardment of the same elements with polonium α-particles of 5.3 Mev. energy. As these yields are much less than those listed in Table I, (α, n) reactions cannot account for the fast neutrons observed in the thermal column in the presence of lithium compounds. Therefore the fast neutrons are attributed to (T, n) reactions of the type shown in Table III. For the following reasons it is believed that the neutrons observed are chiefly from the reactions of tritons on

TABLE II

THICK TARGET YIELDS FOR (α, n) REACTIONS (13)

Reaction	Q Mev.	Target material	Neutrons/10^7 α-particles
$Li^6(\alpha, n)B^9$	−3.96	Li_2CO_3	6.6
$Li^7(\alpha, n)B^{10}$	−2.78		
$O^{16}(\alpha, n)Ne^{19}$	−12	O_2	0.6
$C^{12}(\alpha, n)O^{15}$	−8.4	C	1.0
$F^{19}(\alpha, n)Na^{22}$	−0.4	CF_2	75
		CaF_2	50

TABLE III

Neutron producing reactions	Q, Mev.	Competing particle reactions (exothermic)	Q, Mev.
$D(T, n)\alpha$	+17		
$Li^6(T, n)Be^8$ $\hookrightarrow \alpha + \alpha$	+16	$Li^6(T, d)Li^7$	+1.4
$Li^6(T, n)2\alpha$	+16	$Li^6(T, p)Li^8$	+0.8
$Li^6(T, \alpha)He^5$ $\hookrightarrow \alpha + n$	+13.6		
$Li^7(T, n)Be^9$	+10.5		
$Li^7(T, \alpha n)He^5$ $\hookrightarrow \alpha + n$	+10.5	$Li^7(T, \alpha)He^6$	+9.3
$Li^7(T, 2n)Be^8$ $\hookrightarrow \alpha + \alpha$	+8.9		
$Li^7(T, 2n)2\alpha$	+8.9		
$F^{19}(T, n)Ne^{21}$	+12.1	$F^{19}(T, \alpha)O^{18}$	+11.9
$F^{19}(T, 2n)Ne^{20}$	+4.6	$F^{19}(T, p)F^{21}$	+7.0
$O^{16}(T, n)F^{18}$	+1.5	$O^{16}(T, \alpha)N^{15}$	+7.8
		$O^{16}(T, p)O^{18}$	+3.8
$C^{12}(T, n)N^{14}$	+4.1	$C^{12}(T, p)C^{14}$	+4.7
		$C^{12}(T, \alpha)B^{11}$	+3.8
$H^1(T, n)He^3$	−0.76*		

* *Threshold = 3.04 Mev. for tritons as bombarding particle (18).*

lithium and tritons on deuterium with contributions of less than 10% of the observed yields due to the other elements in the compounds:

(1) For all the substances used except the deuterides, the observed relative yields agree with the relative yields calculated on the assumption that all the neutrons are from the reaction of tritons on lithium.

(2) The neutron yield per triton for the lithium deuteroxide paste is greater than for the hydroxide and is much greater than the yield, relative to the other compounds, expected from the T + Li reaction. The increased yield is believed to be caused by neutrons from the reaction $D(T, n)\alpha$.

(3) In Fig. 7 the curves of Ar^2 vs. r are normalized to the same area, i.e., the same number of neutrons from the source. Within experimental error the points for lithium carbonate and lithium fluoride fall along a common curve, indicating that the neutrons from these compounds have the same energy distribution and are from the (T, n) reaction on lithium which is the only element common to both substances. In the case of lithium hydroxide the large slowing down power* of the hydrogen affects the distribution of the indium resonance neutrons about the source and alters the shape of the distribution curve.

* *Slowing down power = (scattering cross section per unit volume) × (average logarithmic energy loss).*

Quantitative corrections for these effects are difficult to calculate, and the slowing down distribution for the hydroxide cannot be compared exactly to the others. Qualitatively the presence of hydrogen is expected to decrease the slowing down length of the fast neutrons and therefore shift the distribution curve towards the source, as shown in Fig. 7.

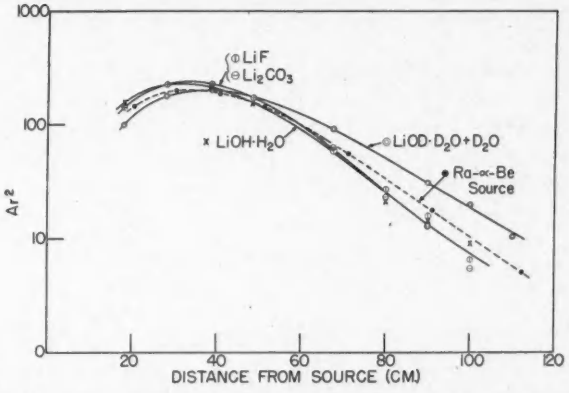

FIG. 7. *Plot of Ar^2 vs. r normalized to equal area under the curves. The curve for the compound containing deuterium lies higher at large distances from the source than the curve for the compounds without deuterium, which indicates that the neutrons from the T(d, n)α reaction are more energetic than those from the (T, n) reactions on lithium.*

(4) Table III shows that most of the possible (T, *n*) reactions on lithium lead to three product particles. This means that, depending on the angular distribution of the emitted particles, the neutrons have any energy between zero and the maximum possible. Therefore the mean energy of the neutrons from the Li (T, *n*) reactions is expected to be less than the maximum energy calculated from the *Q* value. This is known to be so for the Li^7 (*d*, *n*) reactions, which show resonances at deuteron energies of 0.65 and 1.02 Mev., corresponding to excitation levels of 17.17 and 17.45 in the Be^9 nucleus. The Li^6 (T, *n*) reactions also form the compound nucleus Be^9 excited to nearly the same energy (17.7 Mev.+ 2/3 of bombarding energy) as calculated from the masses and can be expected to produce a similar neutron distribution. Therefore the average energy of the neutrons from tritons on lithium is expected to be less than that of the neutrons from the T(*d*, *n*)α reaction, which emits only two particles and has a higher *Q* value than any of the lithium reactions shown in Table III. This expectation is supported by Fig. 7, which shows that the curve for the deuteroxide lies above those for the other compounds at large distances from the source, indicating that the deuteroxide yields more energetic neutrons, which have a longer slowing down length than the lithium neutrons.

(5) Table III shows that, with the exception of hydrogen, (T, *n*) reactions are energetically possible on all the elements present in the compounds used. However, it is believed that if the carbon, oxygen, or fluorine contributed more

than 10% of the total yield a noticeable difference in the shape of the distribution curves would appear unless the neutrons produced in each case have similar energy spectra. This similarity is unlikely in view of the very different Q values for these three elements. Moreover, the relative yields of neutrons from Li_2CO_3, LiF, and $LiOH.H_2O$ would not agree with the relative yields calculated on the assumption that all the neutrons are due to lithium (Table I) if there were appreciable contributions to the neutron yield from the other elements.

Average Cross Sections

The atomic cross section, σ, for the production of neutrons by bombardment of lithium with tritons is a function of the triton energy, i.e., of the residual range of the triton. The thick target* yield of neutrons produced by 2.6 Mev. tritons may be expressed as follows:

$$\text{No. of neutrons per triton} = N_{Li}\int_{R_t}^{0}\sigma(x)dx$$
$$= N_{Li}\sigma_{av}R_t,$$

where N_{Li} = number of atoms of lithium per cubic centimeter of target,
σ = cross section for neutron production per atom of lithium,
= a function of the residual range of the triton.
x = residual range of the tritons in the target,
R_t = range of 2.6 Mev. tritons in the target,
σ_{av} = average atomic cross section for 2.6 Mev. tritons.

Since the range of the tritons is inversely proportional to the stopping power of the target

we have $R_t = R_a \dfrac{\text{(Stopping power of air)}}{\text{(Stopping power of target)}} = R_a(N_a S_a/N_t S_t)$,

where R_a = range in air at S.T.P. of 2.6 Mev. tritons,
S_a = molecular stopping power of air,
S_t = molecular stopping power of target,
N_a = Number of molecules per cubic centimeter of air at S.T.P.,
N_t = Number of molecules per cubic centimeter of target.

We have therefore:

$$\text{No. of neutrons per triton} = N_{Li}\,\sigma_{av}\,R_a\frac{(N_a S_a)}{(N_t\,S_t)}.$$

Substituting the known values:

Range of tritons in air (6) = R_a = 6.0 cm. at 15°C. and 760 mm. press.,

Molecular stopping power of air (11) = S_a = 2,

Number of molecules per cubic centimeter of air = $N_a = 2.55 \times 10^{19}$ at 15°C. and 760 mm. press.,

* *Thick target: target in which the tritons are completely stopped.*

we obtain:

$$\text{Number of neutrons per triton} = 30.6 \times 10^{19} \frac{(N_{Li})}{(N_t S_t)} \sigma_{av}.$$

For a pure chemical $\frac{N_{Li}}{N_t}$ is the number of lithium atoms per molecule and is independent of the density or physical form of the compound. For the powders used about half of the volume was air but as the stopping power of the solid is about 1000 times as great as air the tritons expend most of their energy in the solid and a negligible amount in the air. Table IV shows the average cross section for neutron production by 2.6 Mev. tritons as calculated from the observed yields. The mean value is 1.5×10^{-24} cm.^{2} for lithium.

TABLE IV

Substance	No. of neutrons per 10^6 tritons	$30.6 \frac{N_{Li}}{N_t S_t}$	σ_{av}, cm.$^2 \times 10^{24}$
LiF	26.8	18.3	1.46
Li_2CO_3	17.2	11.8	1.45
$LiOH.H_2O$	15.2	9.11	1.67

Mean value $\sigma_{av} = 1.5 \times 10^{-24}$cm.^{2}

Using the average cross section given in Table IV we can calculate the yield of neutrons from the reaction of tritons on lithium in the deuterides and obtain:

Observed yield for $LiOD.D_2O + D_2O$ = 21.4×10^{-5} neutrons per triton
Estimated yield of tritons on lithium = 9.3×10^{-5} neutrons per triton
Difference = 12.1×10^{-5} neutrons per triton
= yield due to tritons on deuterium.

Observed yield for LiOD = 23.7×10^{-5} neutrons per triton.
Estimated yield of tritons on lithium = 20.3×10^{-5} neutrons per triton
Difference = 3.4×10^{-5} neutrons per triton
= yield due to tritons on deuterium.

Using these yields we obtain the average cross section of 2.6 Mev. tritons on deuterium:

$LiOD.D_2O + D_2O$ $\sigma_{av} = 0.41 \times 10^{-24}$ cm.^{2}
LiOD $\sigma_{av} = 0.31 \times 10^{-24}$ cm.^{2}

The value for LiOD depends on the difference of two nearly equal quantities (observed yield − estimated yield of tritons on lithium) and is much less accurate than the value from $LiOD.D_2O + D_2O$ where this difference is larger.

The D(T, n)α cross section can be compared to the cross section measured by Bretscher and French (5), Baker *et al.* (4) and Taschek *et al.* (17) up to 3.7

Mev. triton energy. By using the range-energy relation for tritons (11) and their results, σ was plotted against x and the integral $\int_{R_t}^{0} \sigma(x)dx = 3.0 \times 10^{-24}$ cm.^{2} obtained graphically for 2.6 Mev. tritons. This gives:

$$\sigma_{av} = \frac{3.0 \times 10^{-24}}{6.0} = 0.50 \times 10^{-24} \text{ cm.}^2$$

which may be compared with 0.41×10^{-24} cm.^{2} obtained in this experiment.

It appears that with 2.6 Mev. tritons the average cross section for neutron production is greater with lithium than with deuterium. This in part may be due to the fact that some of the lithium reactions can produce two neutrons per disintegration. For a thick target of pure lithium the yield would be one neutron per 1130 incident tritons of 2.6 Mev. energy.

Slowing Down Lengths

In Fig. 7 the curves of Ar^2 vs. r have been normalized to the same area and are plotted together with the curve obtained with a Ra-α-Be source in the same graphite.

Assuming a spherical shell source, corrections can be calculated to obtain the distribution from a point source (20). The activity at a distance r from the shell source is multiplied by a factor $\left(\exp.\frac{R^2}{4\theta}\right) \Big/ \left(\frac{2\theta}{rR}\sinh\frac{rR}{2\theta}\right)$ to obtain the activity at the same distance from a point source with the same total emission. R = radius of shell, $\theta = L_s^2$ = symbolic age, r = distance from center of source. The symbolic age obtained from the uncorrected curves was used to calculate the correction factor to be applied to convert the readings to a point source. The corrections are less than 2% up to 60 cm., 4% at 80 cm., and 7% at 100 cm. Calculations by Mr. S. Kushneriuk also showed that the corrections due to lack of symmetry in the source are small.

Examination of Fig. 7 shows that the curve for (T + Li) neutrons lies lower at large values of r than the curve for the Ra-α-Be source, indicating that there are fewer very high energy neutrons from (T + Li) than from the Ra-α-Be. The curve for $LiOD.D_2O + D_2O$ lies higher at large r than any of the others, indicating that the neutrons from this are more energetic. The slowing down lengths L_s obtained are shown in Table V. These were obtained by graphical integration of the expression:

$$L_s^2 = \frac{1}{6}\int_0^\infty Ar^4dr \Big/ \int_0^\infty Ar^2dr.$$

About 20% of the integral of the Ar^4 curve is due to points beyond 80 cm. from the source where the statistical accuracy was poor. The common curve shown in Fig. 7 beyond 80 cm. from the source for the lithium compounds not containing deuterium was used to extrapolate the Ar^4 curves to infinity in the cases of LiF, Li_2CO_3, and $LiOH.H_2O$. Subtracting the effect due to T + Li

neutrons from the curves for the $LiOD.D_2O + D_2O$ gives the slowing down length for $T(d, a)n$ neutrons = 23.4 cm. which is much less than expected from the elementary age-velocity theory (about 33 cm. for 14 Mev. neutrons). Owing to the low intensity at large distances from the source the measured value of slowing down length for the $T(d, a)n$ neutrons may be considerably in error, but it is believed to be significantly lower than the calculated value. This indicates that inelastic scattering of the fast neutrons occurs in the graphite so that fewer collisions are necessary to degrade their energy to indium resonance than would be expected assuming elastic scattering.

TABLE V

Target	$\int_0^\infty Ar^4dr$ Counts/min.	$\int_0^\infty Ar^2dr$ Counts/min.	Slowing down length (cm.) in graphite (Density 1.64 gm./cc.)
	$\times 10^{-11}$ cm.^{5}	$\times 10^{-8}$ cm.^{3}	
LiF	33.0	14.8	19.3
Li_2CO_3	19.6	9.01	19.0
$LiOH.H_2O$	12.3	5.91	18.6
$LiOD.D_2O$	30.9	10.96	21.6
LiOD	28.7	12.4	19.7
Ra-α-Be	5.73	2.35	20.2

Errors

The counting rates of the indium resonance detectors were such that the statistical standard deviation was less than 2.5% out to r = 50 cm., equal to 10% at r = 80 cm., 20% at 90 cm., and about 35% at 100 cm. These are per cent errors in the activity due to neutrons from the source after background is subtracted. Since only about one-third of the area under the Ar^2 curves is beyond 50 cm. and only one-eighth beyond 80 cm., the error in the area due to statistics is about 5%.

The greatest uncertainty in the experiment is in calculating the number of neutrons captured by the lithium from the neutron flux measured at the surface of the shells by means of manganese foils. The flux as measured by the foils depends on the scattering properties of the shells as well as on the absorption cross section and cannot easily be related to the number of neutrons captured by the lithium. Approximate calculations, carried out by Mr. Kushneriuk, are believed to be accurate to about 10%.

Owing to the flux gradient in the thermal column the thermal neutron distribution is not symmetrical about the source, and hence the shell source is not symmetrical. Calculations by Mr. Kushneriuk have shown that the yield obtained from the Ar^2 vs. r curves due to this are 5% low. This has been corrected for.

The absolute yields depend on the value of the neutron emission from the Ra-α-Be source which was measured in terms of two standards and is believed

to be known to 5%. However the method of comparing this yield with the yields of the lithium compounds by the spatial integral of the resonance activities is not believed to give better than 10% accuracy, owing to the difficulty of locating the foils and source accurately in the thermal column and the poor statistics at large distances from the source and the high background of fast neutrons in the thermal column.

The absolute value of the thermal neutron flux as determined by the manganese flux monitor at the face of the shell is estimated to be accurate to about 10%.

Considering all errors the absolute yields are believed accurate to 20%.

Acknowledgments

The writer wishes to thank Dr. B. W. Sargent for suggesting the problem and for his interest in the work. He is also indebted to Mr. S. Kushneriuk, who carried out the calculations of the number of thermal neutrons captured per second by the samples, and to Mr. W. F. Merritt of the Chemical Control Laboratory, who prepared the lithium deuteroxide.

References

1. AMALDI, E. and FERMI, E. Phys. Rev. 50: 899. 1936.
2. AMALDI, E., HAFSTAD, L. R., and TUVE, M. A. Phys. Rev. 51: 896. 1937.
3. ANDERSON, H. L., FERMI, E., and SZILARD, L. Phys. Rev. 56: 284. 1939.
4. BAKER, C. P., HOLLOWAY, M. G., KING, L. D. P., and SCHREIBER, R. E. The cross section for the reaction D(T, α)n. Declassified report AECD-2226, United States Atomic Energy Commission.
5. BRETSCHER, E. and FRENCH, A. P. Phys. Rev. 75: 1154. 1949.
6. BHGGILD, J. K. and MINNHAGEN, L. Phys. Rev. 75: 782. 1949.
7. CØADWICK, J. and GOLDHABER, M. Nature, 135: 65. 1935.
8. FENNING, F. W. Calibration of a manganese foil for the absolute measurement of a flux of thermal neutrons. Unpublished report MP-252, Montreal Laboratory, National Research Council of Canada. 1946.
9. GLUCKAÜF, E. Preliminary report on the number of neutrons emitted by a beryllium-radium photo-source. Unpublished report BR-674, British Atomic Energy Establishment. 1945.
10. GLUCKAÜF, E. and PANETH, F. A. Proc. Roy. Soc. (London), A, 165: 229. 1938.
11. LIVINGSTON, M. S. and BETHE, H. A. Revs. Modern Phys. 9: 272. 1937.
12. MUNN, A. M. and PONTECORVO, B. Can. J. Research, A, 25: 157. 1947.
13. ROBERTS, J. H. Neutron yields of several light elements bombarded with polonium alpha particles. Declassified report MDDC-731, United States Atomic Energy Commission.
14. SARGENT, B. W. Can. J. Research, A, 17: 103. 1939.
15. SEABORG, G. T. and PERLMAN, I. Revs. Modern Phys. 20: 585. 1948.
16. SEIDL, F. G. P. and HARRIS, S. P. Rev. Sci. Instruments, 18: 897. 1947.
17. TASCHEK, R. F., EVERHART, G., GITTINGS, H. T., HEMMENDINGER, A., and JARVIS, G. Preliminary results on the cross section of the reaction $T^3(d, n)He^4$ between 1.0 and 2.5 Mev. deuteron energy. Declassified report AECD-2250, United States Atomic Energy Commission.
18. TASCHEK, R. F., JARVIS, G. A., ARGO, H. V., and HEMMENDINGER, A. Phys. Rev. 75: 1268. 1949.
19. TASCHEK, R. F. and TURNER, C. M. Cross sections by the Be^7 and Mn-bath methods. Parts I and II. Declassified report MDDC-737, United States Atomic Energy Commission.
20. WALLACE, P. R. and LECAINE, J. Elementary approximations in the theory of neutron diffusion. Declassified report MT-12, Montreal Laboratory, National Research Council of Canada. 1943.
21. WAY, K. and HAINES, G. Thermal neutron cross section for elements and isotopes, H–Bi. Declassified report AECD-2138, United States Atomic Energy Commission.

ON THE DIFFERENTIAL EQUATIONS OF DIFFUSION[1]

By J. D. Babbitt

Abstract

The fundamental bases of the differential equation of diffusion are examined. From a dynamical equation defining the motion of the gas, an equation of continuity expressing the law of conservation of mass, and an equation of state giving the relation between concentration and pressure, the differential equations are derived for the interdiffusion of two gases, for the diffusion of vapors, and for the diffusion of gases and vapors through solids. For the diffusion of gases through adsorbing solids, the dynamical equation of the flow is obtained by equating the space derivative of the spreading pressure of the adsorbed film to a resistive force equal to the product of the coefficient of resistance and the velocity of the film. The differential equations derived on this assumption agree qualitatively with measurements for the diffusion of gases through metals when the adsorption can be represented by Langmuir's equation. When the adsorption follows the BET equation, qualitative agreement is found with the diffusion of water vapor through hygroscopic materials. It is also shown that Fick's law is not generally valid as the fundamental equation of diffusion.

Introduction

During recent years, the flow of gases and vapors through solid materials has been extensively studied. The solids investigated have ranged from metals to materials of high porosity, and an attempt has been made to explain the flow by a great variety of mechanisms. Where the flow has been through finite pores within the solid and where there has been an absolute pressure difference so that the flow has been hydrodynamical rather than diffusive, the amount of gas transferred has been satisfactorily explained over all ranges of pressures and degrees of porosity by various theoretical formulas. Where, however, the flow has been diffusive, either the interdiffusion of two gases through a porous barrier or the diffusion of a single gas into a nonporous solid such as a metal, the results have not been satisfactorily explained, and, in consequence, it is desirable to re-examine the fundamental assumptions of diffusion.

Whenever a theory of the diffusion of gases through solids is presented, Fick's law is invariably used as the fundamental equation. Barrer (3) gives this law in two forms, first, as the equation for the steady state of flow,

$$\mathbf{P} = -D_c \frac{\partial c}{\partial x}, \tag{1}$$

where the rate of permeation $\mathbf{P}$ is given in terms of the concentration gradient, $\frac{\partial c}{\partial x}$, and the diffusion coefficient, D_c, and, second, in the form,

$$\frac{\partial c}{\partial t} = D_c \frac{\partial^2 c}{\partial x^2}, \tag{2}$$

[1] *Manuscript received February 25, 1950.*
Contribution from the Division of Physics, National Research Laboratories, Ottawa, Canada. Issued as N.R.C. No. 2172.

which gives the variation of the concentration with time and which is analogous to Fourier's equation for the flow of heat.

These equations have long been used with great success to describe the interdiffusion of gases and solutions. With both gases and solutions, however, an assumption can safely be made which does not necessarily hold when a solid is present, namely, that the concentration is linearly proportional to the pressure. When this assumption is true, the substitution of p for c in Equation (1) results only in a change of the numerical value of the constant D_c and it is not necessary to distinguish carefully between the part played by the pressure and the concentration. When, however, the diffusion is through solids the relation between pressure and concentration is seldom linear owing to the complexities of adsorption, and it is essential to know whether Equation (1) or the equivalent equation in terms of the pressure gradient is the correct statement of the law governing the diffusion.

It is very probable that the tendency to use Equations (1) and (2) as the fundamental equations for diffusion without examining explicitly the assumptions involved arises from a confusion between the kinetic picture of diffusion represented by Meyer's equation and the macroscopic picture represented by a differential equation such as (2). Although in Meyer's equation (cf. Jeans: The Dynamical Theory of Gases—Chapter XIII) the number of molecules transferred is proportional to the concentration gradient, it does not automatically follow that, in an equation such as (2), which is essentially a field equation, the concentration is the correct quantity to use. A study of the analogous differential equations for the flow of heat, electricity, and magnetism shows that the fundamental equation of flow expresses the flux as proportional to the gradient of a potential function (the temperature, electromotive force, and the magnetic potential, respectively). In diffusion, the corresponding potential function is the pressure and not the concentration and from analogy one should infer that the fundamental equation should be expressed in terms of the pressure.

A second source of confusion has been the failure to distinguish diffusion from other flow mechanisms. The term diffusion has been used so loosely that it is often difficult to know what is precisely meant. In this paper, we shall restrict the term diffusion to two mechanisms of flow corresponding to two distinct kinds of resistive forces. Where the flow is confined to the gaseous phase, we shall use the term diffusion only when the total pressure is everywhere equal and only differences of partial pressure exist. Under these conditions, we assume that the force resisting the movement of gas A through gas B is due predominantly to the interference which the molecules of gas B offer to the movement of the molecules of gas A, and conversely that the force resisting the movement of gas B is due predominantly to the interference of the molecules of A. When, on the other hand, the flow is through an adsorbing solid, gas may be transported in the adsorbed phase, and we shall also apply the term diffusion to such transport when there is a movement of the gas in the

adsorbed phase from points of high to those of low concentration. Restricting ourselves to these two specific mechanisms of flow we shall proceed to derive the differential equation which shall govern such diffusion.

In deriving the differential equation, we are indebted to Muskat (9) who was faced with a similar problem in studying the flow of gases and liquids through sands. There are differences between Muskat's problem and ours. We are limiting ourselves to diffusion in the restricted sense outlined above. Muskat was interested only in flow with an absolute pressure gradient and he assumed that his flow could be defined by Darcy's equation. When these differences are kept in mind, however, Muskat's problem is exactly the same as ours, namely, to derive the partial differential equation for the flow, and it is possible to adapt his analysis to our problem. Therefore, to show what is involved, we shall proceed to outline very briefly the treatment used by Muskat and shall then use this method as a model to derive the differential equations of diffusion.

Muskat's Development of the Equations for the Flow of a Homogeneous Fluid Through Porous Media

In developing the equations for the flow of a homogeneous fluid through porous media, Muskat has pointed out that three separate conditions must be satisfied. These conditions are expressed by:

(i) The dynamical equation of motion,

(ii) The equation of continuity,

and (iii) The equation of state.

The dynamical equation defines the nature of the flow, the equation of continuity is the mathematical expression of the law of conservation of mass, and the equation of state expresses the relation between the density and the pressure of the gas.

To develop the dynamical equation we know that, in general, a volume element of fluid will be subject to three types of forces. These are (1) the pressure gradients of components $\frac{\partial p}{\partial x}$, $\frac{\partial p}{\partial y}$, and $\frac{\partial p}{\partial z}$, (2) the external "body forces", such as gravity, of components F_x, F_y, and F_z acting on unit volume of the fluid, and (3) the forces opposing the motion of the fluid, which are due to the internal resistance of friction and which may be written in the form A_x, A_y, and A_z. By equating these forces to the product of the mass and acceleration of the volume element, we obtain the generalized equation of motion. Thus, in one dimension,

$$\rho \frac{Du}{Dt} = -\frac{\partial p}{\partial x} + F_x + A_x, \tag{3}$$

where, following common usage, $\frac{D}{Dt}$ denotes a differentiation following the

motion of the fluid, ρ is the density and, u the component of velocity in the x-direction. (Note: Throughout this paper we shall, for convenience, write all formulas in one dimension only. The expansion to three dimensions will be readily apparent.)

As Muskat points out, when the velocity of flow is small, the inertial or accelerative forces will be negligible compared to the other forces, so that the term on the left of (3) may be taken as zero. Although the effect of the gravitational forces will be appreciable in the interdiffusion of two gases of different densities, we are not, at present, interested in that aspect of the problem and we shall neglect all external forces. With these assumptions the dynamical equation reduces to

$$\frac{\partial p}{\partial x} - A_x = 0, \tag{4}$$

which states simply that the pressure gradient is balanced by the internal resistance or frictional forces.

For the type of flow in which he was interested, Muskat used Darcy's law as his fundamental dynamical equation. Darcy's law states that the velocity of a fluid flowing through a porous medium is directly proportional to the pressure gradient acting on the fluid. Mathematically this can be expressed

$$\frac{\partial p}{\partial x} + \frac{\mu}{k} u = 0, \tag{5}$$

where μ is the viscosity of the fluid and k is a factor depending on the permeability of the medium. Thus in Muskat's treatment

$$A_x = - \frac{\mu}{k} u. \tag{6}$$

The equation of continuity that applies to flow through porous bodies is that commonly used in hydrodynamics, namely,

$$\text{div } (\rho v) = \frac{\partial}{\partial x} (\rho v_x) + \frac{\partial}{\partial y} (\rho v_y) + \frac{\partial}{\partial z} (\rho v_z) = - \frac{\partial \rho}{\partial t}, \tag{7}$$

except that it is necessary to introduce the porosity f to compensate for the fact that the area of flow has been taken as the area of medium plus pores, whereas the volume containing the gas is that of the pores alone. Introducing the porosity and considering flow in one dimension only, we get

$$\frac{\partial}{\partial x} (\rho u) = - f \frac{\partial \rho}{\partial t}. \tag{8}$$

Muskat takes as his equation of state the general relation

$$\rho = \rho_0 p^m e^{\beta p},$$

where ρ_0 is the density at unit pressure and m and β are constants. With this

equation the particular fluids of physical significance may be classified as follows:

Liquids: $m = 0$,

incompressible liquids, $\beta = 0$,

compressible liquids, $\beta \neq 0$,

Gases: $\beta = 0$

isothermal expansion $m = 1$,

adiabatic expansion $m = \dfrac{\text{Spec. heat at const. vol.}}{\text{Spec. heat at const. pres.}}$

In the work that follows we shall be interested in gases only so that throughout we shall take $\beta = 0$.

By combining the dynamical equation with the equations of continuity and of state, Muskat obtains for the differential equation of flow, the expression

$$\frac{\partial \rho}{\partial t} = \frac{k}{(1+m) f \mu \rho_0^{1/m}} \frac{\partial^2 \rho^{\frac{m+1}{m}}}{\partial x^2}. \tag{9}$$

This equation occupies in Muskat's theory of the flow of fluids the same position that is occupied in the theory of the flow of heat by the equation

$$\frac{\partial \theta}{\partial t} = \kappa \frac{\partial^2 \theta}{\partial x^2}, \tag{10}$$

where θ is the temperature and κ the thermal diffusivity. Muskat goes on to point out the implications of this equation and, in particular, to derive the expression for the pressure gradient in steady flow and to show the difference between isothermal and adiabatic flow. We are not, however, directly interested in flow obeying Darcy's law, and having derived this equation as a model for diffusive problems we shall proceed no further with it.

The Differential Equation for the Interdiffusion of Two Gases

In applying this analysis to diffusion, we find that the fundamental dynamical equation for diffusion was developed by Stefan and Maxwell in the nineteenth century but that, in the meantime, the hydrodynamical approach to diffusion represented by such an equation has been neglected. The best presentation is contained in the article on "Diffusion" by G. H. Bryan and A. W. Porter in the fourteenth edition of the Encyclopedia Britannica and we are largely indebted to them for the ideas used in this section.

The fundamental concept of this picture is that, in the interdiffusion of two gases A and B, the portion of the gas A contained in a small element of volume v will experience from the gas B a resistance to its motion equal to $C\rho_1\rho_2 v(u_1 - u_2)$, where ρ_1, ρ_2, and u_1, u_2 are the densities and velocities of the gases A and B respectively and C is a quantity called the coefficient of resistance. It is ap-

parent that the gas B contained in the same volume element will experience an equal and opposite resistance $C\rho_1\rho_2 v(u_2 - u_1)$.

With this concept the dynamical equations can easily be set up. Thus Maxwell gives for the gas A the equation

$$\rho_1 \frac{Du_1}{Dt} + \frac{\partial p_1}{\partial x} - X\rho_1 + C\rho_1\rho_2 (u_1 - u_2) = 0, \tag{11}$$

where p_1 is the partial pressure of A and $X\rho_1$ the external forces. It is easy to show as before that the effects of inertia and of external forces are negligible so that we get,

$$\left.\begin{aligned} &\frac{\partial p_1}{\partial x} + C\rho_1\rho_2 (u_1 - u_2) = 0. \\ \text{Similarly for } B \qquad &\frac{\partial p_2}{\partial x} + C\rho_1\rho_2 (u_2 - u_1) = 0. \end{aligned}\right\} \tag{12}$$

These are the fundamental dynamical equations for the interdiffusion of two gases.

The total pressure of the system, $P = p_1 + p_2$, must remain constant and it follows that the fluxes of partial pressure due to the two gases must everywhere be equal and opposite so that $p_1u_1 + p_2u_2 = 0$. Also, since in diffusion all the motions are very slow compared with those set up by mechanical actions, we can assume that the flow is isothermal and can take as our equation of state that $p_1 = k_1\rho_1$ where k_1 is a constant. Thus

$$k_1\rho_1u_1 + k_2\rho_2u_2 = 0.$$

Now

$$\frac{u_1}{p_2} = -\frac{u_2}{p_1} = \frac{u_1 - u_2}{p_1 + p_2} = \frac{u_1 - u_2}{P},$$

so that

$$p_1u_1 = -p_2u_2 = \frac{p_1p_2(u_1 - u_2)}{P} = \frac{k_1k_2\rho_1\rho_2(u_1 - u_2)}{P}.$$

Substituting in the dynamical equations, we get

$$\frac{\partial p_1}{\partial x} + \frac{CP}{k_1k_2}(p_1u_1) = 0 \text{ and } \frac{\partial p_2}{\partial x} + \frac{CP}{k_1k_2}(p_2u_2) = 0. \tag{13}$$

Whence, substituting $p_1 = k_1\rho_1$ and $p_2 = k_2\rho_2$ and transposing we obtain

$$\rho_1u_1 = -\frac{k_1k_2}{CP}\frac{\partial \rho_1}{\partial x} \text{ and } \rho_2u_2 = -\frac{k_1k_2}{CP}\frac{\partial \rho_2}{\partial x}. \tag{14}$$

If we put $\frac{k_1k_2}{CP}$ equal to D, the coefficient of diffusion, we obtain Fick's law as expressed in Equation (1). We see, therefore, that (1) is a legitimate expression for the interdiffusion of two gases.

Substituting Equations (14) into the equation of continuity

$$\frac{\partial(\rho u)}{\partial x} = -\frac{\partial \rho}{\partial t},$$

we get the differential equation

$$\frac{\partial \rho}{\partial t} = D\frac{\partial^2 \rho}{\partial x^2}, \tag{15}$$

which is equivalent to Equation (2).

It is apparent, therefore, that according to this picture Fick's law is a correct and adequate representation of the interdiffusion of two gases. It should not be overlooked, however, that even here the fundamental dynamical equation,

$$\frac{\partial p_1}{dx} + C\rho_1\rho_2(u_1 - u_2) = 0$$

is expressed in terms of the pressure gradient and it has been possible to transform this into the commonly used concentration form of the law only by the assumption of Boyle's law as the equation of state.

The Diffusion of a Condensing Vapor

It has been pointed out by Stefan (13) that, where the diffusion is that of a condensing or evaporating vapor, there is no transfer of the second gas. Consider the evaporation of a gas from a liquid surface in a cylinder. Let p_1 and p_2 be the partial pressures and let the suffix 1 apply to the vapor and 2 to the permanent gas. Since there is no movement of the permanent gas $u_2 = 0$. As before we assume Boyle's law as the equation of state and put $p_1 = k_1\rho_1$ and $p_2 = k_2\rho_2$.

The fundamental dynamical equations are

$$\frac{\partial p_1}{\partial x} + C\rho_1\rho_2 u_1 = 0 \text{ and } \frac{\partial p_2}{\partial x} - C\rho_1\rho_2 u_1 = 0. \tag{16}$$

Since $p_1 + p_2 = P$, these reduce to

$$\frac{\partial p_1}{\partial x} + \frac{C(P - p_1)}{k_1 k_2}(p_1 u_1) = 0 \text{ and } \frac{\partial p_2}{\partial x} - \frac{C(P - p_1)}{k_1 k_2}(p_1 u_1) = 0. \tag{17}$$

Introducing the equation of state, we get

$$\rho_1 u_1 = -\frac{k_1 k_2}{C(P - p_1)}\frac{\partial \rho_1}{\partial x}. \tag{18}$$

If we follow Stefan and put $\frac{k_1 k_2}{C} = D_v$, the coefficient of diffusion, we have

$$\rho_1 u_1 = -\frac{D_v}{(P - p_1)}\frac{\partial \rho_1}{\partial x}$$

$$= \frac{D_v}{k_1}\frac{\partial}{\partial x}[\log(P - k_1\rho_1)]. \tag{19}$$

This is the equation for the mass transferred corresponding to Fick's law in the form (1). Introducing the equation of continuity, we get

$$\frac{\partial \rho_1}{\partial t} = -\frac{D_v}{k_1}\frac{\partial^2}{\partial x^2}[\log (P - p_1)]. \tag{20}$$

Thus we see that, in the diffusion of a vapor, the function $\log (P - k_1\rho_1)$ replaces the density ρ_1 used in the interdiffusion of two gases.

It is instructive to study how this equation works in practice. To determine the rate of diffusion of a vapor the common procedure is to measure the mass transferred from a region of high partial pressure, which we shall denote by ${}_1p_1$, to one of low pressure, which we shall denote by ${}_2p_1$. The equation for the mass transfer may be written

$$\rho_1 u_1 = \frac{D_v}{k_1}\frac{\partial}{\partial x}[\log (P - p_1)].$$

Since by the equation of continuity $\rho_1 u_1$ is constant when the flow is steady, we can integrate this equation. Hence

$$\rho_1 u_1 = -\frac{D_v}{k_1}\frac{1}{L}\log\frac{(P - {}_1p_1)}{(P - {}_2p_1)}, \tag{21}$$

where L is the distance between the points where $p_1 = {}_1p_1$ and $p_1 = {}_2p_1$. We can write this equation

$$\rho_1 u_1 = -\frac{D_v}{k_1}\frac{1}{L}\log\left(1 - \frac{{}_1p_1 - {}_2p_1}{P - {}_2p_1}\right), \tag{22}$$

and expanding the logarithmic term

$$\rho_1 u_1 = \frac{D_v}{k_1}\frac{1}{L}\left[\frac{{}_1p_1 - {}_2p_1}{P - {}_2p_1} - \frac{1}{2}\left(\frac{{}_1p_1 - {}_2p_1}{P - {}_2p_1}\right)^2 + \ldots\ldots\right]. \tag{23}$$

In most experiments on vapors the partial pressures p_1 will be much smaller than the total pressure P and all terms in the series except the first may be neglected. Also, in most diffusion experiments ${}_2p_1$ is zero or very close to it so that ${}_2p_1$ may be neglected in comparison with P. Our equation thus becomes

$$\rho_1 u_1 = \frac{D_v}{k_1}\frac{1}{P}\frac{{}_1p_1 - {}_2p_1}{L}, \tag{24}$$

or, if we express it in terms of the densities

$$\rho_1 u_1 = \frac{D_v}{P}\frac{{}_1\rho_1 - {}_2\rho_1}{L}. \tag{25}$$

If we write $D = \frac{D_v}{P}$ this equation is identical with the integrated form of the equation for the interdiffusion of two gases and we see that, when the partial pressure of the vapor is small in comparison with the total pressure, the error introduced by using Fick's law in the form

$$\rho_1 u_1 = -\frac{k_1 k_2}{CP}\frac{\partial \rho_1}{\partial x}$$

$$= -D\frac{\partial \rho_1}{\partial x}$$

is negligible.

Diffusion Through an Inert Porous Medium

It is obvious that when we have two gases separated by a porous barrier the resistance to the mixing of the gases will be greater than if the barrier were not present. In general, there will be two effects:

(i) Since the area available for diffusion will be much less and since, in general, owing to the tortuosity of the paths, the molecules will have to diffuse a longer distance, the rate of diffusion will be less than if the barrier were not present. To represent this reduction, we can assume that the diffusion coefficient is reduced proportionally to the reduction in area (which, in turn, is proportional to the porosity f of the medium) and also that it is reduced by a factor $r = \frac{l}{l_e}$ = ratio of length of barrier to effective path traveled by the molecules. Hence the equation of mass transfer becomes

$$\rho_1 u_1 = -frD\frac{\partial \rho_1}{\partial x}. \tag{26}$$

(ii) In developing the equations for diffusion it has been assumed that the resistance to the movement of the gases is the result of the mutual interference of the two gases only, and that, in particular, this resistance is so great and the movement of the gases is so slow that any hydrodynamic or viscous resistance can be neglected. When we are considering the diffusion through porous bodies it is not immediately obvious that these assumptions will hold, for if the pores are very small it is conceivable that the resistance to hydrodynamic flow might be comparable to the diffusive resistance. According to a kinetic picture, this would take place when the collisions of the molecules with the walls of the pores became comparable in number to the collisions with molecules of the second gas. For the present, however, we shall neglect any hydrodynamic or viscous resistance and assume that all resistance to the flow is diffusive. The measurements of Penman (10) indicate that this assumption is valid, at least for diffusion through soils. The theoretical justification for the assumption is that at atmospheric pressure the size of the pores would have to be very small ($< 10^{-5}$ cm.) to be comparable to the mean free path of the molecules.

Writing Equation (26) in the form

$$\rho_1 u_1 = -D'\frac{\partial \rho_1}{\partial x} \tag{27}$$

we take it as our equation of transfer for the diffusion through an inert porous medium and we can proceed, as for simple diffusion, to develop the differential equation.

The equation of continuity is similar to that used by Muskat for the hydrodynamic flow through such media, namely,

$$\frac{\partial(\rho_1 u_1)}{\partial x} = -f\frac{\partial \rho_1}{\partial t}.$$

Combining this with Equation (27) we obtain

$$f\frac{\partial \rho_1}{\partial t} = D'\frac{\partial^2 \rho_1}{\partial x^2},$$

or,

$$\frac{\partial \rho_1}{\partial t} = rD\frac{\partial^2 \rho_1}{\partial x^2}. \tag{28}$$

Thus the differential equation is similar to that for the interdiffusion of two gases except for the constant factor r. This result is confirmed by the measurements of Penman (10).

Diffusion of a Vapor Through an Inert Porous Medium

It is obvious that, in the range of vapor pressures where the approximation developed above is applicable, the diffusion of a vapor through an inert porous medium will follow the same laws as the interdiffusion of two gases.

Diffusion of a Vapor through an Adsorbing Medium that is not Permeable to Nonadsorbed Gases

In discussing the movement of a gas through a medium by which it is adsorbed, we shall restrict ourselves, in this section, to consideration of a nonporous medium in the sense that there are no channels or pores of sufficient size to allow the penetration of a nonadsorbed gas. It is necessary, therefore, to conceive of the gas as being adsorbed on the external surface and migrating through the medium as an adsorbed film on internal surfaces. There is considerable supporting evidence for such a picture and it is not necessary to make any assumptions about the internal surfaces save that they are accessible to adsorbed molecules and nonaccessible to the gas phase. We shall be limited only by the assumption that, once adsorbed, the gas migrates as an adsorbed atom or molecule until it reaches the external surface on the low pressure side of the barrier where it evaporates.

It is obvious that, on such a picture, some of the fundamental ideas of diffusion must be modified. In the interdiffusion of two gases, the basic assumption is that the resistance to the movement of the two gases is due to the relative motions of the two kinds of molecules, and that this relative motion gives rise to a resistive force proportional to the densities of the two gases and to their

relative velocities. In the diffusion of an adsorbed gas, as pictured above, no second gas is present within the adsorbent to resist the motion of the diffusing gas, and it is only possible to conceive of the resistance as residing in the "friction" between solid and adsorbed film. In the modern treatment of adsorption, such a resistance is related to the energy required to move an atom over the potential barriers between adsorbing sites on the surface.

It is evident, according to this picture, that the second gas, if present, plays no function in the diffusion save that of hindering the movement of the diffusing gas up to the external surface of the medium. Since the resistance thus offered is in general, negligible compared to the resistance within the medium, there will be no distinction here between hydrodynamical flow, where there is only one gas, and diffusion, where a permanent nondiffusing gas is present in addition to the adsorbed gas. In such a diffusion, it is immaterial whether the pressure difference of the diffusing gas is a total or a partial pressure difference.

To find the differential equation governing the movement of a gas under these considerations we return to our fundamental dynamical equation which we express in the simplified form

$$\frac{\partial p}{\partial x} - A_x = 0.$$

The problem is (1) what is the pressure gradient that applies to such a diffusion and (2) how are the resistive forces A_x related to the physical characteristics of the system.

In the statistical treatment of adsorption, an adsorbed layer is found to have the properties of a two-dimensional gas. In particular, it is possible to derive a potential function ϕ which has, for an adsorbed film, exactly the same thermodynamic properties that the pressure p has for a three-dimensional gas. ϕ has been called the spreading pressure and is related to the free energy of the adsorbed film by the relation $\phi = -\frac{\partial F_{ads}}{\partial A}$, where A is the area of the film. ϕ is a measure of the force that must be applied to keep the film from spreading. It would seem, therefore, from these qualitative considerations that the spreading pressure ϕ is the appropriate potential function for the fundamental dynamical equation.

In considering the hydrodynamical picture of the movement of an adsorbed film, it is necessary to think of the film as moving as a whole over the surface with a velocity of motion u just as, in viscous flow, a gas is pictured as moving as a whole even though it is known that the viscous forces are due to random motions of the molecules. We shall, therefore, treat the adsorbed film as having a velocity of motion u relative to the surface and shall assume, as is natural, that the resistive force to the motion will be proportional to u. We shall put the resistive force equal to Cu where C is again the coefficient of resistance.

There is, at first sight, no reason for thinking that the resistive force will be independent of the number of molecules adsorbed. To the contrary, in the kinetic picture of adsorption, it is sometimes assumed that the molecules adsorbed at low pressures are bound more tightly, and consequently would offer greater resistance to flow, than the molecules that are adsorbed at higher pressures. It would seem, therefore, that, from kinetics, the resistive force might be taken as dependent on the number of molecules adsorbed. On the other hand, from the statistical point of view, variation of binding force with concentration is already taken care of in the expression for the spreading pressure—when the atoms are bound firmly they contribute a small effect to the spreading pressure and vice versa—and it is not necessary to introduce the influence of binding force into the resistive force. We shall, therefore, express our resistive force as Cu and assume, as justified by results, that C is a constant, characteristic of the gas and the medium.

The fundamental dynamical equation is, therefore,

$$\frac{\partial \phi}{\partial x} + Cu = 0, \tag{29}$$

where the sign is positive since u is in the direction of decreasing pressure.

The equation of state for such a diffusion is given by the relation between ϕ and the concentration of adsorbed molecules. This relation, of course, depends on the adsorption isotherm and is readily available only for those isotherms that have been statistically derived. We shall not then, at this time, attempt to give the generalized differential equation for flow through adsorbing media but shall confine ourselves to those types of adsorption for which a statistical expression for ϕ is available.

The Differential Equation for the Diffusion of a Mobile Monolayer

The simplest model of an adsorbed film on a solid is that designated by Fowler and Guggenheim (5) as a mobile monolayer. In a mobile monolayer some point in the adsorbed molecule (for example its center of mass) is bound tightly to the surface in the normal direction but can move with complete freedom in the two directions on the surface. It is unlikely that such an idealized picture will represent the behavior of any film actually adsorbed on solids but since it is the simplest representation of adsorption we commence with a discussion of it.

For a mobile monolayer, Fowler and Guggenheim give for the spreading pressure ϕ, the relation

$$\phi = \frac{NkT}{A}, \tag{30}$$

where N is the number of atoms adsorbed on a surface of area A. For convenience we take A as the area of surface per unit volume so that N equals

number of atoms adsorbed per unit volume. It is apparent from the similarity with the equation

$$p = \frac{NkT}{V}$$

in three dimensions that a mobile monolayer is the two-dimensional analogue of a perfect gas.

When we substitute this value for ϕ in Equation (29), we get

$$u = -\frac{kT}{CA}\frac{\partial N}{\partial x}, \tag{31}$$

and for the mass transfer

$$Nu = -\frac{kT}{CA}N\frac{\partial N}{\partial x}. \tag{32}$$

Since ρ, the density of adsorbed gas, is clearly proportional to N, we may write the equation of continuity in the form

$$\frac{\partial(Nu)}{\partial x} = -\frac{\partial N}{\partial t}, \tag{33}$$

which is more convenient when we are considering adsorbed gases.

From (32) and (33) we obtain the differential equation for the flow, namely,

$$\frac{\partial N}{\partial t} = \frac{kT}{CA}\frac{\partial}{\partial x}\left(N\frac{\partial N}{\partial x}\right)$$

$$= \frac{kT}{2CA}\frac{\partial^2 N^2}{\partial x^2}. \tag{34}$$

It is perhaps worth while to look at the implications of this equation. For steady-state flow, since $\frac{dN}{dt} = 0$, we have

$$\frac{\partial^2 N^2}{\partial x^2} = 0. \tag{35}$$

To find how the concentration would vary with distance we consider a barrier of thickness L, with concentration N_0 at surface $x = 0$ and N_L at $x = L$. Integrating (35) and putting in the boundary conditions, we find

$$N^2 = (N_L^2 - N_0^2)\frac{x}{L} + N_0^2. \tag{36}$$

Thus the concentration varies as the square root of the distance.

We find how the diffusion coefficient of the commonly used equation

$$\mathbf{P} = -D_c\frac{\partial C}{\partial x} \tag{37}$$

might be expected to vary with concentration we write the equation for the mass transfer in the form

$$Nu = -\frac{kT}{2CA}\frac{\partial N^2}{\partial x} \tag{38}$$

and integrate from $x = 0$ to $x = L$, remembering that, by the equation of continuity, Nu is independent of x. Thus

$$Nu = \frac{kT}{2CA}\frac{N_0^2 - N_L^2}{L}. \tag{39}$$

Similarly we integrate (37) bearing in mind that $\mathbf{P}$ is equivalent to Nu and C to N. Thus

$$Nu = \mathbf{P} = D_c\frac{N_0 - N_L}{L}. \tag{40}$$

Equating and writing $\frac{kT}{CA} = D$, we get

$$D_c = D\,\frac{N_0 + N_L}{2}. \tag{41}$$

Thus we see that, according to this picture of a mobile monolayer, we should expect the diffusion coefficient as commonly derived from Fick's law to be proportional to the mean concentration.

The Differential Equation for the Diffusion of an Ideal Localized Monolayer (Langmuir Adsorption)

According to the model of a localized monolayer developed by Langmuir, the molecules are attached to the surface at definite points of attachment which are generally referred to as sites. From a kinetic argument, Langmuir was able to show that the isotherm for such an adsorption is represented by an equation of the form

$$\theta = \frac{p}{p_0 + p} = \frac{ap}{1 + ap}, \tag{42}$$

where θ is the fraction of sites occupied and $p_0 = \frac{1}{a}$ is a constant.

Fowler has shown how this equation may be statistically derived and has obtained an expression for the spreading pressure (5). He gives

$$\phi = \frac{N_s kT}{A}\log\frac{1}{1 - \theta}, \tag{43}$$

where N_s may be taken as the number of sites, and A the surface area, per unit volume.

Substituting this value of ϕ into our fundamental dynamical Equation (29), we get

$$\frac{N_s kT}{A}\frac{\partial}{\partial x}\left(\log\frac{1}{1-\theta}\right)+Cu=0. \tag{44}$$

Putting $\theta=\frac{N}{N_s}$, where N = number of adsorbed atoms and transposing we find

$$u=-\frac{N_s kT}{CA}\frac{\partial}{\partial x}\left(\log\frac{N_s}{N_s-N}\right). \tag{45}$$

Whence the equation of mass transfer can be written

$$\begin{aligned} Nu &= -\frac{N_s kT}{CA}\cdot N\cdot\frac{\partial}{\partial x}\left(\log\frac{N_s}{N_s-N}\right)\\ &= -\frac{N_s kT}{CA}\frac{N}{N_s-N}\frac{\partial N}{\partial x}. \end{aligned} \tag{46}$$

On comparing this equation with Fick's law

$$\mathbf{P}=-D_c\frac{\partial c}{\partial x},$$

we see that

$$\begin{aligned} D_c &= \frac{N_s kT}{CA}\frac{N}{N_s-N}\\ &= \frac{N_s kT}{CA}\frac{\theta}{1-\theta}. \end{aligned} \tag{47}$$

In Fig. 1, $D_c\Big/\frac{N_s kT}{CA}$ has been plotted against θ, and the resulting curve shows how the diffusion coefficient of Fick's law would vary with θ.

Equation (47) and Fig. 1 give the instantaneous value of D_c at any concentration θ but in practice it is always an integrated value that is measured. To see how the measured values will vary with concentration we proceed with our analysis.

The equation of continuity is again

$$\frac{\partial(Nu)}{\partial x}=-\frac{\partial N}{\partial t},$$

and introducing the fundamental dynamical Equation (45), we obtain

$$\begin{aligned} \frac{\partial N}{\partial t} &= \frac{N_s kT}{CA}\frac{\partial}{\partial x}\left(\frac{N}{N_s-N}\frac{\partial N}{\partial x}\right)\\ &= \frac{N_s kT}{CA}\frac{\partial^2}{\partial x^2}\left[N_s-N-N_s\log\left(N_s-N\right)\right]. \end{aligned} \tag{48}$$

This is the differential equation for diffusion in an adsorbing solid when the adsorption obeys Langmuir's isotherm.

In the steady state, we should have

$$\frac{\partial^2}{\partial x^2}[N_s - N - N_s \log (N_s - N)] = 0, \tag{49}$$

and the equation giving the variation of the number of adsorbed atoms with the distance x is

$$N_s - N - N_s \log (N_s - N) = \left(N_0 - N_L - N_s \log \frac{N_s - N_L}{N_s - N_0}\right)\frac{x}{L} + N_s - N_0 - N_s \log (N_s - N_0). \tag{50}$$

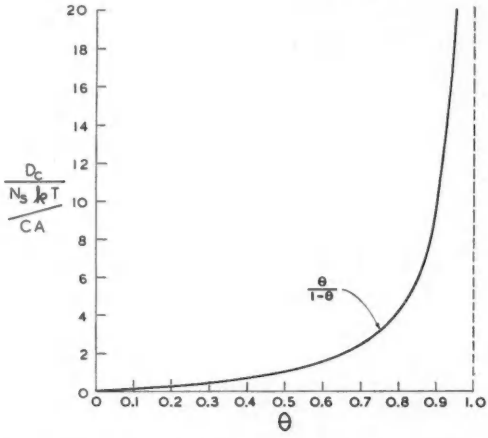

FIG. 1. *Variation of the coefficient of the differential equation when the adsorption obeys Langmuir's equation.*

The rate of diffusion of a gas through a solid is most commonly determined by measuring the mass transferred through a definite thickness of the solid with a constant pressure difference. We shall now calculate the amount that, on our picture, would diffuse in such an experiment.

The equation for the mass transfer can be expressed

$$Nu = -\frac{N_s kT}{CA}\frac{\partial}{\partial x}[N_s - N - N_s \log (N_s - N)], \tag{51}$$

and integrating from $x = 0$ to $x = L$, we get

$$Nu = \frac{N_s kT}{CA}\frac{1}{L}\Big[N_s - N - N_s \log (N_s - N)\Big]_{N=N_L}^{N=N_0}$$

$$= -\frac{N_s kT}{CA}\frac{1}{L}\left[N_0 - N_L + N_s \log \frac{N_s - N_0}{N_s - N_L}\right], \tag{52}$$

or if we wish the expression in terms of $\theta = \frac{N}{N_s}$,

$$Nu = -\frac{N_s^2 kT}{CA}\frac{1}{L}\left[\theta_0 - \theta_L + \log\frac{1-\theta_0}{1-\theta_L}\right]. \tag{53}$$

This expression gives the amount of gas diffusing through a barrier when $\theta = \theta_0$ on one surface and $\theta = \theta_L$ on the other. To find, in practice, a diffusion following these laws we turn to the diffusion of gases in metals. It is well known that certain gases are adsorbed by metals in such a manner that the isotherm can be represented by the Langmuir equation and, according to our picture, the diffusion of such gases through the metals should follow the equations developed above.

To test these equations the experimental results of Smithells and Ransley (12) are most convenient. Their measurements give the volume of gas at N.T.P. diffusing per second through unit area of metal, 1 mm. thick when there is zero pressure on one side and pressure p on the other. Since volumes at N.T.P. will be proportional to the mass, Smithells and Ransley have essentially measured Nu as given by Equation (53) and their results may be used as a direct test for that equation.

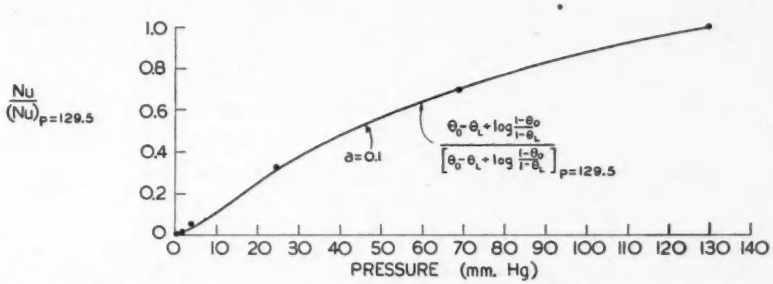

FIG. 2. *Diffusion of hydrogen through copper.* • *Experimental values from Smithells and Ransley.*

In Fig. 2 we present the results of Smithells and Ransley for the diffusion of hydrogen through copper at 723°K. and in Fig. 3 the results for the diffusion of hydrogen through iron (etched) at 686°K. The results have been expressed as a fraction of the weight diffusing at the highest measured pressure and the equation is made to agree with experiment at that pressure. As a second adjustable constant we have a in the expression $\theta = \frac{ap}{1+ap}$ and the curve for the value of a giving the closest fit to the experimental results is shown in the figures. At present it is impossible to deprive supporting evidence for the theory by comparing the value of a from diffusion with that from the isotherm since the isotherms have been determined only at temperatures considerably lower than those at which diffusion experiments have been made. It can only

be said about a that the value used in Fig. 2 is the same as that considered satisfactory by Smithells and Ransley when derived from another theory.

The agreement with experimental results shown in Figs. 2 and 3 is encouraging but, since it is not the intention in this paper to study in detail the diffusion through metals and its relation to the equations above, we shall proceed no further with this analysis. We wish to point out only that the simple

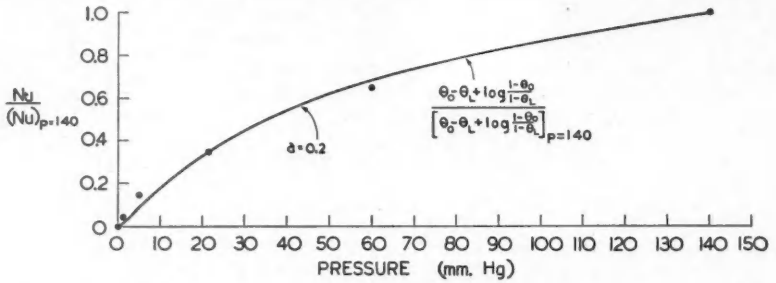

FIG. 3. *Diffusion of hydrogen through iron (etched).* • *Experimental values from Smithells and Ransley.*

assumptions made in deriving our differential equation are sufficient to lead to an equation that is, at least, in qualitative agreement with measurements, and that the theoretical basis of this equation is more substantial than that of the semi-empirical equation that has hitherto been used.

The Differential Equation for the Diffusion of a Gas Obeying the BET Isotherm

There is one other class of adsorption isotherm that has been represented by a statistical equation and that has great importance because of the variety of solids that adsorb vapor in that way. This is the equation of Brunauer, Emmett, and Teller for polymolecular adsorption. The BET equation was originally derived, like Langmuir's equation, from kinetics but recently Cassie (4) and Hill (6) have shown how it may be obtained from statistics, and from their analysis it is possible to derive an expression for the spreading pressure ϕ. We shall, therefore, proceed to discuss how a gas adsorbed by the BET mechanism would, on our theory, diffuse through an adsorbing solid.

To obtain the expression for the spreading pressure ϕ, we have that

$$\phi = -\frac{\partial F_{ads}}{\partial A},$$

and from Hill we find that

$$F_{ads} = -kT \log Q, \tag{54}$$

where Q is the complete partition function for BET adsorption. Evaluating

Q in terms of the total number of adsorbed molecules N, the number of localized sites B, the number of molecules X adsorbed on the localized sites, and the partition functions $j_s e^{\frac{\epsilon_1}{kT}}$ and $j_L e^{\frac{\epsilon_L}{kT}}$ for the molecules adsorbed in the first layer and in higher layers respectively, we find for F_{ads} the expression

$$F_{ads} = -kT\Big[N\log N + B\log B - (N-X)\log(N-X) - (B-X)\log(B-X) - 2X\log X + X\frac{\epsilon_1}{kT} + (N-X)\frac{\epsilon_L}{kT} + X\log j_s + (N-X)\log j_L\Big]. \quad (55)$$

Whence

$$\phi = -\frac{\partial F_{ads}}{\partial A} = -\frac{B}{A}\frac{\partial F_{ads}}{\partial B} = \frac{BkT}{A}\log\frac{B}{B-X}. \quad (56)$$

Substituting this value of ϕ in our fundamental dynamical equation (29), we get

$$\frac{BkT}{A}\frac{\partial}{\partial x}\left(\log\frac{B}{B-X}\right) + Cu = 0,$$

or

$$u = -\frac{BkT}{CA}\frac{\partial}{\partial x}\left(\log\frac{B}{B-X}\right), \quad (57)$$

and the equation for mass transfer becomes

$$Nu = -\frac{BkT}{CA}N\frac{\partial}{\partial x}\left(\log\frac{B}{B-X}\right) = -\frac{kT}{CA}N\frac{B}{B-X}\frac{\partial X}{\partial x}. \quad (58)$$

To eliminate X, we use the equation given by Cassie that

$$(N-X)(B-X) = \beta X^2$$

where

$$\beta = \frac{j_L}{j_s}e^{\frac{\epsilon_L-\epsilon_1}{kT}}. \quad (59)$$

Thus

$$\frac{\partial X}{\partial x} = \frac{B-X}{N+B-2(1-\beta)X}\frac{\partial N}{\partial x}, \quad (60)$$

and

$$X = \frac{N+B\pm\sqrt{(N+B)^2-4(1-\beta)NB}}{2(1-\beta)}. \quad (61)$$

Following Cassie, we use the minus sign for X as giving the minimum free energy, and substituting, we get

$$Nu = -\frac{kT}{CA}\frac{NB}{\sqrt{(N-B)^2+4\beta NB}}\cdot\frac{\partial N}{\partial x}. \quad (62)$$

It is very difficult to observe N experimentally and in practice the measured quantity is almost always the pressure p. We shall use the notation $P = \frac{p}{p_0}$, where p_0 is the saturation vapor pressure. In this notation the BET equation can be written

$$\frac{N}{B} = \frac{CP}{(1-P)(1-P+CP)}, \tag{63}$$

where

$$C = 1/\beta.$$

With the BET equation we can eliminate N from (62) and we get

$$Nu = -\frac{B^2kT}{CA} \frac{1}{\sqrt{1 + \frac{(4\beta-2)(1-P)(1-P+CP)}{CP} + \frac{[(1-P)(1-P+CP)]^2}{C^2P^2}}} \cdot \frac{C(1-P^2+CP^2)}{[(1-P)(1-P+CP)]^2} \cdot \frac{\partial P}{\partial x}. \tag{64}$$

In experimental work on adsorbing solids it has been usual to express the results in terms of an equation

$$\text{Mass transfer} = Nu = -D_p \frac{\partial P}{\partial x}. \tag{65}$$

By a comparison of (65) with (64) we see that D_p would be expected to vary with P according to the relation

$$D_p = \frac{B^2kT}{CA} \frac{1}{\sqrt{1 + \frac{(4\beta-2)(1-P)(1-P+CP)}{CP} + \frac{[(1-P)(1-P+CP)]^2}{C^2P^2}}} \cdot \frac{C(1-P^2+CP^2)}{[(1-P)(1-P+CP)]^2}. \tag{66}$$

In Fig. 4 $D_p \Big/ \frac{kTB^2}{CA}$ has been plotted against P and the curve shows the way the diffusion coefficient of the simple equation (65) will vary with pressure if the adsorption follows the BET isotherm and our assumptions are correct. In calculating D_p from (67) β and C have been given the values that would be appropriate to spruce wood, that is, $C = \frac{1}{\beta} = 11.80$ (1). Although spruce wood, being permeable to nonadsorbed gases, does not come within the class of solids we are considering we have taken this value for C as being readily available and as giving a reasonable figure. We are interested at this stage in only a qualitative comparison and wish only to see the general behavior.

In practice it is difficult to measure the differential value of the diffusion coefficient as given by (66); nearly always Equation (64) is integrated

before it is applied. We shall, therefore, proceed to derive such an integrated equation and show how the commonly measured coefficient of diffusion is related to the mean pressure. The first step is to obtain the differential equation.

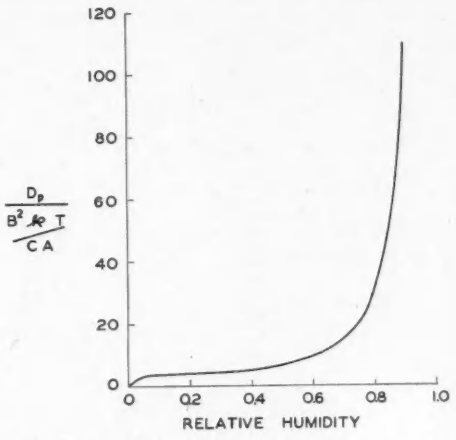

FIG. 4. *Variation of the coefficient of the differential equation when the adsorption obeys the BET equation.*

We may write the equation of mass transfer (62) in the form

$$Nu = -\frac{BkT}{CA}\frac{N}{\sqrt{Y}}\cdot\frac{\partial N}{\partial x}, \tag{67}$$

where

$$Y = (N - B)^2 + 4\beta NB. \tag{68}$$

Equation (67) is equivalent to

$$Nu = -\frac{BkT}{CA}\frac{\partial}{\partial x}\left\{\sqrt{Y} - B(2\beta - 1)\log\left[\sqrt{Y} + N + B(2\beta - 1)\right]\right\}, \tag{69}$$

and using the equation of continuity in the form

$$\frac{\partial(Nu)}{\partial x} = -\frac{\partial N}{\partial t},$$

we obtain for the differential equation

$$\frac{\partial N}{\partial t} = \frac{BkT}{CA}\frac{\partial^2}{\partial x^2}\left\{\sqrt{Y} - B(2\beta - 1)\log\left[\sqrt{Y} + N + B(2\beta - 1)\right]\right\}. \tag{70}$$

To find the expression for the integrated mass transfer, we consider the movement of a gas through a barrier of adsorbing material from the surface $x = 0$ where $P = P_0$ to the surface $x = L$ where $P = P_L$. Integrating Equation (69) we get

$$Nu = \frac{BkT}{CA} \cdot \frac{1}{L} \cdot \left\{ \sqrt{Y} - B(2\beta - 1) \log \left[\sqrt{Y} + N + B(2\beta - 1) \right] \right\}_{N=N_L}^{N=N_0} \cdot \quad (71)$$

Similarly integrating Equation (65) we have

$$Nu = D_P \frac{P_0 - P_L}{L} \cdot \quad (72)$$

Hence equating (71) and (72) we get for D_p

$$D_P = \frac{BkT}{CA} \frac{\left\{ \sqrt{Y} - B(2\beta - 1) \log \left[\sqrt{Y} + N + B(2\beta - 1) \right] \right\}_{N=N_L}^{N=N_0}}{P_0 - P_L} \cdot \quad (73)$$

Substituting in this the value of Y and using the BET equation (63) to change the independent variable from N to P, we get

$$D_P = \frac{B^2 kT}{CA} \frac{1}{P_0 - P_L} \left\{ \sqrt{\frac{C^2P^2}{[(1-P)(1-P+CP)]^2} + \frac{(4\beta - 2)CP}{(1-P)(1-P+CP)} + 1} \right.$$
$$- (2\beta - 1) \log \left[B \sqrt{\frac{C^2P^2}{[(1-P)(1-P+CP)]^2} + \frac{(4\beta - 2)CP}{(1-P)(1-P+CP)} + 1} \right.$$
$$\left. \left. + \frac{BCP}{(1-P)(1-P+CP)} + B(2\beta - 1) \right] \right\}_{P=P_L}^{P=P_0}, \quad (74)$$

or reverting to our former notation where

$$Y = \frac{C^2P^2}{[(1-P)(1-P+CP)]^2} + \frac{(4\beta - 2)CP}{(1-P)(1-P+CP)} + 1,$$

we have

$$D_P = \frac{B^2kT}{CA} \cdot \frac{1}{P_0 - P_L} \cdot \left\{ \sqrt{Y_0} - \sqrt{Y_L} - (2\beta - 1) \log \right.$$
$$\left. \frac{\sqrt{Y_0} + \dfrac{BCP_0}{(1-P_0)(1-P_0+CP_0)} + B(2\beta - 1)}{\sqrt{Y_L} + \dfrac{BCP_L}{(1-P_L)(1-P_L+CP_L)} + B(2\beta - 1)} \right\} \cdot \quad (75)$$

The value of $D_p \Big/ \frac{B^2kT}{CA}$ given by Equation (75) has been plotted in Fig. 5 as a function of the mean relative humidity $\frac{P_0 + P_L}{2}$. In this calculation P_L has been taken as zero. The values of B and C have again been taken from the data on spruce wood (1) ($C = 11.80$ and $B = 6.17$).

There are not at present sufficient measurements to test this equation quantitatively but the measurements that are available do indicate that the

experimental relation between D_p and P is represented qualitatively by Equation (75). All measured results for wood seem to indicate a diffusion coefficient very small at low humidities and increasing very rapidly at humidities approaching saturation (2, 8, 11). A curve of similar shape has been obtained by King (7) from his measurements on the diffusion of water vapor through horn keratin. In fact, all available measurements indicate that this shape of curve is general for diffusion whenever the adsorption can be represented by the sigmoid isotherm peculiar to BET adsorption.

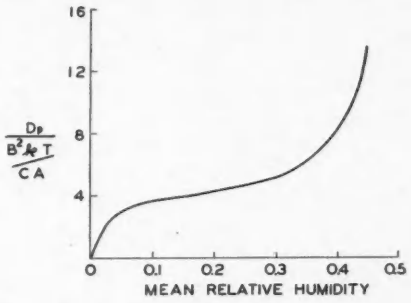

FIG. 5. *Variation of the coefficient of the integrated equation when the adsorption obeys the BET equation.*

The part of the theoretical curves of Figs. 4 and 5 that has not been observed experimentally is the reversed curvature and sharp decrease to zero at low relative humidities. In the experiments, however, few measurements have been made at the lowest humidities and it might well be that this reversed curvature has been overlooked. More measurements at low humidities will be necessary to delineate the experimental curve in this region. The theoretical curves do show, however, the large increase of diffusion at high humidities that is so striking a characteristic of diffusion through adsorbing solids.

It should be pointed out that these diffusion equations have been derived on the assumption that the adsorption can be represented by the BET equation. It has been shown by numerous workers that the BET equation gives satisfactory values for the amount of gas adsorbed only at relative humidities below 50% and therefore we should not expect results derived from this theory to hold outside of that range. Although it does not give quantitative agreement at high humidities, the BET equation does indicate, however, the large increase of adsorption that is so characteristic of the adsorption of water vapor as saturation is approached and, in consequence, the equations can be considered as giving a qualitative indication of the behavior at high humidities.

Flow Through a Medium that is Both Porous and Adsorbing

There remains for consideration the problem of a medium that is porous in the sense that it is permeable to a nonadsorbed gas and that is at the same

time an adsorbent for the gas whose flow is being measured. It is obvious that with such a medium there will be a movement of the gas both through the pores and through the material itself. It is also obvious that through the pores the quantity of flow will depend on whether we have hydrodynamical flow with an absolute pressure difference or diffusive flow with a difference only of partial pressure, whereas through the medium proper, as shown above, the flow will depend only on the gradient of ϕ and will be disturbed by the presence of the second gas only indirectly through the altered pressure gradient in the pores.

Although at first sight one might suppose that such a flow could be represented by the sum of the mass transfer through the pores and through the medium, this is not so since in general there will be throughout the medium a free exchange of gas from the adsorbed phase within the medium to the vapor phase within the pores. In a small element of internal surface there will be a balance between the mass flowing into the element, the mass flowing out, the mass that evaporates into the pores and the mass that condenses on the surface from the vapor in the pores. Similarly in a small element of volume in the pores, the adsorption and desorption of the gas by the medium must be taken into consideration in addition to the flow.

Mathematically, this amounts to the fact that it is not valid to apply the equation of continuity separately to the diffusion through the medium and to the flow in the pores, but instead the equation of continuity must only be applied to the total mass transferred, that is, to the sum of the mass transferred by diffusion through the medium and by flow through the pores. Thus although it is simple to set up the fundamental dynamical equations for the flow it is not possible, in general, to obtain from them the differential equations since the equation of continuity could only be written if we knew precisely the size and distribution of pores in the medium and could calculate at each point the distribution of gas between gaseous and adsorbed phase. We shall not at present attempt to do this but shall rest content with having pointed out the difficulties.

Conclusion

We have in this paper derived from first principles the differential equations governing the diffusion of gases and vapors and have endeavored to point out the modifications that must be made to these equations when the diffusion is through a solid medium. In particular we have shown that, where there is an interaction between the diffusing gas and the solid, as in adsorption, the use of Fick's law as the fundamental equation of diffusion is not valid. An attempt has also been made to distinguish between hydrodynamic flow and diffusion and to point out the assumptions and features peculiar to diffusion.

In conclusion, a general comparison of the derivation of the differential equations of four equalization processes is given in Table I. In this table the equivalent fundamental quantities are set down and from these quantities

step by step the analogous equations are derived. Such a comparison is useful to show where the processes differ and whence the variations in the form of the final equation.

There are one or two points that are brought out by this table that are worth emphasizing. In the first place it is essential to note that the pressure (and its analogous quantity θ) is the potential function whose space derivative gives the force that is balanced by the resistive forces. This fundamental fact has been obscured by the tendency to use Fick's law in the form $\mathbf{P} = -D_c \frac{\partial c}{\partial x}$ as the fundamental equation of motion. As brought out in this paper, only when c is directly proportional to the pressure is such an approach correct.

TABLE I

	Conduction of heat	Flow according to Darcy's equation	Diffusion of gases	Diffusion through absorbing media
Fundamental quantities	Energy Quantity of heat = energy per cc. $= q$ Velocity of flow of energy $= v$ Flux of heat $= f = qv$ Temperature $= \theta$	Mass Density = mass per cc. $= \rho$ Velocity of flow $= v$ Flux $= \rho v$ Pressure $= p$	Mass Density = mass per cc. $= \rho$ Velocity of diffusion $= u$ Flux = rate of flow of gas $= \rho u$ Partial pressure $= p$	Mass Number of adsorbed molecules per cc. $= N$ Velocity of diffusion $= u$ Flux = rate of flow of adsorbed gas $= Nu$ Spreading pressure $= \phi$
Fundamental law	Conservation of energy	Conservation of mass	Conservation of mass	Conservation of mass
Statement of fundamental dynamical law	$f = -k\frac{\partial\theta}{\partial x}$ or $qv = -k\frac{\partial\theta}{\partial x}$, where k = thermal conductivity	$v = -\frac{k}{\mu}\frac{\partial p}{\partial x}$, where k = permeability μ = viscosity	$\rho_1(u_1 - u_2) = -\frac{1}{C\rho_2}\frac{\partial p_1}{\partial x}$, where C = coefficient of resistance	$u = -\frac{1}{C}\frac{\partial\phi}{\partial x}$, where C = coefficient of resistance
Equation of continuity	$\frac{\partial(f)}{\partial x} = -\frac{\partial q}{\partial t}$ or $\frac{\partial(qv)}{\partial x} = -\frac{\partial q}{\partial t}$	$\frac{\partial(\rho u)}{\partial x} = -f\frac{\partial\rho}{\partial t}$, where f = porosity	$\frac{\partial(\rho_1 u_1)}{\partial x} = -\frac{\partial\rho_1}{\partial t}$	$\frac{\partial(Nu)}{\partial x} = -\frac{\partial N}{\partial t}$
Equation of state	$q = \rho c\theta$, where ρ = density c = specific heat	$\rho = \rho_0 p^m$ Isothermal flow: $m = 1$ Adiabatic flow: $m = c_\rho/c_v$	$\rho_1 = k_1 p_1$ (flow assumed isothermal)	$\phi = f(N)$ The relation between ϕ and N is dependent on the nature of the adsorption and is related to the adsorption isotherm
Differential equations	$\frac{\partial q}{\partial t} = k\frac{\partial^2\theta}{\partial x^2}$ or $\frac{\partial\theta}{\partial t} = \frac{k}{\rho c}\frac{\partial^2\theta}{\partial x^2} = \kappa\frac{\partial^2\theta}{\partial x^2}$, where $\kappa = k/\rho c$ = thermal diffusivity or $\frac{\partial q}{\partial t} = k\frac{\partial^2 q}{\partial x^2}$	$f\frac{\partial\rho}{\partial t} = \frac{k\rho_0}{\mu(m+1)}\frac{\partial^2 p^{m+1}}{\partial x^2}$ or $f\frac{\partial\rho}{\partial t} = \frac{k}{\mu}\frac{1}{1+m}\frac{1}{\rho_0^{1/m}}\frac{1+m}{m}\frac{\partial^2\rho}{\partial x^2}$	$\frac{\partial\rho_1}{\partial t} = Dk_1\frac{\partial^2 p_1}{\partial x^2}$ $\frac{\partial p_1}{\partial t} = D\frac{\partial^2 p_1}{\partial x^2}$ or $\frac{\partial\rho_1}{\partial t} = D\frac{\partial^2\rho_1}{\partial x^2}$	$\frac{\partial N}{\partial t} = \frac{1}{C}\frac{\partial}{\partial x}\left(N\frac{\partial\phi}{\partial x}\right)$ $\frac{\partial N}{\partial t} = \frac{1}{C}\frac{\partial}{\partial x}\left(N\frac{\partial f(N)}{\partial x}\right)$

The second point that should be noted is that the dynamical equation has two essentially different forms; in the conduction of heat and in the interdiffusion of two gases, the flux is proportional to the potential gradient, whereas in flow according to Darcy's equation and in the diffusion in an adsorbing medium it is the velocity of flow. Since in all four processes the equation of continuity pertains to the flux, this difference in the dynamical equation leads to a difference in the final equations.

It would scarcely be necessary to mention the effect of the equations of state were it not for the confusion that has arisen from the indiscriminate use of Fick's law. The classical example of the influence of the equation of state, although never expressed in that way, is the difference between the thermal conductivity and the thermal diffusivity as shown in the different forms of the final differential equation for the flow of heat. If we look at the analogous equations in the interdiffusion of gases, we find that the diffusion coefficient D is the counterpart of the thermal diffusivity κ whereas Dk_1, is analogous to the conductivity. It is necessary, therefore, to keep these relations constantly in mind so that the pressure and the density are not indiscriminately used in the equations of diffusion.

Finally it is essential to point out that this approach to the diffusion through adsorbing media is tentative, pending greater confirmation than it has here been possible to obtain; the assumption that C is independent of the number of molecules adsorbed may not be valid and it may be necessary to take C as some function of N. There is no doubt, however, that the true differential equation for the diffusion of a gas in such a medium can result only from a combination of the equations of continuity and of state with an expression defining the fundamental dynamical law of the system.

References

1. BABBITT, J. D. Can. J. Research, A, 20: 143. 1942.
2. BABBITT, J. D. Pulp and Paper Mag. Can. 49: 83. 1948.
3. BARRER, R. M. Diffusion in and through solids. Cambridge: The University Press, London. 1941.
4. CASSIE, A. B. D. Trans. Faraday Soc. 41: 450. 1945.
5. FOWLER, R. H. and GUGGENHEIM, E. A. Statistical thermodynamics, Chapter X. Cambridge; The University Press, London. 1939.
6. HILL, T. L. J. Chem. Phys. 14: 263. 1946.
7. KING, G. Trans. Faraday Soc. 41: 479. 1945.
8. MARTLEY, J. F. D.S.I.R. For. Prod. Research Tech. Paper 2. 1926.
9. MUSKAT, M. The flow of homogeneous fluids through porous media. Edwards Bros., Inc., Ann Arbor, Mich. 1937.
10. PENMAN, H. L. J. Agr. Sci. 30: 437. 1940.
11. PFALZNER, P. Can. J. Research, A, 28: 389. 1950.
12. SMITHELLS, C. J. and RANSLEY, C. E. Proc. Roy. Soc., (London), A, 150: 172. 1935.
13. STEFAN, J. Sitzber. Akada. Wiss. Wien. Math-naturw. Klasse. Abt. IIa. 83. 1881.

VIRGIN

CANADIAN JOURNAL OF RESEARCH

Notes on the Preparation of Copy

GENERAL:—Manuscripts should be typewritten, double spaced, and the **original and one extra copy** submitted. Style, arrangement, spelling, and abbreviations should conform to the usage of this Journal. Names of all simple compounds, rather than their formulae, should be used in the text. Greek letters or unusual signs should be written plainly or explained by marginal notes. Superscripts and subscripts must be legible and carefully placed. Manuscripts should be carefully checked before being submitted, to reduce the need for changes after the type has been set. If authors require changes to be made after the type is set, they will be charged for changes that are considered to be excessive. **All pages, whether text, figures, or tables, should be numbered.**

ABSTRACT:—**An abstract of not more than about 200 words, indicating the scope of the work and the principal findings, is required.**

ILLUSTRATIONS:

(i) *Line Drawings:*—All lines should be of sufficient thickness to reproduce well. Drawings should be carefully made with India ink on white drawing paper, blue tracing linen, or co-ordinate paper **ruled in blue only**; any co-ordinate lines that are to appear in the reproduction should be ruled in black ink. Paper ruled in **green, yellow, or red should not be used** unless it is desired to have all the co-ordinate lines show. Lettering and numerals should be neatly done in India ink preferably with a stencil (**do not use typewriting**) and be of such size that they will be legible and not less than one millimeter in height when reproduced in a cut three inches wide. All experimental points should be carefully drawn with instruments. Illustrations need not be more than two or three times the size of the desired reproduction, but the ratio of height to width should conform with that of the type page. **The original drawings and one set of small but clear photographic copies are to be submitted.**

(ii) *Photographs:*—Prints should be made on glossy paper, with strong contrasts; they should be trimmed to remove all extraneous material so that essential features only are shown. Photographs should be submitted **in duplicate**; if they are to be reproduced in groups, one set should be so arranged and mounted on cardboard with rubber cement; the duplicate set should be unmounted.

(iii) *General:*—**The author's name, title of paper, and figure number should be written in the lower left hand corner (outside the illustration proper) of the sheets on which the illustrations appear.** Captions should not be written on the illustrations, but typed on a separate page of the manuscript. All figures (including each figure of the plates) should be numbered consecutively from 1 up (arabic numerals). **Each figure should be referred to in the text.** If authors desire to alter a cut, they will be charged for the new cut.

TABLES:—Titles should be given for all tables, which should be numbered in Roman numerals. Column heads should be brief and textual matter in tables confined to a minimum. **Each table should be referred to in the text.**

REFERENCES:—**These should be listed alphabetically by authors' names, numbered in that order, and placed at the end of the paper.** The form of literature citation should be that used in the respective sections of this Journal. **Titles of papers should not be given in references listed in Sections A, B, E, and F, but must be given in references listed in Sections C and D.** The first page only of the references cited in papers appearing in Sections A, B, and E should be given. **All citations should be checked with the original articles.** Each citation should be referred to in the text by means of the key number; in Sections C and D the author's name and the date of publication may be included with the key number if desired.

Reprints

Fifty reprints of each paper without covers are supplied free. Additional reprints, if required, will be supplied according to a prescribed schedule of charges. On request, covers can be furnished at cost.